A GENERALIZED ONO-KONDO LATTICE MODEL

FOR HIGH PRESSURE ADSORPTION ON

CARBON ADSORBENTS

By

MAHMUD SUDIBANDRIYO

Bachelor of Science
Bandung Institute of Technology
Bandung, Indonesia
May 1986

Master of Science
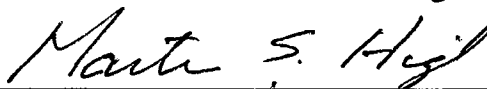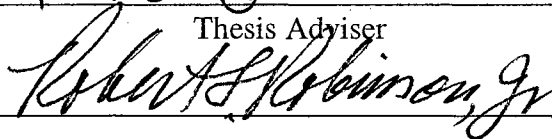Oklahoma State University
Stillwater, OK
May 1991

Submitted to the Faculty of the
Graduate College of the
Oklahoma State University
in partial fulfillment of
the requirements for
the Degree of
DOCTOR OF PHILOSOPHY
December, 2003

A GENERALIZED ONO-KONDO LATTICE MODEL

FOR HIGH PRESSURE ADSORPTION ON

CARBON ADSORBENTS

Thesis Approved:

_____
Thesis Adviser

_____

_____

_____
Dean of the Graduate College

PREFACE

A new Coalbed Methane (CBM) recovery technology has the potential to sequester greenhouse gas carbon dioxide at a net profit. The economic viability of this technology can be enhanced through better theoretical understanding of the adsorption behavior and developing a model capable of predicting high-pressure pure and mixture adsorption isotherm on heterogeneous system using accessible characterizations. Among the various theories that can be used for describing the adsorption of high-pressure fluids, the Ono-Kondo (OK) lattice theory provides a viable model for this purpose.

The Ono-Kondo (OK) lattice model was further developed to facilitate precise representations and accurate predictions for high-pressure, supercritical adsorption isotherms encountered in Coalbed Methane (CBM) recovery and CO_2 sequestration. Specifically, the parameters of the OK model were regressed to obtain reliable representation of pure-gas, high-pressure adsorption on carbon adsorbents for adsorbates in the near-critical and supercritical regions. Following a thorough analysis, the OK model parameters were generalized, and the model was extended to mixture adsorption.

Systematically-selected measurements were conducted to supplement existing data on high-pressure adsorption. These data were used to support the model development. The measurements were conducted for pure methane, nitrogen, and CO_2

and their mixture gas adsorption on an activated carbon and on selected coals at temperatures of 319 K and 328 K, and pressures to 13.8 MPa.

The OK monolayer model appears effective in modeling pure-gas adsorption on carbon matrices at supercritical and near-critical regions. The model can represent adsorption on activated carbon and coals within their expected experimental uncertainties.

The generalized model, which relates the OK model parameters to gas properties and accessible adsorbent characterization, can predict the adsorption isotherms on activated carbon with about 7% average absolute deviation or twice the expected experimental uncertainties. The generalized model can also predict the adsorption isotherms of various gases based on the adsorption isotherm of one gas on the same adsorbent. In addition, the generalized model appears effective in modeling pure-gas adsorption on wet coals when the coal moisture content is above its equilibrium value. However, the model parameter values in this case are affected by the presence of water.

The OK model is capable of predicting binary and ternary gas adsorption within twice the experimental uncertainties, on average. Further, the total and individual component adsorption can be represented to within the expected experimental uncertainties with the use of one binary interaction parameter.

ACKNOWLEDGMENTS

TABLE OF CONTENTS

LIST OF TABLES

LIST OF FIGURES

NOMENCLATURE

A Helmholtz free energy; surface area per unit mass of adsorbent

a attractive term parameter in equation of state (EOS)

b co-volume parameter in equation of state; Langmuir adsorption isotherm model parameter

b_o pre-exponential factor in Langmuir adsorption isotherm model

C maximum adsorption capacity in OK model; BET adsorption isotherm model parameter

C_a surface adsorbed-phase density

$C_{a,o}$ maximum surface adsorbed-phase density at T_o

C_{ij} binary interaction parameter for OK model and EOS model

C_{Lond} constant in London's equation

E_{ij} binary interaction parameter for OK model

E_0 parameter in the theory of volume filling of micropores

F number of degrees of freedom

$\widehat{f}_i^{\,g}$ fugacity of component i in a gas-phase mixture

G Gibbs free energy

k Two-dimensional (2D)-EOS model parameter; Boltzman constant

$k_{d\infty}$ the rate of desorption constant at infinite temperature in the Langmuir model

L maximum adsorption capacity in the Langmuir and BET models; slit width

M total number of lattice cells; molecular weight

m number of layers in the lattice model; 2-D EOS model constant;

           mass in gravimetric adsorption measurement

N_{av} Avogadro number

N_i number of molecules of component i

n number of components; parameter in the theory of volume filling of micropores

n_{ads}^{Gibbs} the amount of gas adsorbed

n_{inj} amount of gas injected from the pump section into the cell section

n_{sol} number of moles of gas dissolved in water

P pressure

P_s saturated pressure corresponding to the maximum adsorption capacity

Q configurational partition function in the lattice theory; heat of adsorption in

           the Langmuir model

R universal gas constant

r_e equilibrium distance of an incoming molecule interacting with a surface

S entropy

T temperature

T_o normal boiling point of the adsorbate (or triple point for CO_2)

U internal energy

V volume

V_{ads} adsorbed-phase volume

V_s micropore saturation volume in the theory of volume filling of micropores

V_{void} void volume

x_{ads} fractional coverage of a pure component in the monolayer lattice model

x_i mole fraction of component i in an adsorbed-phase

$x_{i,b}$ fraction that gas molecule i that occupies cells in a layer of the lattice model

$x_{i,t}$ fractional coverage of component i in t^{th} layer of the lattice model

x_t fractional coverage of pure component in t^{th} layer of the lattice model

y_i mole fraction of component i in the gas phase

z distance from a molecule to the surface

Z compressibility factor

Z_a compressibility factor as defined in 2-D EOS

z_i feed gas mole fraction

z_0 lattice coordination number

z_1 parallel coordination number representing the number of primary nearest-neighbor cells in parallel direction

Greek Symbols

α 2-D EOS model constant; a coefficient related to non-perfect sticking in the Langmuir model

β 2-D EOS model constant

δ thermal expansion coefficient of the adsorbed phase

ε^* well depth of the Lennard-Jones 12-6 potential

ε_{ij} fluid-fluid interaction energy parameter in the OK model

ε_{is} fluid-solid interaction energy parameter in the OK model

Φ adsorbate-adsorbent potential; potential energy

Φ_D dispersion energy

Φ_R close-range repulsion energy

Φ_{Ind} induction energy (interaction between electric field and an induced dipole)

$\Phi_{F\mu}$ interaction between electric field (F) and a permanent dipole (μ)

$\Phi_{\dot{F}Q}$ interaction between field gradient ($\dot{F}$) and a quadrupole (with quadrupole moment Q)

$\hat{\phi}_i^a$ fugacity coefficient of component i in an adsorbed-phase mixture

Γ Gibbs excess adsorption per unit mass of adsorbent

Ψ_{ij} correlation coefficient in the lattice model representing the deviations of a non-random mixture from its random limit

μ_i chemical potential for component i

π number of phases; spreading pressure

ρ density

ρ_{ads} adsorbed-phase density

ρ_{mc} adsorbed-phase density corresponding to the maximum adsorption capacity

ρ_s density of atoms or molecules on the surface

σ diameter of a molecule; the expected experimental uncertainty

θ fractional coverage in the Langmuir adsorption isotherm model

ω amount of gas adsorbed per unit mass of adsorbent

Subscripts

ads   the adsorbed amount within the equilibrium cell

b   bulk phase or the gas phase

He   properties obtained with the use of helium gas

i,j   component *i,j*

unads the un-adsorbed amount within the equilibrium cell

o   reference state

Superscripts

Abs   absolute adsorption

a   adsorbed phase

Gibbs Gibbs excess adsorption

s   solid phase

t   total

v   vapor phase

CHAPTER 1

INTRODUCTION

Coalbed methane is a proven gas reserve that needs to be produced effectively. Coalbeds can also sequester carbon dioxide (CO_2) for mitigation of CO_2 emissions, with or without the attendant goal of methane gas production. The potential for large-scale incremental methane recovery and carbon sequestration from coal is significant. A recent assessment (Stevens et al., 1998) estimates that U.S. coalseams can provide an incremental gas resource via enhanced coalbed methane (ECBM) of 150 Tcf, and have the capacity to sequester 90 Gt of CO_2. This capacity is sufficient to store about 15 year of CO_2 emissions. Importantly, much of the sequestration (25-30 Gt) can be performed at a profit, and almost all of it can be achieved at costs of less than $5/ton. Initial results from an enhance coalbed methane pilot project in the San Juan and nearby basins revealed that this technology may be profitable at prevailing wellhead natural gas prices of $0.06 to $0.07/m^3 ($1.75 to $2.00 /Mcf), with an estimated 8.5 Gt of CO_2 sequestration potential (Stevens et al., 1999).

The economic viability of this technology, however, is dependent on a number of technical factors including coal seam thickness, adsorption isotherm (gas adsorption capacity), reservoir pressure, permeability, porosity, water saturation, diffusion, etc. Among these contributing factors, the adsorption isotherm is the most critical. Specifically, accurate adsorption isotherms for CO_2, methane, nitrogen and their mixtures

1

are required to develop optimized processes for enhanced methane recovery.

Development of coalbed methane (CBM) gas production is impeded by the uncertainties in predicting the economics of the process. These uncertainties are largely attributed to incomplete understanding of the production process and lack of accurate prediction (simulation) methods for the phenomena involved including adsorption. Studies have established that the variability in the coal chemical and geometric structures affecting coal adsorption capacity may produce a 70% uncertainty in the predicted gas production rates (Wong et al., 1999). This is a clear indication that improved understanding of coal adsorption behavior using CO_2/N_2 injection is a critical knowledge gap that needs to be filled if production of the large (ECBM) gas resource (and carbon sequestration sink) that coals represent is to become an economic reality.

Theoretically-based models for adsorption behavior which elucidate the effect of its major contributing factors are needed to develop optimal strategies for ECBM recovery operations. A practically useful theory should be capable of (a) handling different adsorbate/adsorbent systems over the whole range of operation conditions and (b) predicting multicomponent adsorptions based on the data for single component adsorptions.

Among the theories widely used for adsorption are the Langmuir model, ideal adsorbed solution (IAS) theory (Myers and Prausnitz, 1965), heterogeneous ideal adsorbed solution (HIAS) (Myers, 1987), vacancy solution model (VSM) (Suwanayuen and Danner, 1980; Cochran et al., 1985), theory of volume filling micropores (TVFM) (Dubinin, 1966), two-dimensional equation of state model (2-D EOS) (Hoory and Prausnitz, 1967; Hall et al., 1994; Zhou et al, 1994; Sudibandriyo et al., 2003), and the

simplified local density (SLD) model (Chen et al., 1997; Fitzgerald et al., 2003). In general, all the models work well for low-pressure adsorption. However, for high-pressure adsorption, where the effect of adsorbed-phase density becomes significant, the models that do not include this effect are inadequate. The 2-D EOS has been reported to be more accurate than the Langmuir or IAS for high-pressure adsorption on Fruitland coal (De Gance, 1992; Hall et al., 1994). The accuracy of the model, however, depends on the 2-D EOS used, and the less satisfactory results for mixture adsorption reveal that further development of the EOS mixing rules is still needed. The SLD framework has many theoretical attributes that suit the modeling demands incumbent of coalbed methane reservoirs. However, the model suffers from additional computational complexity associated with integrations across the adsorbed-phase density profile [Fitzgerald et al., 2003].

In this study, we evaluate and further develop the Ono-Kondo (OK) lattice model to correlate high-pressure, supercritical adsorption isotherms encountered in CBM recovery and CO_2 sequestration. In general, the OK model lies between the SLD and 2-D EOS models in the practicality of its theory and its ease of computation and applicability. Specifically, the OK model:

1. Is based on a well-developed lattice theory

2. Describes monolayer and multilayer adsorption

3. Describes adsorption behavior based on the physical properties of the adsorbates and the accessible characterization of the adsorbent

Application of the model to pure-gas adsorption on activated carbon has been demonstrated by Aranovich and Donohue (1996) and Benard and Chahine (1997 and 2001). The results show that the model is in good agreement with the experimental data considered. However, the regressed model parameters obtained in their study were not suitable for other similar systems in the high-pressure, supercritical region. These results reveal that, even though the OK model has the potential to represent gas adsorption, the model parameters must be determined with care. This includes: (a) determination of the optimal number of layers used to describe the adsorbed phase for a specific system, (b) a general formulation that will produce reasonable estimates for each parameter, and (c) describing the parameters in terms of accessible adsorbate-adsorbent characteristics. These general formulations are important for predicting adsorption of systems beyond those where experimental data are available. Moreover, the temperature dependence of the parameters must also be evaluated.

The goal of the proposed study is to improve the OK model capability to represent and predict pure and multicomponent high-pressure adsorptions on carbon adsorbents in the near critical and supercritical regions. The specific objectives of this study are to:

1. Investigate multilayer adsorption on activated carbon and selected coals at near-critical and supercritical conditions

2. Delineate the temperature dependence of the OK model parameters

3. Present a generalized form of the OK model parameters in terms of accessible adsorbate and adsorbent characteristics

4. Extend the OK model to adsorption mixture modeling

Specifically, the resultant model should correlate within the experimental uncertainties the sorption of pure fluids, multicomponent mixtures, and individual components in a mixture on the adsorbents of interest and the sorption behavior over the ranges of temperature and pressure of interest.

If the model is successful in correlating adsorption data within the desired level of uncertainty, then the model is to be developed for its corresponding predictive ability. In this case, the model is expected, for a specified matrix, to provide accurate predictions for:

1. Sorption isotherm at one temperature from data at another temperature

2. Sorption behavior of various gases from data on one gas on the same matrix

3. The multicomponent gas sorption behavior of several gases from their pure-gas sorption data

Systematically-selected measurements were conducted to supplement existing data on high-pressure adsorption. These data were used to support the above specific objectives. The measurements were conducted for pure methane, nitrogen, and CO_2 and their mixture gas adsorption on an activated carbon and on selected coals at temperatures of 319 K and 328 K, and pressures to 13.8 MPa.

The format of this dissertation is as follows. Chapter 2 presents a review of fundamental adsorption theory and thermodynamics. In Chapter 3, relevant adsorption models are briefly reviewed, followed by a review on adsorbent characterization. Chapter 3 also presents a general overview of various experimental methods and procedures for adsorption measurements and some adsorption data sources. Chapter 4 describes the experimental method and procedures used in the OSU adsorption laboratory. An outline

for the Ono-Kondo (OK) lattice model is given in Chapter 5, including the proposed extension to mixtures. Chapter 6 is devoted to the OK modeling for pure-component adsorption and Chapter 7 presents the OK modeling for multicomponent adsorption. Chapter 8 presents conclusions and recommendations.

This study was part of an extensive research project dealing with high-pressure gas-adsorption modeling (Gasem, et al., 2003). As such, materials included in Chapters 3 and 4, as well as the adsorption database used in model development are a product of a collective effort involving the author, Zhejun Pan (2003), and James Fitzgerald (2003).

CHAPTER 2

FUNDAMENTALS OF ADSORPTION

Phenomenon of Adsorption

When a certain number of molecules strike continually upon a surface and stay there for a certain length of time before re-evaporating, the concentration of molecules at this surface will be higher than in the bulk of the gas (de Boer, 1968). This "condensed" phase is called the adsorbed phase and this phenomenon is called adsorption. The adsorption concept is widely applied in separation processes, gas storage, and also in coalbed methane recovery process. It also plays a fundamental role in reaction engineering.

The nature of the adsorbing surface is a determining factor in adsorption. The molecular characterization of solid surfaces is not yet fully developed; however, current knowledge allows a helpful description. To be useful as an adsorbent, a solid must present a large surface area per unit mass. This can only be achieved with porous solids such as activated carbon, zeolites and aluminas, which contain many cavities or pores with diameters as small as a fraction of a nanometer. Details on the solid surface characteristics is given in Chapter 3.

Depending upon the strength of the forces binding the adsorbate molecules to the surface, these adsorbate molecules may be mobile or fixed in position. In gas adsorption,

the number of molecules attracted to a solid surface depends on the conditions in the gas phase. For very low pressures, relatively few molecules are adsorbed, and only a fraction of the solid surface is covered. As the gas pressure increases at a given temperature, surface coverage increases. When the thickness of the adsorbed phase on solid surface is about equal to the adsorbed molecule diameter, the adsorption is said to form a monolayer. Further increase in pressure may result in multilayer adsorption. However, the complexity of the solid surface makes it possible for multilayer adsorption to occur on one part of a porous surface while vacant sites still remain on another part.

The three basic types of contributions to the adsorbate-adsorbent interactions are dispersion, repulsion, electrostatic, and chemical bond (Yang, 2003). Chemical bonds lead to chemical adsorption, which is not within the scope of this work. For physical adsorption, the adsorbate-adsorbent potential may be described by (Yang, 2003):

$$\Phi = \Phi_D + \Phi_R + \Phi_{Ind} + \Phi_{F\mu} + \Phi_{\dot{F}Q} \tag{2-1}$$

where Φ_D is dispersion energy, Φ_R is close-range repulsion energy, Φ_{Ind} is induction energy (interaction between electric field and an induced dipole), $\Phi_{F\mu}$ is interaction between electric field (F) and a permanent dipole (μ), $\Phi_{\dot{F}Q}$ is interaction between field gradient ($\dot{F}$) and a quadrupole moment Q.

Fundamental Equations for Adsorption Equilibrium

Although many adsorption theories are available in the literature, the thermodynamic framework is independent of any particular theoretical or empirical description of the adsorption behavior. For adsorption in microporous adsorbents, we can use the familiar framework of solution thermodynamics, with the distinction that the

solvent is a solid. The starting point is the fundamental differential equation for the energy of microporous adsorbent containing n gaseous adsorbate (Callen, 1985):

$$dU = TdS - PdV + \sum_{i=1}^{n} \mu_i dN_i + \mu dm$$

(2-1)

The intensive variables for this system are the temperature, T, the pressure, P, the chemical potentials of the adsorbates, μ_i, and the chemical potential of the solid adsorbent, μ. The extensive variables are the internal energy, U, entropy, S, the amount of each adsorbate, N_i, and the mass of solid adsorbent, m. Equation (2-1) is written for the condensed phase (the solid phase plus the adsorbed phase).

This fundamental treatment is different from that which presents adsorption as a two-dimensional phenomenon (Pan, 2003).

For a system containing a constant mass m of adsorbent:

$$dU = TdS + \sum_{i=1}^{n} \mu_i dN_i$$

(2-2)

The PdV term vanishes because a constant V is assumed, and the differential equation governing the adsorbed phase can be written as (Myers, 2002):

$$dU^a = TdS^a + \sum_{i=1}^{n} \mu_i dN_i^{\,a}$$

(2-3)

The differential equation for the Gibbs free energy is:

$$dG^a = -S^a dT + \sum_{i=1}^{n} \mu_i dN_i^{\,a}$$

(2-4)

For a gas adsorption system shown in Figure.1, the total energy is given by

$$G^t = G^v + G^s + G^a$$

(2-5)

Differentiating Equation (2-5) results in:

$$dG^t = dG^v + dG^s + dG^a \qquad (2\text{-}6)$$
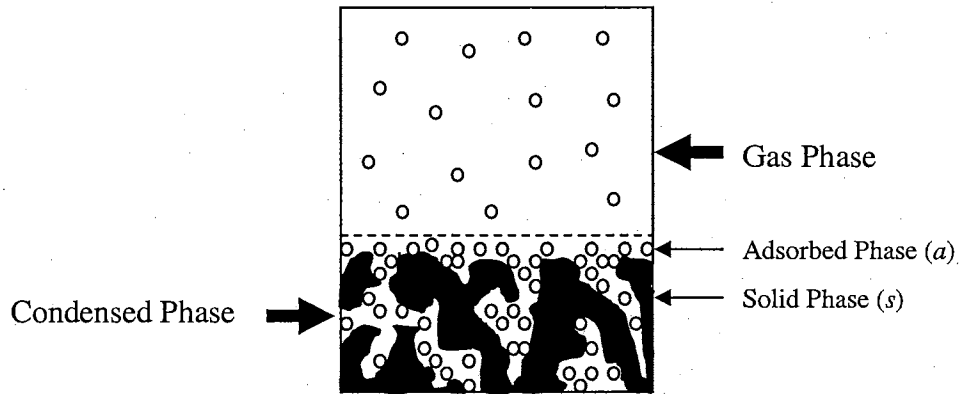
Figure1. Gas Adsorption on Solid Material at Equilibrium

For the bulk-gas phase (Sandler, 1998),

$$dG^v = -S^v dT^v + V^v dP^v + \sum \mu_i^v dN_i^v \qquad (2\text{-}7)$$

The pure solid is assumed to be incompressible so that $V^s = V^{s*}$, $U^s = U^{s*}$, and $S^s = S^{s*}$, where the asterisk refers to the clean adsorbent *in vacuo*. However, the pressure affect the enthalpy and free energy, thus $H^s = H^{s*} + PV^s$, $G^s = G^{s*} + PV^s$, and $\mu^s = \mu^{s*} + PV^s$. Further, the Gibbs free energy for the solid phase can be expressed as (Myers, 2002):

$$dG^s = d\mu^s = -S^s dT + V^s dP \qquad (2\text{-}8)$$

Combining Equations (2-4) through (2-8), and minimizing G^t at constant T and P under the constraint $N_i^t = N_i^a + N_i^v = $ constant, gives:

$$dG^t = \sum \mu_i^a dN_i^a + \sum \mu_i^v dN_i^v = \sum (\mu_i^a - \mu_i^v) dN_i^v = 0 \qquad (2\text{-}9)$$

Equation (2-9) shows that the equality of chemical potentials $\mu_i^a = \mu_i^v$ corresponds to the equilibrium state ($dG^t = 0$). Any adsorption model used always refers to these

thermodynamics criteria for equilibrium; albeit, the calculation of the adsorbed-phase chemical potentials may be different.

Degree of Freedom and Independent Variables

The number of degrees of freedom from the Gibbs phase rule is

$$F = n - \pi + 2 \tag{2-10}$$

where n is the number of chemical components present and π is the number of phases. Since the adsorbent is one of the components (Myers, 2002),

$$F = n - \pi + 3 = n - 2 + 3 = n + 1 \tag{2-11}$$

Thus for adsorption of one component, $n=1$ and

$$F = 1 + 1 = 2 \tag{2-12}$$

Two variables, e.g., T and P or T and ω (moles adsorbed), must be fixed independently to establish an equilibrium state.

Relationship between Gibbs and Absolute Adsorption

Adsorption data may be reported in terms of *Gibbs* or *absolute* adsorption. Calculation for the Gibbs and absolute adsorptions differs in the manner by which n_{unads} is calculated. The Gibbs adsorption calculation, which is inferred from experimental measurement, neglects the volume occupied by the adsorbed phase in calculating the amount of unadsorbed gas (i.e., the entire void volume, V_{void}, in the following expression, is viewed as being available for the case of an unadsorbed gas).

$$n_{unads}^{Gibbs} = \left(\frac{P V_{Void}}{ZRT} \right)_{cell} \tag{2-13}$$

This leads to a physical interpretation of Gibbs adsorption as the amount adsorbed *in excess* of the amount that would be present if the total void volume was filled with bulk gas.

If Equation (2-13) is modified to account for the volume of the adsorbed phase, then V_{void} in Equation (2-13) is replaced by the volume occupied by the equilibrium gas, $V_{gas} = V_{void} - V_{ads}$, and V_{ads} can be expressed as $V_{ads} = n_{ads}^{Abs} / \rho_{ads}$. Using these expressions, the following relationship can be derived between Gibbs and absolute adsorption in terms of the phase densities:

$$n_{ads}^{Abs} = n_{ads}^{Gibbs} \left(\frac{\rho_{ads}}{\rho_{ads} - \rho_{gas}} \right) \tag{2-14}$$

or $\quad n_{ads}^{Abs} = n_{ads}^{Gibbs} + V_{ads}\rho_{gas}$ (2-15)

where ρ is the density of the specified phase. Equation (2-15) shows that the absolute adsorption is always greater that the Gibbs adsorption. At low pressures (thus, low values of ρ_{gas}), the correction from Gibbs to absolute adsorption is negligible, but at higher pressures it becomes very significant.

An important consideration in the calculation of the absolute adsorption is that it requires knowledge of the adsorbed phase density, ρ_{ads} or V_{ads}, which is not readily accessible by experimental measurement. Thus, estimates of ρ_{ads} or V_{ads} must be employed. Explanation of the estimates is given in the experimental section (Chapter 4).

Types of Adsorption

The amount of adsorption is decided by the interactions among the gas molecules and the surface; thus, the nature of the various adsorbent and adsorbate will lead to different adsorption behavior. For example, the characteristic of the adsorbent, whether it is porous or not, and/or the conditions of the adsorbate, whether it is sub-critical or super-critical, will affect the shape of the adsorption isotherms. For absolute adsorption, five types of adsorption isotherms are shown in Figure 2 (Brunauer, 1940). Type I is the Langmuir type, roughly characterized by a monotonic approach to a limiting adsorption that presumably corresponds to a complete monolayer. Type II is very common in the case of physical adsorption with multilayer formation. Type III is relatively rare and seems to be characterized by a heat of adsorption equal to or less than the heat of liquefaction of the adsorbate. Type IV and V are considered to reflect capillary condensation phenomena and may show hysteresis effects.
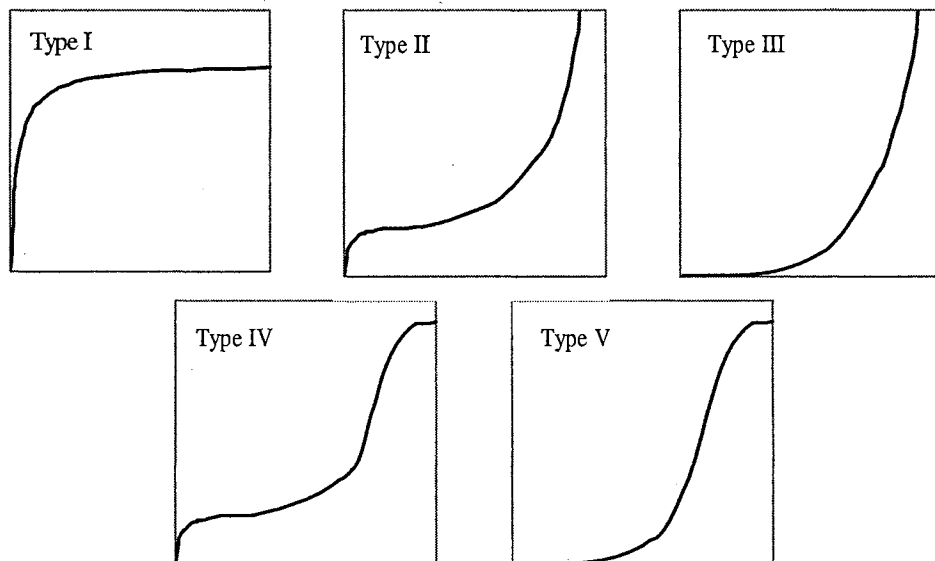
Figure 2. Five Types of Adsorption Isotherms

CHAPTER 3

LITERATURE REVIEW

Adsorption Models

Numerous theories and models have been developed to correlate pure adsorption data and to predict gas mixture adsorption. Among them are the extended Langmuir model, ideal adsorbed solution (IAS) theory, heterogeneous ideal adsorbed solution (HIAS), vacancy solution model (VSM), theory of volume filling micropores (TVFM), 2-D equations of state, simplified local density (SLD) model, and Ono-Kondo (OK) lattice model. In this chapter, a number of relevant adsorption models are reviewed briefly, followed by a review for various carbon adsorbents.

Langmuir Model

The most basic theory in adsorption is the Langmuir theory (1918). This theory describes the monolayer surface adsorption on an ideal surface. As depicted in Figure 3, an ideal surface means that the energy fluctuations, E, on the surface are periodic with the same magnitude, and the magnitude of this fluctuation is larger than the thermal energy of a molecule, kT; hence, the trough of the energy fluctuation is acting as the adsorption site. If the distance between the two neighboring troughs is much larger than the diameter of the adsorbate molecule, the adsorption process is called localized and each adsorbate molecule will occupy only one site.
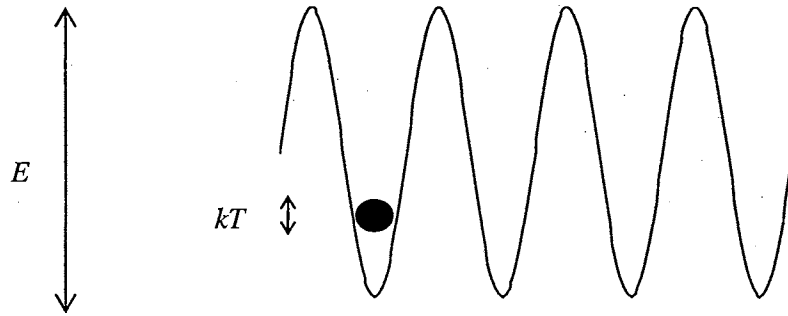
Figure 3. Surface Energy Fluctuation

Although the Langmuir model can be derived from the equilibrium thermodynamic point of view, the best way to describe this model is by using kinetic theory.

When a molecule hits the surface, the molecule might be adsorbed or reflected, as shown in Figure 4. If a molecule hits a site that is already occupied by a molecule, the molecule will be reflected. Thus, the adsorption rate will be proportional to the fraction of empty sites. After a certain time, this adsorbed molecule may then evaporate. The rate of evaporation therefore depends on the occupied sites. Equating the rates of adsorption and desorption (evaporation), we can obtain the Langmuir isotherm written in terms of fractional loading:

$$\theta = \frac{\omega}{L} = \frac{bP}{1+bP} \quad or \quad bP = \frac{\theta}{1-\theta} \tag{3-1}$$

This equation will follow Henry's law at low pressure: $\theta = bP$, and for mixture adsorption, the Langmuir model takes the following form:

$$\omega_i = \frac{L_i(T)b_i(T)Py_i}{1+\sum_j b_j(T)Py_j} \tag{3-2}$$

The parameter b is called the affinity constant or the Langmuir constant. It is a measure of how strongly an adsorbate molecule is attached onto a surface. This parameter is related to the heat of adsorption, Q, as shown in the following expression:

$$b = b_o \exp(\frac{Q}{RT})$$

(3-3)
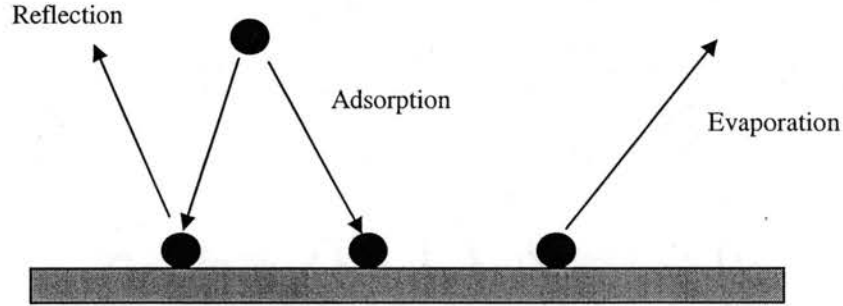
Figure 4. Schematic Diagram for the Langmuir Adsorption Mechanism

where the pre exponential factor b_o is also temperature dependent,

$$b_o = \frac{\alpha}{k_{d\infty} \sqrt{2\pi MRT}}$$

(3-4)

where α is a coefficient related to non-perfect sticking, and $k_{d\infty}$ is the rate desorption constant at infinite temperature.

The potential energy approach is used to explain how the heat of adsorption can be related to the intrinsic parameters of the system (solid + adsorbate). When one adsorbate molecule approaches the solid surface, it will be at an equilibrium distance (Figure 5). The potential energy of adsorbate-surface interaction can be approximated using the London equation (Masel, 1996):

$$\Phi(z) = \rho_s \pi C_{Lond} \left(\frac{0.2(r_e)^6}{z^9} - \frac{1}{z^3} \right)$$

(3-5)

16
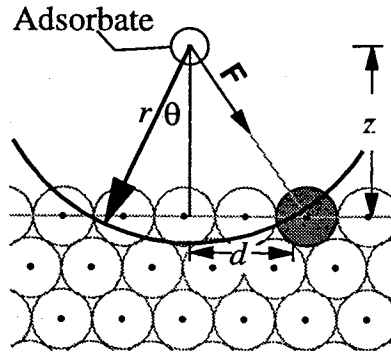
Figure 5. Adsorbate-Solid Surface Interaction (Masel, 1996)

Comparison of the calculated heat of adsorption, using this equation, with the measured values of some gases on metal and graphite surface show a good agreement between the calculated and measured values (Masel, 1996).

The Langmuir model can only represent Type I adsorption. However, further development of this theory by Brunauer, Emmett and Teller (1938) brought the capability of the model to represent other types of adsorption.

The BET (Brunauer, Emmett and Teller) Model

The Langmuir model is for monolayer coverage. However, in the adsorption of sub-critical adsorbates, molecules are adsorbed onto the solid surface in a layering process, and when the pressure is sufficiently high multiple layers are formed. The BET theory was first developed by Brunauer et al., in 1938, which yielded the following model:

$$\frac{\omega}{L} = \frac{CP}{(P_s - P)[1 + (C-1)(P/P_s)]}$$
(3-6)

The assumptions made in developing the BET model are:

1. The surface is homogeneous; the adsorption energy is constant over all sites.

2. Adsorption on a surface is localized; the adsorbed atoms or molecules are adsorbed at definite, localized sites.

3. Each site accommodates only one molecule or atom.

4. The number of layers is infinite.

The first three assumptions are the same as the assumptions made in Langmuir model.

The BET model can represent the adsorption isotherms from Types I to III by adjusting the parameters L and C in Equation (3-6). A further modification of the BET model was capable of representing Type IV and Type V adsorption (Brunauer et al., 1940).

The BET model is widely used to determine the surface area of an adsorbent using measured nitrogen adsorption at 77K.

Ideal Adsorbed Solution (IAS) Theory

The ideal adsorbed solution (IAS) theory was introduced first by Myers and Prausnitz in 1965. The IAS is an adsorption analog to Raoult's Law for vapor-liquid equilibria. The equilibrium condition for the adsorbed phase and the gas phase is given by:

$$y_i P = P_{s,i}(\pi)x_i \tag{3-7}$$

$P_{s,i}(\pi)$ is the equilibrium gas-phase pressure corresponding to the solution temperature and to the solution spreading pressure, π, for the adsorption of pure component i. The spreading pressure is defined as the difference in surface tension between a clean surface and a surface covered with (monomolecular) adsorbate (Yang, 2003).

In order to apply the above mixed-gas adsorption calculation, a pure-component isotherm model is needed. Any pure isotherm model can be utilized in the IAS

18

calculation. Valenzuela et al. (1988) used Langmuir isotherms for several adsorption systems while Zhou (1994) and Hall et al. (1994) used a 2-D Equation of State model.

Two-Dimensional Equation-of-State Models

The generalized 2-D EOS is analogous to the three-dimensional equation of state, by simply replacing pressure P with the spreading pressure, π, and volume, V, with the surface area, A.

The assumptions made in the 2-D EOS model are (DeGance, 1992):

1. The actual interfacial region is treated as an imaginary mathematical surface, with its own thermodynamic properties.

2. The adsorbent is thermodynamically inert.

3. The adsorbent possesses a temperature-invariant area, which is equally accessible to all adsorbates.

4. The surface is homotattic; i.e., it is made up of many homogeneous sub-regions.

5. The absolute adsorption definition is applied.

In 1967, Hoory and Prausnitz used the two-dimensional analogue of van der Waals' to model multicomponent adsorption. A more general two-dimensional analog was developed later, and can be written as follows (Hall et al., 1994 and Zhou et al., 1994):

$$\left[A\pi + \frac{\alpha\omega^2}{1 + u\beta\omega + w(\beta\omega)^2} \right]\left[1 - (\beta\omega)^m\right] = \omega RT \tag{3-8}$$

A is the specific surface area, π is the spreading pressure, ω is the specific amount adsorbed, and α and β are model parameters. The model coefficients u, w, and m must be specified to give various forms of the 2-D equations of state.

Equilibrium between an adsorbed phase and a vapor phase is required to calculate an adsorption isotherm. The following form may be applied for a pure component:

$$Ax_i\pi\hat{\phi}_i^a = k_i RT\hat{f}_i^g \tag{3-9}$$

To perform the modeling of multicomponent adsorption, Equation (3-8) combined with Equation (3-9) must be fitted to a single component isotherm data to obtain model parameter k, α, and β for each component. Then, for a given gas phase mole fraction at specific pressure and temperature, Equations (3-8) and (3-9) are solved simultaneously to obtain the amount of gas adsorbed, ω, for each component. In this case, the appropriate mixing rules must be applied to calculate parameters α and β for the mixture, the fugacity coefficient in the adsorbed phase, and the fugacity in the gas phase for each component.

The specific surface area, A, and the spreading pressure, π, are not required in the equilibrium calculations. The combined $A\pi$ can be calculated from Equation (3-8) and the following compressibility factor relation:

$$Z_a = \frac{A\pi}{RT\omega} \tag{3-10}$$

Theory of Volume Filling of Micropores

The theory of volume filling of micropores (TVFM) was extended from the Polanyi's potential theory developed by Dubinin in 1966. Dubinin assumed that, in micropores, the adsorbate fills the adsorption space via the mechanism of volume filling and hence does not form a discrete monolayer in the pores. The pure-component isotherms for the Dubinin-Astakhov (D-A) equation are given as follow:

$$V = V_s \exp\left\{ -\left(\frac{RT}{E_0} ln\frac{P_{s,i}}{P} \right)^n \right\} \tag{3-11}$$

V is the adsorption volume, V_s is the micropore saturation volume corresponding to the saturated pressure $P_{s,i}$, while n and E_0 are temperature-invariant fitting parameters. To extend TVFM into multicomponent adsorption, mixture equilibrium models such as IAS may be applied.

The Simplified Local Density (SLD) Model

The framework of the SLD model was based on the assumption that the chemical potential of a fluid inside a slit at a distance z from the solid surface is the result of fluid-fluid and fluid-solid interaction (Chen et al., 1997; Fitzgerald et al., 2003):

$$\mu(z) = \mu_{ff}(z) + \mu_{fs}(z) = \mu_{bulk} \tag{3-12}$$

where the chemical potential of a nonideal bulk fluid can be written in terms of fugacity:

$$\mu_{bulk} = \mu_o + RT \ln(f_{bulk} / f_o) \tag{3-13}$$

and the chemical potential due to fluid-fluid interactions at a distance z can be written as:

$$\mu_{ff}(z) = \mu_o + RT \ln(f_{ff}(z) / f_o) \tag{3-14}$$

where the subscript "$_o$" refers to a reference state. The fluid-solid chemical potential can be represented by:

$$\mu_{fs}(z) = N_A [\Phi(z) + \Phi(L - z)] \tag{3-15}$$

where L is the width of the slit.

From Equation (3-12) to (3-15), the following expression was obtained:

$$f_{ff}(z) = f_{bulk} \, exp\left[-\frac{\Phi(z) + \Phi(L - z)}{kT} \right] \tag{3-16}$$

Peng-Robinson EOS can be used to calculate the pure-component bulk fugacity as suggested by Chen (1997), while a similar expression was adopted for the fugacity of the adsorbed phase. To calculate the adsorbed-phase fugacity, changes of density and the

attractive term "*a*" with distance z must be taken into account. The equation for $a(z)$ depends on the ratio of the slit width L to the molecular diameter σ_{ff}.

The fluid-solid interaction potential is defined as:

$$\Phi(z) = 4\pi\rho_s \varepsilon_{fs} \sigma_{fs}^2 \left(\frac{\sigma_{fs}^{10}}{5(z')^{10}} - \frac{1}{2}\sum_{i=1}^{4} \frac{\sigma_{fs}^4}{(z'+(i-1)\sigma_{ss})} \right)$$

(3-17)

where ε_{fs} is the fluid-solid interaction energy parameter which can be fitted to the experimental data, and $\rho_s = 0.382$ atom/Å^2 for carbon atoms. The distance z' is defined as $z' = z + \sigma_{ss}/2$, where $\sigma_{ss} = 3.35$ Å for a carbon atom. σ_{ff} is taken from available literature and the distance parameter of the fluid-solid interaction σ_{fs} is calculated as $\sigma_{fs} = (\sigma_{ff} + \sigma_{ss})/2$.

Given the bulk fluid pressure and temperature, Equation (3-16) is used to solve for a "local density" $\rho(z)$. The Gibbs adsorption per unit mass of adsorbent is calculated as follows:

$$\Gamma = A \int_{\sigma_{ff}/2}^{L-\sigma_{ff}/2} [\rho(z) - \rho_b] dz$$

(3-18)

To calculate the Gibbs adsorption, the surface area per unit weight of the adsorbent, A, and the slit width, L, must be known or regressed from experimental data.

Application of the SLD model to the multicomponent adsorption is possible through one-fluid mixing rules (Fitzgerald et al., 2003).

The Lattice Theory of Adsorption

An adsorption model based on the lattice theory was proposed first by Ono and Kondo in 1960. Aranovich et al. (1996 and 1997) and Hocker et al. (1999) recently

developed a more general formalism of this model, in the context of adsorption of solutes in liquid solutions.

The assumptions of the OK Lattice model are:

1. The fluid system is composed of layers of lattice cells that contain fluid molecules and vacancies.

2. Molecular interactions exist only between a molecule and its nearest neighboring molecules.

3. Chemical equilibrium between the adsorbed layers and the bulk is given by the equality of the chemical potential in each layer and bulk.

Detail discussion of this model are given in Chapter 5.

Literature Review on Carbon Adsorbents

Understanding the structure of solid surfaces is very important for developing a better model for gas adsorption. In this study, we are only concerned with adsorption on the carbon adsorbents; therefore, the discussion is limited to the structure of activated carbon and coal.

Activated Carbon

Activated carbon is a powerful adsorbent because of its high ability to adsorb various substances both from gases and liquids. It is a processed carbon material with a highly developed porous structure and a large internal specific surface area. It consists mainly of carbon (87-97%) and also contains such elements as hydrogen, oxygen, sulfur and nitrogen, as well as various compounds either originating from the raw material used or generated during its production. The pore volume of activated carbon is usually greater

than 0.2 cm^3/g; sometimes it even exceeds 1.0 cm^3/g. The inner specific surface area is generally greater than 400 m^2/g but in many instances it is greater than 1000 m^2/g.

The principal properties of manufactured activated carbons depend on the type and properties of the raw material used. Most important raw materials are wood (sawdust), charcoal, peat, peat coke and coals. Coconut shells are also used to produce higher-surface area activated carbon. However, hard coals are currently still the greatest potential for the raw materials. About 60% of activated carbon production in the United States is based on hard coal.

When coal is used for the production of activated carbon, the following processing scheme is usually applied (Jankowska, 1991):

1. Grinding of the coal and spraying it with water

2. Briquettting of the ground product

3. Crushing the briquettes

4. Sieve fractionation

5. Oxidation to prevent swelling or baking

6. Carbonization

7. Activation

The last three are very important steps, since they have a major impact on the final properties of the produced activated carbon.

Oxidation is usually done in the temperature range of 150-350°C by passing an oxidizing gas, where the oxygen content varying within wide limits (1-50%) depending on the type of coal and the process used. The carbon is kept in contact with oxygen for about 19 hours in the case of a stationary layer, and for 30 minutes in the case of a

fluidized bed. Water, the excess of lower boiling fractions of the binding agent (binding agent such as tars are used to produce activated carbon granules) and some volatile matters are removed during this process. The mechanical strength of the carbonized granules increases due to a reduced baking of the oxidized coal and a resulting reduced swelling of the granules.

The carbonization process takes place in hot steam at 500-800°C. The granules acquire mechanical strength in this process, and due to evolution of volatile matter, the material becomes richer in carbon and an initial porous structure develops. The heat destroys the organic matter of the initial coal as well as the binding material. The initial porous structure of the coal significantly changes during the thermal treatment. The coal passes to the plastic state and its initial porous structure is destroyed. Further heating produces the evolution of volatile substances from the solidified plastic mass resulting in the formation of a branched system of pores. The structure of the carbonization product consists of a system of crystallites similar to those of graphite bonded by aliphatic-type bonds to yield a spatial polymer. The spaces between the neighboring crystallites constitute the primary porous structure of the carbon. The pores of the carbonized granules are often filled with decomposition products and are blocked with amorphous carbon (Jankowska, 1991).

The product of carbonization has a weakly developed porous structure, so without additional activation it cannot be used in practice as an adsorbent. The basic treatment of activating coal-based granules consists of their treatment with oxidizing gases (steam, carbon dioxide, oxygen) at elevated temperature (900-1000 °C). In the process of activation, carbon reacts with the oxidizing agent, and the resulting carbon dioxide

diffuses from the carbon surface. The amorphous carbon blocking the pore reacts in the initial oxidation step, and as a result the closed pores open up and new ones are formed. In further oxidation, the carbon of the elementary crystallites enters into reaction due to which the existing pores widen. The schematic of the activated carbon structure is illustrated in Figure 6. Each line in this figure represents a layer of hexagonal carbon rings arranged similar to the ones in a crystal of graphite. Despite their structural similarity, some deviations exist. Figure 7 shows a comparison between the structure of graphite and activated carbon. The difference lies mainly in the orientations of the respective layers. The interlayer distance in activated carbon ranges from 0.34 to 0.35 nm (compared to 0.335 nm in a crystal of graphite) (Jankowska, 1991). The number of layers in activated carbon is also more limited (usually up to five layers) compared to the layers in crystal graphite.
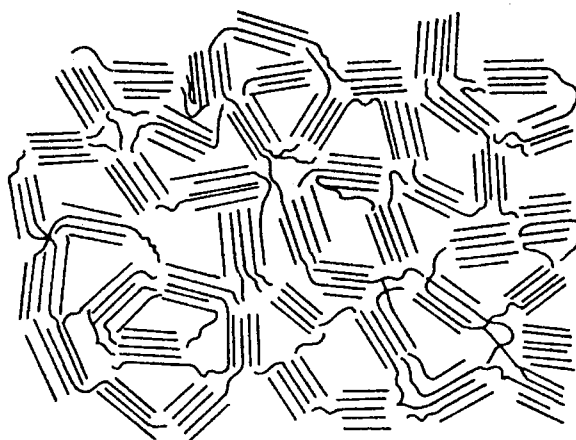
Figure 6. Schematic Illustration for the Structure of Activated Carbon (Jankowska, 1991)
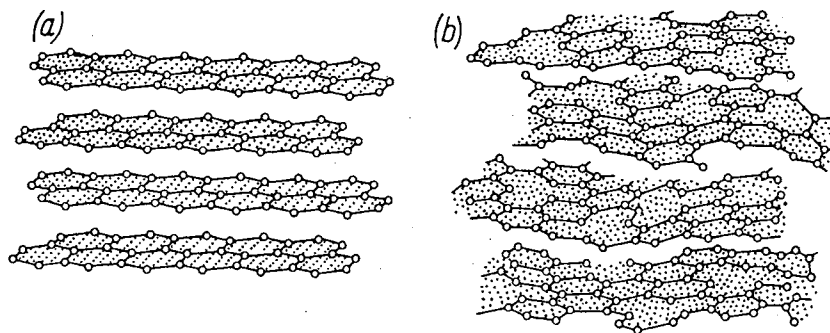
Figure 7. (a) Comparison of Three-Dimensional Crystal Graphite
and (b) the Activated Carbon Structure (Walker, 1969)

Another major difference between the two structures is the existence of surface

functional groups in the activated carbon surface. Surface functional groups can originate

from the starting material from which a particular activated carbon is produced. This is

especially so for activated carbons produced from raw materials relatively rich in oxygen,

such as wood, following their incomplete carbonization. In general, activated carbon

may contain some chemically bound oxygen and a small quantity of hydrogen combined

with surface carbon atoms either directly or through oxygen. Figure 8 illustrates a model

of a fragmented activated carbon surface with its functional groups.
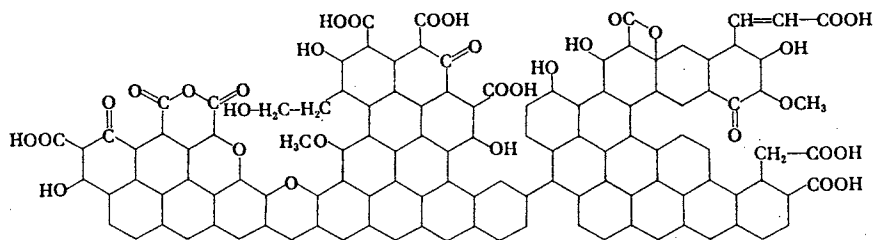
Figure 8. Model of a Fragment of Activated Carbon Surface (Jankowska, 1991)

Among the activated carbon properties, the pore distribution is the most important

one affecting its gas adsorption behavior. The volume of macropores, mesopores and

micropores in activated carbons are usually in the range 0.2-0.8 cm^3/g, 0.1-0.5 cm^3/g and 0.2-0.6 cm^3/g, respectively. The surface area of the micropores, however, might contribute up to 99% of the total surface area of the carbon (Kadlec et al., 1984).

Coal Structure

A thorough knowledge of the nature of the coal structure is a necessity for understanding the behavior of coal in CBM and sequestration processes. Physical and chemical structures of coal include (Meyers, 1982):

1. Lithotype region of 10^{-2}-10^{-1} m in size; mainly contains organic hydrocarbons which differ in density, reflectivity, strength, and volatiles content.

2. Lithotype boundaries of 10^{-3}-10^{-2} m in size; mainly contains non-hydrocarbon elemental composition and density at least 50% more than that of the lithotype.

3. Microscopic organic regions of 10^{-6}-10^{-4} m in size, from which the lithotypes are built; known as macerals whose origin is vegetable life.

4. Pores within the organic matrix, which are of varying sizes and shapes of 10^{-9}-10^{-5} m. These pores affect the strength, density, molecular transport properties and the adsorption capacity of the coal.

Figure 9a shows a scanning electron photomicrograph (SEM) of a maceral. Pore opening of 10^{-6}-10^{-5} m can be seen in this figure. Minerals and organic debris can often be seen lodged within the pores. Embedded water containing dissolved salts is also present. The organic matrix around the pores is composed of organic molecules linked and cross-linked to form polymers with possible repeating chemical structures. Minerals dispersed in the matrix can be obtained as filler material trapped within the polymeric system or pores (Figure 9b).
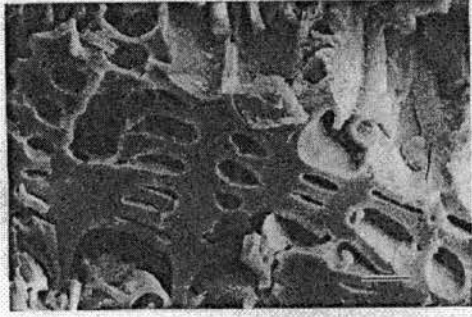
Figure 9a. Scanning of a Maceral
(Meyers, 1982)
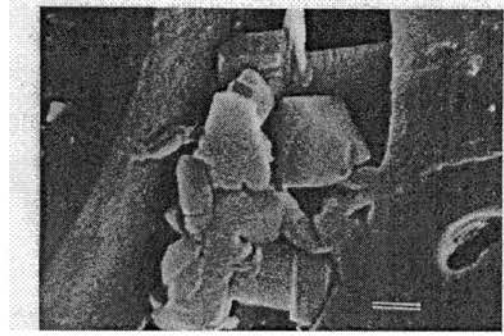
Figure 9b. Calcite Mineral Trapped in
Pores (Meyers, 1982)

The structure of coal at the molecular level of 10^{-9}-10^{-8} m consists of submicroscopic chemical species aggregated into crystalline and amorphous zones in both organic and mineral regions. This can be observed only by spectroscopic techniques and by analysis of chemical reactivity. From the information observed using X-ray diffraction for coals with carbon content of 65-95 %, the following features are observed (Ergun, 1959):

1. Carbon-carbon distances similar to those of graphite, with C-C bands about 0.14 nm in length.

2. Interlayer distances between lamellae similar to those of graphite 0.343-0.354 nm for coals with carbon content of 84-94%.

3. Poly-nuclear aromatic rings ranging from two to four condensed structures in coals with carbon content in the range 65-90%.

Figure 10 shows chemical functionality in the coals as obtained using NMR (Nuclear Magnetic Resonance). As shown in the figure, the coal contains mainly two regions, namely aromatic region and aliphatic region. In both regions a variety of the functional groups are also observed.
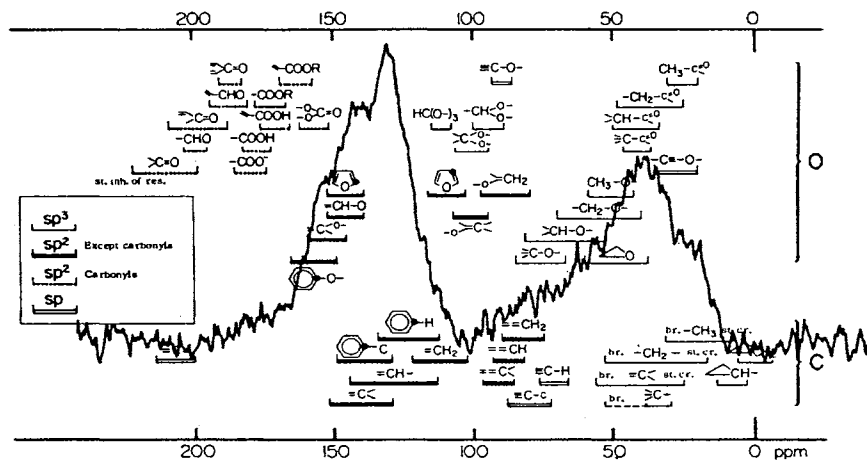
Figure 10. High-Resolution Solid-State Carbon Spectrum of a Whole Coal (Meyers, 1982)

Distribution of the surface area and pore volume in pores of different sizes is an important parameter for gas adsorption. Table 1 shows the pore volumes in different diameter range for the highest (anthracite) and the lowest (lignite) rank of coal (Gan et al., 1972). Pore volume contained in pores > 30 nm in diameter was estimated from mercury porosimetry. Pore volume contained in pores in the diameter range 1.2-30 nm was estimated from the adsorption branch of the nitrogen isotherms using the Cranston and Inkey method (1957). Pore volume contained in pores < 1.2 nm in diameter was calculated by subtracting the total open volume accessible to helium with the volume obtained from both mercury porosimetry and nitrogen adsorption. The results showed that the higher the coal rank, the higher the percent pore volume contained in the micropores (IUPAC defined macropores, mesopores and micropores as pores in the diameter range of > 50 nm, 2-50 nm and < 2nm, respectively). These results are also in good agreement with the pore size distribution obtained by Medek (1977) using the CO_2 adsorption isotherm in his method. The surface area distribution given in Table 1 indicates that the micropores play a major role for the adsorption of a small molecule.

30

The results also suggest that for the adsorption of molecules such as nitrogen ($\sigma_{N_2} = 0.38$ nm), methane $\sigma_{CH_4} = 0.376$ nm) and CO_2 $\sigma_{CO_2} = 0.394$ nm) on coal, a maximum of three adsorption layers is more likely.

Table 1. Gross Open-Pore Distribution in Coals

	Anthracite	Lignite
% Volume		
>30 nm	11.9	77.2
1.2-30 nm	13.1	3.5
<1.2 nm	75.0	19.3
% Area		
>30 nm	0.4	7.3
1.2-30 nm	1.1	1.2
<1.2 nm	98.5	91.5

Experimental Techniques

The aim of this section is to introduce the major experimental procedures for determination of adsorption isotherms. A general overview of the methods is important since the experimental data used in this study are obtained from various experimental methods and procedures. Most of the experimental apparatuses discussed in this chapter are designed for low-pressure gas adsorption measurements; albeit, they can be modified for high-pressure adsorption. The volumetric apparatus for high-pressure gas adsorption measurement used in our laboratory will be described separately in the next chapter.

Volumetric Gas Adsorption

This method calls for measuring the adsorbate gas pressure in a calibrated constant volume, at a set temperature. A simple volumetric gas adsorption apparatus is shown in Figure 11. The pressure and temperature of each dose of gas are measured and

31

the gas is allowed to enter the adsorption bulb. After adsorption equilibrium has been established, the amount adsorbed is calculated from the change in pressure. This technique can only be used to measure the gas adsorption point-by-point, which is referred to as a discontinuous procedure. In order to measure a complete isotherm, the addition of successive errors may result from the dosing device. Because of its simplicity, however, many researchers are still using this technique (Reich et al., 1980; Vermesse et al., 1996; Krooss et al., 2002).
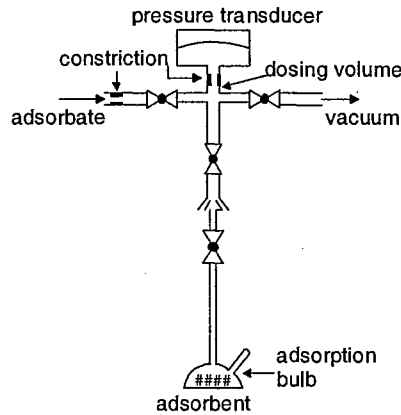
Figure 11. Simple Volumetric Gas Adsorption

Sometimes, the dosing device is replaced by an expansion cell, in which the amount of gas injected in the system is calculated after adsorption by expanding the gas in the adsorption cell into this expansion cell (Stacy et al., 1968; Talu and Zwiebel, 1986; Benard and Chahine, 1997; Zhou et al., 2000).

Figure 12 shows a volumetric gas adsorption with reservoir and a double pressure measurement. One pressure transducer is used to determine the amount of adsorbate remaining in the reservoir, while the second is used to determine the adsorption equilibrium pressure and also the amount of unadsorbed gas in the central cross and the

adsorption bulb. This arrangement gives an integrated measurement of the amount adsorbed and avoids the addition of successive errors resulting from a dosing device (Rouquerol et al., 1999). This type of arrangement was used by Lewis (1950), Payne (1968), Ritter (1987), Clarkson (1997) and many other researchers.
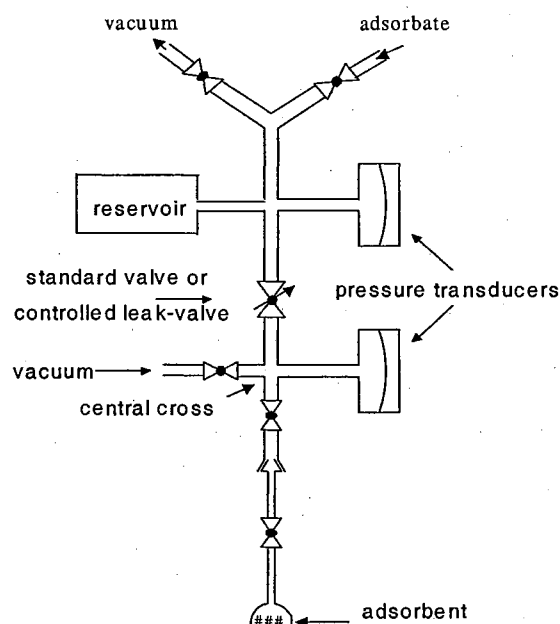
Figure 12. Volumetric Gas Adsorption with Reservoir
and Double Pressure Measurement

Continuous measurement is also possible with the help of a controlled leak-valve. In continuous measurement, the adsorbate is continuously fed on to the adsorbent, so that the point on the adsorption isotherm is continuously moving along the path of the isotherm. Here, the flow rate must be adjusted so that the system is always at thermodynamic equilibrium (or "quasi-equilibrium").

Another type of volumetric gas adsorption is the one used by Camp and Stanley (1991) and Webb (1992), as shown in Figure 13. Here they use two identical bulbs

(reference and adsorption) and two reservoirs. The two reservoirs are filled with the adsorbate gas at the same pressure, before the gas adsorption measurement begins. Then, the leak-valve on the reference side is opened to provide the desired rate of pressure increase. The leak-valve above the sample is automatically adjusted to cancel any unbalance of Transducer 2. The pressure difference recorded by Transducer 1 provides a direct measurement of the amount adsorbed at a certain equilibrium pressure (provided by Transducer 3). The differential assembly allows one to eliminate the dead volume correction, provided that the dead volume of the reference side is properly adjusted by means of the glass beads. However, this technique requires a new calibration for any new type of sample.
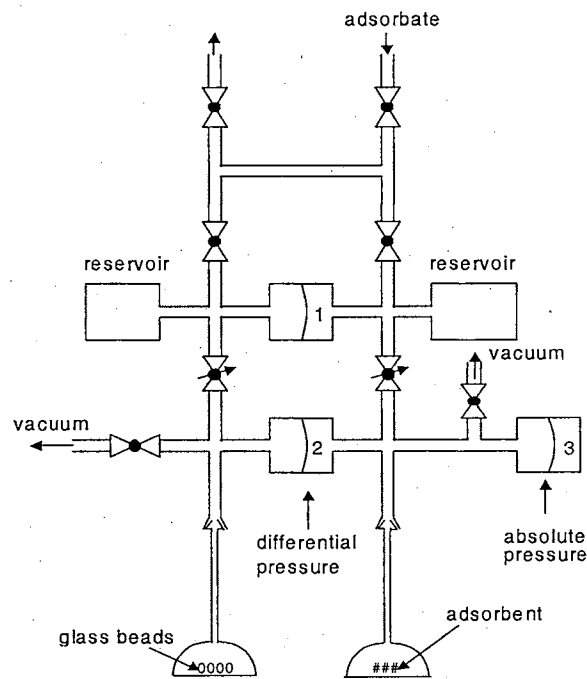
Figure 13. Differential Volumetric Gas Adsorption

Void Volume Determination: The void volume is needed for the volumetric adsorption techniques to express the adsorption data in terms of the surface excess (Gibbs excess adsorption). Two main methods are available for evaluating this void volume. The direct one (which is considered to be more accurate) is by measuring the volume accessible to a gas that is not adsorbed at the temperature and pressure of the void volume determination (usually helium gas is used). This method will be described in detail in the next chapter. The indirect void volume method calls for simply subtracting the volume of the empty bulb from the estimated volume of the sample. This volume can be obtained in two ways: from the theoretical density, or from pycnometric measurements (in liquid or gas) carried out separately.

Gas Flow Techniques

In this technique, a gas flowmeter is used to determine the amount of gas adsorbed. The flowmeter can be of a differential type (Nelsen and Eggertsen, 1958) or a thermal detector (Pieters and Gates, 1984). The thermal detector provides a signal, which depends on the heat capacity, thermal conductivity and mass flow of the gas. This method is usually referred to as a "mass" flow meter method although there is no direct measurement of mass. This gas flow techniques can also be used for continuous or discontinuous procedure.

Gas Adsorption Gravimetry

The amount adsorbed in the gravimetric technique is directly determined from the increase in mass measured by a balance. A simple gravimetric method uses a spring balance to determine the amount of gas adsorbed. However, in recent years spring balances have been largely superseded by electronic microbalances (Salem et al., 1998;

Vaart et al., 2000; Humayun and Tomasko, 2000; Beutekamp and Harting, 2002; Frére et al., 2002) as shown in Figure 14. A sensitive gravimetric technique is based on the effect of change of mass on the resonance frequency of a vibrating quartz crystal. In this case, the adsorbent must be firmly attached to the crystal (Krim and Watts, 1991).
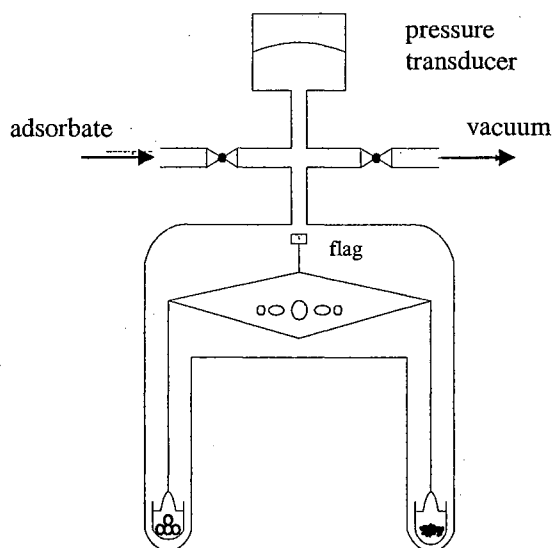
Figure 14. Gravimetric Measurement Apparatus

As in the volumetric methods, the gravimetric methods can also be used for continuous or discontinuous measurements. Also, it should be noted that the direct measurement of mass does not eliminate the problem of dead volume (or void volume) encountered in the volumetric technique. The adsorbent volume correction is now transformed into a buoyancy correction.

Due to the large volume of adsorption balances in the gravimetric technique, some difficulties may occur in measuring the pressure change accurately. In this case, a considerable amount of the adsorbent must be placed on the balance pan, which usually has only small space.

A gravimetric method can also be applied simultaneously with the volumetric method. Dreisbach in 1999 used this technique with a magnetic suspension balance.

Buoyancy Correction: The buoyancy correction needed in gravimetric adsorption has the same origin as the void volume determination in the volumetric measurement. It is due to the volume of the sample or, more precisely, to the adsorbed-phase volume and the resulting change in the apparent amount adsorbed. Both the direct and indirect methods can also be used to determine this buoyancy correction.

The following illustrates the procedure for determining the buoyancy correction. For the gravimetric measurements as shown by Figure 14, the recorded apparent mass change caused by the adsorption is:

$$\Delta m_T = m_{P,T} - m_{0,T} \tag{3-19}$$

where $m_{P,T}$ is the mass on the right side pan of the balance at the equilibrium pressure P and the adsorption temperature T, and $m_{0,T}$ denotes the mass at the same temperature but in a vacuum. The total buoyancy consists of the following individual terms:

$$m_i^B = M_g \rho_g V_i \tag{3-20}$$

where subscript i refers, respectively, to the right-hand pan (r), the left-hand pan (l), the adsorbent (s), the absolute adsorbed amount (a), and the tare weight (w) on the left side pan. M_g and ρ_g are the molar mass and the density of the adsorbate; and V is the volume of the above-mentioned elements. The buoyancy of the absolute amount adsorbed, m_a^B, cannot be determined, because the adsorbed-phase volume is unknown. This is the reason why the excess values are obtained by the gravimetric adsorption measurements. The true mass change (subscript tr) is given by:

$$\Delta m_{tr} = \Delta m_T + \Delta m^B + \Delta m_a^B ;$$

$$\Delta m^B = \Delta m_r^B + \Delta m_s^B - \Delta m_l^{B'} - \Delta m_w^B = M_g \rho_g \Delta V ; \qquad (3\text{-}21)$$

$$\Delta V = V_r + V_s - V_l - V_w$$

where Δm^B can be determined by helium measurements under the assumption that helium is not adsorbed at the measurement temperature. Therefore, the following relations exist for Δm^B:

$$\Delta m_{He}^B = M_{He} \rho_{He} \Delta V ;$$

$$\Delta m^B = M_g \rho_g \Delta m_{He}^B / (M_{He} \rho_{He}) ; \qquad (3\text{-}22)$$

$$\Delta m_{He}^B = -\Delta m_{T,He}$$

and the Gibbs excess adsorption can be calculated by the following formula:

$$n^{Gibbs} = (\Delta m_T + \Delta m^B) / (m_A M_g) \qquad (3\text{-}23)$$

where m_A is the amount of adsorbent.

Chromatographic Technique

The chromatographic technique for measuring adsorption involves a column packed with the adsorbent to separate the flowing species (Haydel and Kobayashi, 1967). The chromatographic analysis method is simple and fast in producing data but suffers from inherently larger errors (de Boer, 1968).

Literature Data

The data in the literature on gas adsorption primarily focus on two adsorbents: activated carbon and zeolites. Because the ultimate goal of this study is modeling of gas adsorption on coals, attention is paid mainly to the data on carbon adsorbents (i.e. activated carbon). Experimental data for high-pressure gas adsorption on coals are scarce

38

and complicated by (a) the difficulty in characterizing the coal matrix adequately, and (b) assessing the effect of water (found in essentially all coalbeds) on the resulting data (Joubert et al., 1973; Hall et al., 1994; Levy et al., 1997). Therefore, the gas adsorption data on activated carbon were used to evaluate the model prior to extending the model to include the effects of the complex adsorbent structure of coals and/or the presence of water.

The selected literature data for gas adsorption on activated carbon are documented in Tables 2 and 3. The data cover a wide range of temperature, pressure and most pure and mixture components applicable for coalbed methane studies. These data provide a useful source to evaluate adsorption models for the whole range of total loading. In addition, the data can also be used to evaluate models capability of predicting multicomponent adsorption based on pure-component adsorption data.

Table 2. Literature Data Used for Pure-Gas Adsorption Model Evaluation

System No.	Adsorbent	Adsorbent Surface area (m^2/g)	Adsorbate	Temp. Range (K)	Pressure Range (MPa)	Reference
1	AC, Columbia Grade L	1152	N_2	311 - 422	0.028 – 1.50	Ray (1950)
2	AC, Columbia Grade L	1152	CH_4	311 - 422	0.026 – 1.48	Ray (1950)
3	AC, Columbia Grade L	1152	C_2H_6	311 - 478	0.007 – 1.49	Ray (1950)
4	Charcoal	1157	CH_4	283 - 323	0.5 – 13.8	Payne (1968)
5	Charcoal	1157	C_3H_8	293 - 333	8×10^{-4} – 1.35	Payne (1968)
6	AC, BPL	988	CH_4	213 - 301	0.012 – 3.83	Reich (1980)
7	AC, BPL	988	C_2H_6	213 - 301	7×10^{-4} – 1.71	Reich (1980)
8	AC, BPL	988	C_2H_4	213 - 301	7×10^{-4} – 1.70	Reich (1980)
9	AC, BPL	988	CO_2	213 - 301	0.003 – 3.84	Reich (1980)
10	AC, PCB-Calgon Corp.	1150-1250	CH_4	296 - 480	0.27 – 6.69	Ritter (1987)
11	AC, PCB-Calgon Corp.	1150-1250	CO_2	296 - 480	0.11 – 3.67	Ritter (1987)
12	AC F30/470, Chemviron Carbon	993.5	CO_2	278 - 328	0.05 – 3.35	Berlier (1997)
13	AC Norit R1 Extra	1450	N_2	298	0.03 – 5.98	Dreisbach (1999)
14	AC Norit R1 Extra	1450	CH_4	298	0.01 – 5.75	Dreisbach (1999)
15	AC Norit R1 Extra	1450	CO_2	298	0.008 – 6.0	Dreisbach (1999)
16	AC from Coconut shell with KOH activation	3106 (CO_2 ads.)	CH_4	233 - 333	0.09 – 9.40	Zhou (2000)
17	AC -Calgon F-400	850	CO_2	303 to 318	0.02 – 20.2	Humayun (2000)
18	AC-Norit RB1	1100	CH_4	294 - 351	0.05 – 0.8	Vaart (2000)
19	AC-Norit RB1	1100	CO_2	294 - 348	0.05 – 0.8	Vaart (2000)
20	AC from Coconut shell with KOH activation	3106 (CO_2 ads.)	N_2	178 - 298	0.44 – 9.19	Zhou (2001)
21	AC F30/470, Chemviron Carbon	993.5	N_2	303 - 383	0.39 – 9.5	Frére (2002)

40

Table 2. Literature Data Used for Pure-Gas Adsorption Model Evaluation (Continued)

System No.	Adsorbent	Adsorbent Surface area (m^2/g)	Adsorbate	Temp. Range (K)	Pressure Range (MPa)	Reference
22	AC F30/470, Chemviron Carbon	993.5	CH_4	303 - 383	0.44 – 8.98	Frére (2002)
23	AC F30/470, Chemviron Carbon	993.5	C_3H_8	303 - 383	0.05 – 2.20	Frére (2002)
24	AC Norit R1	1262	N_2	298	0.03 – 14.56	Beutekamp (2002)
25	AC Norit R1	1262	CO_2	298	0.03 – 6.04	Beutekamp (2002)
26	Zeolite, Linde 13 X	525	N_2	298 - 348	0.35 – 8.23	Wakasugi (1981)
27	Zeolite, Linde 5A	~400	N_2	298 - 348	0.60 – 17.61	Wakasugi (1981)
28	Zeolite, Linde 5A	~400	CH_4	298 - 348	0.36 – 9. 18	Wakasugi (1981)
29	Zeolite, Linde 5A	~400	CO_2	298 - 348	0.03 – 11. 22	Wakasugi (1981)
30	Zeolite, Linde 5A	~400	C_2H_6	298 - 348	0.07 – 5.07	Wakasugi (1981)
31	H-Modernite, Norton Co: Type Z-900H	~300	CO_2	283 - 333	$3x10^{-4}$ – 0.29	Talu (1986)
32	H-Modernite, Norton Co: Type Z-900H	~300	H_2S	283 - 368	$4x10^{-4}$ – 0.10	Talu (1986)
33	H-Modernite, Norton Co: Type Z-900H	~300	C_3H_8	283 - 324	$2x10^{-5}$ – 0.21	Talu (1986)
34	Zeolite G5	430	CH_4	283 - 303	0.13 – 1.15	Berlier (1995)
35	Zeolite G5	430	C_2H_6	283 - 303	0.056 – 1.10	Berlier (1995)
36	Zeolite G5	430	C_2H_4	283 - 303	0.056 – 1.10	Berlier (1995)
37	Zeolite13 X	383	CH_4	298	0.15 – 15.02	Beutekamp (2002)
38	Zeolite13 X	383	C_2H_6	298	0.14 – 3.95	Beutekamp (2002)

41

Table 3. Literature Data Used for Mixture-Gas Adsorption Model Evaluation

System No.	Adsorbent	Adsorbent Surface area (m^2/g)	Adsorbate	Temp. Range (K)	Pressure Range (MPa)	Reference
39	AC Norit R1 Extra	1450	$N_2 + CH_4$	298	0.03 – 6.00	Dreisbach (1999)
40	AC Norit R1 Extra	1450	$CH_4 + CO_2$	298	0.03 – 6.00	Dreisbach (1999)
41	AC Norit R1 Extra	1450	$N_2 + CO_2$	298	0.03 – 6.00	Dreisbach (1999)
42	AC Norit R1 Extra	1450	$N_2 + CH_4 + CO_2$	298	0.03 – 6.00	Dreisbach (1999)
43	AC, BPL	988	$CH_4 + C_2H_6$	301	0.13 – 2.01	Reich (1980)
44	AC, BPL	988	$CH_4 + C_2H_4$	301	0.12 – 2.03	Reich (1980)
45	AC, BPL	988	$C_2H_6 + C_2H_4$	301	0.14 – 1.98	Reich (1980)
46	AC, BPL	988	$CH_4 + C_2H_6 + C_2H_4$	301	0.12 – 2.97	Reich (1980)

CHAPTER 4

EXPERIMENTAL METHOD FOR HIGH-PRESSURE ADSORPTION

Experimental Methods and Procedures

Adsorption Measurements

The experimental method used in the OSU adsorption laboratory is based on a mass balance principle, which employs precise measurements of pressures, volumes and temperatures. A brief description of the apparatus and procedures follows.

The experimental apparatus, shown schematically in Figure 15, has been used successfully in previous studies (Hall et al., 1994). The pump and cell sections of the apparatus are maintained in a constant temperature air bath at 318.2 K. The equilibrium cell has a volume of 110 cm^3 and is filled with the adsorbent to be studied. The cell is placed under vacuum prior to gas injection. The void volume V_{void} in the equilibrium cell is then determined by injected known quantities of helium from a calibrated injection pump (Ruska Pump). Since helium is not significantly adsorbed, the void volume can be determined from measured values of temperature, pressure and amount of helium injected into the cell. Several injections made into the cell at different pressures show consistency in the calculated void volume. Generally, the void volume calculated from sequential injections varies less than 0.3 cm^3 from the average value (of approximately 100 cm^3)

43
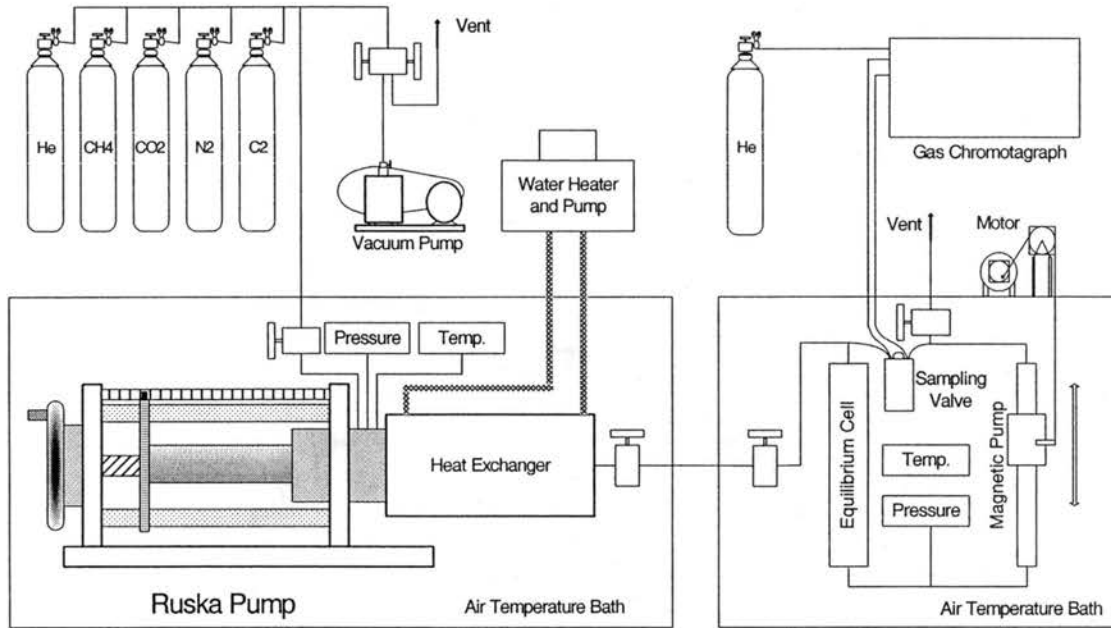
Figure 15. Schematic Diagram of the Experimental Apparatus

based on at least five injections. The mass-balance equation, expressed in volumetric terms, is

$$V_{void} = \frac{\left(\dfrac{P\Delta V}{ZT}\right)_{pump} - n_{sol,He}}{\left(\dfrac{P_2}{Z_2 T} - \dfrac{P_1}{Z_1 T}\right)_{cell}},$$ (4-1)

where ΔV is the volume injected from the pump, Z is the compressibility factor of helium, T is the temperature, P is the pressure, subscripts "cell" and "pump" refer to conditions in the cell and pump sections of the apparatus, respectively, and "1" and "2" refer to conditions in the cell before and after injection of gas from the pump, respectively. The number of moles of helium dissolved in the water, $n_{sol,He}$, is calculated from helium solubility in water data (Pray et al., 1952) and the value is zero for dry adsorbents. This void volume is used in subsequent measurements of adsorption, as follows.

The Gibbs adsorption (also known as the excess adsorption) can be calculated directly from experimental quantities. For pure-gas adsorption measurements, a known quantity, n_{inj}, of gas (e.g., methane) is injected from the pump section into the cell section. Some of the injected gas will be adsorbed, and the remainder, n_{unads}^{Gibbs}, will exist in the equilibrium bulk (gas) phase in the cell. A molar balance is used to calculate the amount adsorbed, n_{ads}^{Gibbs}, as

$$n_{ads}^{Gibbs} = n_{inj} - n_{unads}^{Gibbs} - n_{sol} \qquad (4\text{-}2)$$

The amount injected can be determined from pressure, temperature and volume measurements of the pump section:

$$n_{inj} = \left(\frac{P \Delta V}{ZRT} \right)_{pump} \qquad (4\text{-}3)$$

The amount of unadsorbed gas is calculated from conditions at equilibrium in the cell:

$$n_{unads}^{Gibbs} = \left(\frac{P V_{Void}}{ZRT} \right)_{cell} \qquad (4\text{-}4)$$

The number of moles of gas dissolved in the water, n_{sol}, is calculated from suitable gas solubility in water (Pray et al., 1952; King et al., 1992; Dhima et al., 1998). For nitrogen and methane, the amount of gas dissolved in the water is minimal. For CO_2, about 8 % of the gas might be dissolved in the water. In Equations (4-3) and (4-4), Z is the compressibility of the pure gas at the applicable conditions of temperature and pressure. The above steps are repeated at sequentially higher pressures to yield a complete adsorption isotherm. The amount adsorbed is usually presented as an intensive quantity (mmol adsorbed / g adsorbent or mmol/g) by dividing n_{ads}^{Gibbs} by the mass of adsorbent in the cell. Inspection of Equations (4-2) to (4-4) reveals that the amount

adsorbed may be calculated in a straightforward manner from experimental measurements of pressures, temperatures and volumes, coupled with independent knowledge of the gas compressibility factors, Z (from experimental data or a suitably accurate equation of state).

For mixed-gas adsorption measurements, a volumetrically prepared gas mixture of known composition (z_i) is injected; thus, the total amount of each component in the cell is known. A magnetic pump is used to circulate the fluid mixture to ensure that equilibrium is reached. The composition (y_i) of the gas phase in the cell at equilibrium is determined by chromatographic analysis. A pneumatically controlled sampling valve, contained in the air bath at cell temperature, sends a 20 μL sample to the gas chromatograph (GC) for analysis. The amount of each individual component adsorbed is calculated using component material balances; for component "i" in the mixture, the relations are

$$n_{ads(i)}^{Gibbs} = n_{inj(i)} - n_{unads(i)}^{Gibbs} - n_{sol(i)} = n_{inj}z_i - n_{unads}^{Gibbs}y_i \qquad (4\text{-}5)$$

where

$$n_{inj(i)} = \left(\frac{P\Delta V}{ZRT}\right)_{pump} z_i \qquad (4\text{-}6)$$

and Z is the compressibility of the *feed* gas mixture at pump conditions, and

$$n_{unads(i)}^{Gibbs} = \left(\frac{PV_{Void}}{ZRT}\right)_{cell} y_i \qquad (4\text{-}7)$$

where Z is the compressibility of the *equilibrium* gas mixture at cell conditions.

The number of moles of component i dissolved in the water, $n_{sol(i)}$, is calculated as in pure gas adsorption, using the partial pressure of each component.

Relationship between Gibbs and Absolute Adsorption

Adsorption data may also be reported in terms of *absolute* adsorption. Calculations for the Gibbs and absolute adsorption differ in the manner by which n_{unads} is calculated. The Gibbs adsorption calculation, described above, neglects the volume occupied by the adsorbed phase in calculating the amount of unadsorbed gas (i.e., in Equation (4-4), the entire void volume, V_{void}, is viewed as being available to the unadsorbed gas).

Following is a discussion to clarify the relationships between the Gibbs and absolute adsorption and to highlight the approximate nature of the calculated absolute adsorption. In addition, expressions are presented which facilitate calculation of the absolute component adsorption, $n_{ads(i)}^{Abs}$, and the adsorbed-phase mole fraction, x_i^{Abs}, in terms of the experimental Gibbs adsorption results.

Pure Component Adsorption: First, consider the various volumes that can be used to characterize the state existing in the equilibrium cell. Using a representation that envisions two distinct, homogeneous fluid phases (bulk gas and adsorbed phase), the total system volume (excluding water) V_{total} of the experimental apparatus is the sum of the volumes of solid adsorbent (V_{solid}), gas (V_{gas}), and adsorbed-phase (V_{ads}), as follows:

$$V_{total} = V_{solid} + V_{gas} + V_{ads} \qquad (4\text{-}8)$$

The void volume, having been determined by helium injection, is related to these quantities as follows:

$$V_{void} = V_{gas} + V_{ads} = V_{total} - V_{solid} \qquad (4\text{-}9)$$

Now, consider the amount of material adsorbed at equilibrium, which may be written in molar terms as follows:

$$n_{ads} = n_{total} - n_{unads} \tag{4-10}$$

The difference in the definitions of the Gibbs and total adsorption resides in the manner in which n_{unads} is related to the volume terms. As stated previously, in the Gibbs calculation, the volume occupied by the condensed phase is neglected in calculating n_{unads}, and the amount of unadsorbed gas is calculated using the entire void volume; thus, Equation (4-10) becomes, using Equation (4-9) for V_{void}:

$$n_{ads}^{Gibbs} = n_{total} - V_{void}\, \rho_{gas} \tag{4-11}$$

where ρ denotes density. In the calculation of the absolute adsorption, n_{unads} is determined using the volume actually available to the bulk gas phase (accounting for the reduction of volume accessible to the gas as a result of the volume occupied by the adsorbed phase):

$$n_{ads}^{Abs} = n_{total} - V_{gas}\, \rho_{gas} \tag{4-12}$$

By combining Equations (4-11) and (4-12) to eliminate n_{total}, the following relation between Gibbs and absolute adsorption is obtained:

$$n_{ads}^{Gibbs} = n_{ads}^{Abs} - V_{ads}\, \rho_{gas} \tag{4-13}$$

The volume of the adsorbed phase may be expressed in terms of the amount adsorbed and the density of the adsorbed phase as:

$$V_{ads} = n_{ads}^{Abs} / \rho_{ads} \tag{4-14}$$

48

Combining Equations (4-13) and (4-14) yields:

$$n_{ads}^{Gibbs} = V_{ads} \left(\rho_{ads} - \rho_{gas} \right)$$

(4-15)

Equation (4-15) clearly illustrates the physical interpretation of the Gibbs adsorption, namely, the amount adsorbed in excess of that which would be present if the adsorbed phase volume were filled with bulk gas. Combining Equations (4-14) and (4-15) leads to:

$$n_{ads}^{Abs} = n_{ads}^{Gibbs} \left(\frac{\rho_{ads}}{\rho_{ads} - \rho_{gas}} \right)$$

(4-16)

An important consideration in the calculation of the absolute adsorption is that it requires knowledge of the adsorbed phase density, ρ_{ads}, which is not readily accessible by experimental measurement. Thus, estimates of ρ_{ads} are usually employed. A commonly used approximation is the liquid density at the atmospheric pressure boiling point, as was done by Arri and Yee (1992).

Adsorption from Mixtures: For absolute adsorption, the component mole fractions in the adsorbed phase, x_i^{Abs}, may be calculated from the component Gibbs adsorptions; however, this requires some assumption regarding the density, ρ_{ads}, of the adsorbed phase mixture. In the following discussion, ρ_{ads} is approximated using the assumption of ideal mixing in the adsorbed phase, where the pure-component adsorbed-phase density estimates are used to calculate the mixture adsorbed-phase density. The component Gibbs adsorption (amount of component "i" in the adsorbed phase in excess of the amount that would be present if the bulk equilibrium gas mixture occupied the volume of the adsorbed phase) may be written using a component material balance as:

$$n_{ads(i)}^{Gibbs} = n_{ads}^{Abs} x_i^{Abs} - V_{ads} \rho_{gas} y_i = V_{ads} \left(\rho_{ads} x_i^{Abs} - \rho_{gas} y_i \right) \tag{4-17}$$

For convenience, we define a fractional component Gibbs adsorption, θ_i^{Gibbs}, as

$$\theta_i^{Gibbs} \equiv \frac{n_{ads(i)}^{Gibbs}}{n_{ads}^{Gibbs}} \tag{4-18}$$

(Note that, although Equation (4-18) has the appearance of a mole fraction, the Gibbs adsorption is an excess quantity, not a total quantity for a specified phase; thus θ, rather than x, is used to denote the quantity.)

Inserting this definition into Equation (4-17), we obtain:

$$n_{ads}^{Gibbs} \theta_i^{Gibbs} = n_{ads}^{Abs} \left(x_i^{Abs} - y_i \frac{\rho_{gas}}{\rho_{ads}} \right) \tag{4-19}$$

Combining Equation (4-16) with Equation (4-19),

$$x_i^{Abs} = \theta_i^{Gibbs} \left(1 - \frac{\rho_{gas}}{\rho_{ads}} \right) + y_i \left(\frac{\rho_{gas}}{\rho_{ads}} \right) \tag{4-20}$$

Equation (4-20) reveals that x_i^{Abs} and θ_i^{Gibbs} become identical in the limit of low pressure (where ρ_{gas} becomes small).

Inspection of Equation (4-20) reveals that all quantities on the right hand side can be obtained directly from experimental measurements except ρ_{ads}, for which some approximation must be made. For binary system, if ideal mixing is used to represent ρ_{ads} in terms of the pure component adsorbed-phase densities, we have:

$$\frac{1}{\rho_{ads}} = \frac{x_1^{Abs}}{\rho_{ads(1)}} + \frac{x_2^{Abs}}{\rho_{ads(2)}} \tag{4-21}$$

where the subscripts "1" and "2" refer to pure components. Then, Equation (4-20) may be written as

$$x_1^{Abs} = 1 - x_2^{Abs} = \frac{\theta_1^{Gibbs} \rho_{ads(2)} + \rho_{gas} \left(y_1 - \theta_1^{Gibbs}\right)\left(1 + \rho_{ads(2)}\right)}{\rho_{ads(2)} + \rho_{gas} \left(y_1 - \theta_1^{Gibbs}\right)\left(1 - \dfrac{\rho_{ads(2)}}{\rho_{ads(1)}}\right)} \qquad (4\text{-}22)$$

and the absolute component adsorption can be calculated as follows:

$$n_{ads(i)}^{Abs} = n_{abs}^{Abs} \, x_i^{Abs} \qquad (4\text{-}23)$$

with Equation (4-16) used to calculate the *total* mixture adsorption, n_{ads}^{Abs}, where the densities, ρ_{ads} and ρ_{gas}, refer to mixtures of compositions x_i^{Abs} and y_i, respectively.

Gas Compressibility Factors

As indicated by Equations (4-3) and (4-4), accurate gas-phase compressibility (Z) factors are required for methane, nitrogen and carbon dioxide and their mixtures to properly analyze the experimental data. The compressibility factors for pure methane, nitrogen, and CO_2 were determined from highly accurate equations of state (Angus et al., 1978 and 1979; Span and Wagner, 1996). For void volume determination, the helium compressibility factor is given by (Hall, 1993)

$$Z_{He} = 1 + \left(0.001471 - 0.000004779T + 0.00000000492T^2\right)/P \qquad (4\text{-}24)$$

where T is in Kelvins and P is in atmospheres. This expression is based on the experimental data from National Bureau of Standards Technical Note 631 for helium.

A careful evaluation of the current literature led us to conclude that an adequate predictive capability for mixture Z factors did not exist. Therefore, we elected to use available pure-fluid and binary mixture data to refit the Benedict-Webb-Rubin equation of state (BWR EOS) and improve its accuracy significantly. In general, the new BWR parameters yield deviations in the Z factors of less than 0.5%. This allowed us to address

our compressibility factor needs for binary adsorption mixtures. Details of the BWR equation expressions are given elsewhere (Pan, 2003).

Calibrations

Calibrations were performed routinely during the course of the experiments. The temperature measuring devices were calibrated against a Minco platinum resistance reference thermometer (see Appendix A), and the pressure transducers were calibrated against a Ruska deadweight tester with calibration traceable to the National Institute of Science and Technology (see Appendix B).

The gas chromatograph was calibrated against volumetrically prepared mixtures at the nominal feed-gas concentrations. The GC used for composition analysis is a Varian Chrompack CP-3800 with the helium carrier gas maintained at a 0.25-mL/s flow rate. A 10-ft Haysep D packed-column was used for CH_4/CO_2 and N_2/CO_2 systems, and a molecular sieve 13X column was used for the CH_4/N_2 system; column temperature was $80^\circ C$. A thermal conductivity detector was used for all of the binary systems studied; the bath temperature was set at $100^\circ C$. The chromatographic response factor, defined as $(A_2/A_1)(y_1/y_2)$ where A is the GC response area, was found to depend slightly on pressure; as such, the GC was calibrated for each nominal composition at pressure intervals of 1.4 MPa (see Appendix C for detail calibration).

The uncertainties in the experimentally measured quantities after calibrations were estimated as follows: temperatures, 0.1 K; pressures, 6.9 kPa; injected gas volumes, 0.02 cm^3; gas mixture compositions, 0.002 mole fraction.

52

The OSU Adsorption Database

Table 4 documents the OSU CBM gas adsorption database. The database contains the pure, binary, and ternary mixture adsorption measurements conducted at Oklahoma State University. Included in the database are details regarding the adsorbates, the adsorbent, and the corresponding temperature and pressure ranges for each system.

Pure-gas adsorption measurements are reported for methane, nitrogen, ethane, and carbon dioxide on **ten** solid matrices comprised of wet Fruitland coal (OSU #1 and OSU #2), wet Lower Basin Fruitland coal (OSU #3), wet / dry Illinois #6 coal, wet Tiffany coal, dry Beulah Zap coal, dry Wyodak coal, dry Upper Freeport coal, dry Pocahontas coal, and dry activated carbon.

Binary adsorption measurements are presented for mixtures of methane, nitrogen and CO_2 at a series of compositions on **four** different matrices: Fruitland coal, Illinois #6 coal, Tiffany coal, and activated carbon. Ternary measurements are also presented for methane/nitrogen/CO_2 mixtures on wet, mixed Tiffany coal and on dry activated carbon.

Tables 5 and 6 present the compositional analyses for the various solid matrices considered. The activated carbon used was Filtrasorb 400, 12x40 mesh, from Calgon Carbon company. The activated carbon was dried under vacuum at 431.5 K for two days before the adsorption measurements. The nitrogen BET surface area at 77 K has been reported by Humayun and Tomasko (2000) to be 850 m^2/g. The surface area value provided by the supplier, however, is 998 m^2/g.

Four different wet coals were prepared for adsorption measurements. The Fruitland coal is from the San Juan Basin; it is a medium volatile bituminous coal. This recently prepared sample (OSU #2) has a slightly different composition from the one

Table 4. The OSU Adsorption Database

System No.	Adsorbent	Adsorbate	Temp. (K)	Pressure Range (MPa)
47	Dry AC – F 400	N_2	318 & 328	0.7 – 13.7
48	Dry AC – F 400	CH_4	318 & 328	0.7 – 13.7
49	Dry AC – F 400	CO_2	318 & 328	0.7 – 13.7
50	Dry AC – F 400	C_2H_6	318	0.7 – 13.7
51	Dry AC – F 400	$N_2 + CH_4$	318	0.7 – 12.4
52	Dry AC – F 400	$CH_4 + CO_2$	318	0.7 – 12.4
53	Dry AC – F 400	$N_2 + CO_2$	318	0.7 – 12.4
54	Dry AC – F 400	$N_2 + CH_4 + CO_2$	318	0.7 – 12.4
55	Wet Fruitland Coal	N_2	319	0.7 – 12.4
56	Wet Fruitland Coal	CH_4	319	0.7 – 12.4
57	Wet Fruitland Coal	CO_2	319	0.7 – 12.4
58	Wet Fruitland Coal	$N_2 + CH_4$	319	0.7 – 12.4
59	Wet Fruitland Coal	$CH_4 + CO_2$	319	0.7 – 12.4
60	Wet Fruitland Coal	$N_2 + CO_2$	319	0.7 – 12.4
61	Wet Illinois #6 Coal	N_2	319	0.7 – 12.4
62	Wet Illinois #6 Coal	CH_4	319	0.7 – 12.4
63	Wet Illinois #6 Coal	CO_2	319	0.7 – 12.4
64	Wet Illinois #6 Coal	$N_2 + CH_4$	319	0.7 – 12.4
65	Wet Illinois #6 Coal	$CH_4 + CO_2$	319	0.7 – 12.4
66	Wet Illinois #6 Coal	$N_2 + CO_2$	319	0.7 – 12.4
67	Wet Tiffany Coal	N_2	328	0.7 – 13.7
68	Wet Tiffany Coal	CH_4	328	0.7 – 13.7
69	Wet Tiffany Coal	CO_2	328	0.7 – 13.7
70	Wet Tiffany Coal	$N_2 + CH_4$	328	0.7 – 13.7
71	Wet Tiffany Coal	$CH_4 + CO_2$	328	0.7 – 13.7
72	Wet Tiffany Coal	$N_2 + CO_2$	328	0.7 – 13.7
73	Wet Tiffany Coal	$N_2 + CH_4 + CO_2$	328	0.7 – 13.7
74	Wet LB Fruitland Coal	N_2	319	0.7 – 12.4
75	Wet LB Fruitland Coal	CH_4	319	0.7 – 12.4
76	Wet LB Fruitland Coal	CO_2	319	0.7 – 12.4
77	Dry Illinois #6 Coal	CO_2	328	0.7 – 13.7
78	Dry Beulah Zap Coal	CO_2	328	0.7 – 13.7
79	Dry Wyodak Coal	CO_2	328	0.7 – 13.7
80	Dry Upper Freeport Coal	CO_2	328	0.7 – 13.7
81	Dry Pocahontas Coal	CO_2	328	0.7 – 13.7

Table 5. Compositional Analysis of Solid Matrices Used in this Study

Analysis	Activated Carbon	Fruitland OSU #1	Fruitland OSU #2	Illinois #6	Lower Basin Fruitland OSU #3a	Lower Basin Fruitland OSU #3b	Tiffany Well #1	Tiffany Well #10
Ultimate*								
Carbon %	88.65	68.63	66.58	71.47	38.92	40.20	47.78	56.75
Hydrogen %	0.74	4.27	4.23	5.13	3.08	3.10	2.62	2.77
Oxygen %	3.01	0.89	5.08	9.85	3.75	2.87	6.19	5.16
Nitrogen %	0.40	1.57	1.47	1.46	0.87	0.89	0.92	1.02
Sulfur %	0.73	4.19	0.72	1.27	1.73	2.14	0.57	0.52
Ash %	6.46	20.45	21.92	10.81	51.66	50.81	49.71	47.74
Proximate*								
Vol. Matter %	3.68	20.2	20.33	30.61	20.01	14.00	15.48	15.35
Fixed Carbon %	89.86	59.35	57.75	55.90	28.33	35.19	34.82	36.91
Equil. Moisture Content (%)	35	2.2	2.2	3.9	4.0	4.0	3.8	3.7

* Huffman Laboratories, Inc., Golden, Colorado.

55

Table 6. Compositional Analysis of Coals from Argonne National Laboratory

Analysis*	Beulah Zap	Wyodak	Illinois #6	Upper Freeport	Pocahontas
Ultimate					
Carbon %	72.9	75.0	77.7	85.5	91.1
Hydrogen %	4.83	5.35	5.00	4.70	4.44
Oxygen %	20.3	18.0	13.5	7.5	2.5
Sulfur %	0.80	0.63	4.83	2.32	0.66
Ash %	9.7	8.8	15.5	13.2	4.8
Proximate					
Moisture %	32.2	28.1	8.0	1.1	0.7
Vol. Matter %	30.5	32.2	36.9	27. 1	18.5
Fixed Carbon %	30.7	33.0	40.9	58.7	76.1
Ash %	6.6	6.3	14.3	13.0	4.7

* Analyses were provided by the Argonne National Laboratory

used in previous measurements (OSU #1). The Lower Basin (LB) Fruitland coal is from the same coalbed seam as Fruitland coal, but it was taken from a different location. The Illinois #6 coal is a high volatile bituminous coal. Other coal samples are from BP Amoco Tiffany Injection Wells #1 and #10. The coal samples were ground to 200μm particles and moistened with water. This made the sample moisture content varies from 4 to 15% (by weight), which is higher than the equilibrium moisture content. Equilibrium moisture content was determined gravimetrically by exposing dry coal to 303.1 K air at 96-99% saturation.

In addition, five types of coal samples prepared by Argonne National Laboratory were used to study CO_2 adsorption on dry coals. The coals were dried under vacuum in an equilibrium cell at 353 K for 36 hours before being used in the adsorption measurements (Gasem et al., 2003).

Tables 7a through 7f present samples data from the **OSU Database** for the gas adsorption measurements conducted at OSU. The data are presented in terms of both Gibbs and absolute adsorption since absolute adsorption is the quantity most familiar to practitioners in CBM operations. Also for convenience, the data are reported both in SI and English engineering units. Complete database is available in our report prepared for the US Department of Energy (Gasem et al., 2003).

The database includes the expected experimental uncertainties for the adsorption measurements. The expected experimental uncertainty of the pure-gas adsorption data is about 3%. However, the expected uncertainties in the amount adsorbed for the mixture data vary with pressure and composition. In general, average uncertainties are below 5% for total adsorption; while, the individual-component uncertainties vary from 0.02 to 0.4 mmol/g depending on the mixture composition. Moreover, the expected uncertainties in the amount of individual-component adsorption are significantly higher for the less-adsorbed gas at lower molar feed concentrations (e.g., nitrogen in the 20/80 nitrogen/CO_2 system). Detail error propagation analysis is given in Appendix D.

Table 7. Sample Data from the OSU Database: (a). Nitrogen Adsorption on Activated Carbon at 318.2 K (Run 1)

SI Units

Cell T (K)	318.2
Moisture content (%)	0.0
Void volume (m^3)	0.0001003
Pump pressure (MPa)	6.9
Pump T (K)	307.8
Adsorbent mass (g)	47.1
Adsorbed phase density (g/cm^3)	0.725

Pressure (MPa)	Gibbs Ads (mmol/g)	Abs. Ads (mmol/g)	σ Gibbs (mmol/g)	σ Abs (mmol/g)
0.69	0.996	1.006	0.056	0.057
1.73	1.741	1.786	0.055	0.057
2.86	2.225	2.322	0.055	0.057
4.10	2.566	2.729	0.054	0.058
5.53	2.823	3.070	0.054	0.059
6.97	2.990	3.326	0.054	0.060
8.31	3.086	3.508	0.055	0.062
9.66	3.155	3.664	0.055	0.064
11.10	3.199	3.804	0.056	0.067
12.46	3.199	3.889	0.057	0.069
13.66	3.197	3.965	0.058	0.072

English Engineering Units

Cell T (°F)	113.1
Moisture content (%)	0.0
Void volume (ft^3)	0.003542
Pump pressure (psia)	997.4
Pump T (°F)	94.4
Adsorbent mass (lb)	0.1038

Pressure (psia)	Gibbs Ads (SCF/ton)	Abs. Ads (SCF/ton)	σ Gibbs (SCF/ton)	σ Abs (SCF/ton)
100.7	755.7	763.5	42.7	43.2
250.9	1321.7	1355.9	42.0	43.1
415.4	1688.4	1762.1	41.5	43.3
594.9	1947.5	2071.3	41.2	43.8
801.9	2142.4	2329.9	41.0	44.6
1011.0	2269.3	2524.6	41.2	45.8
1204.6	2342.6	2662.4	41.5	47.1
1401.0	2394.4	2781.3	41.9	48.7
1609.6	2427.9	2886.9	42.6	50.6
1807.8	2427.8	2952.1	43.3	52.7
1981.2	2426.7	3009.2	44.1	54.7

Nitrogen Adsorption on Activated Carbon at 318.2 K (Run 1)
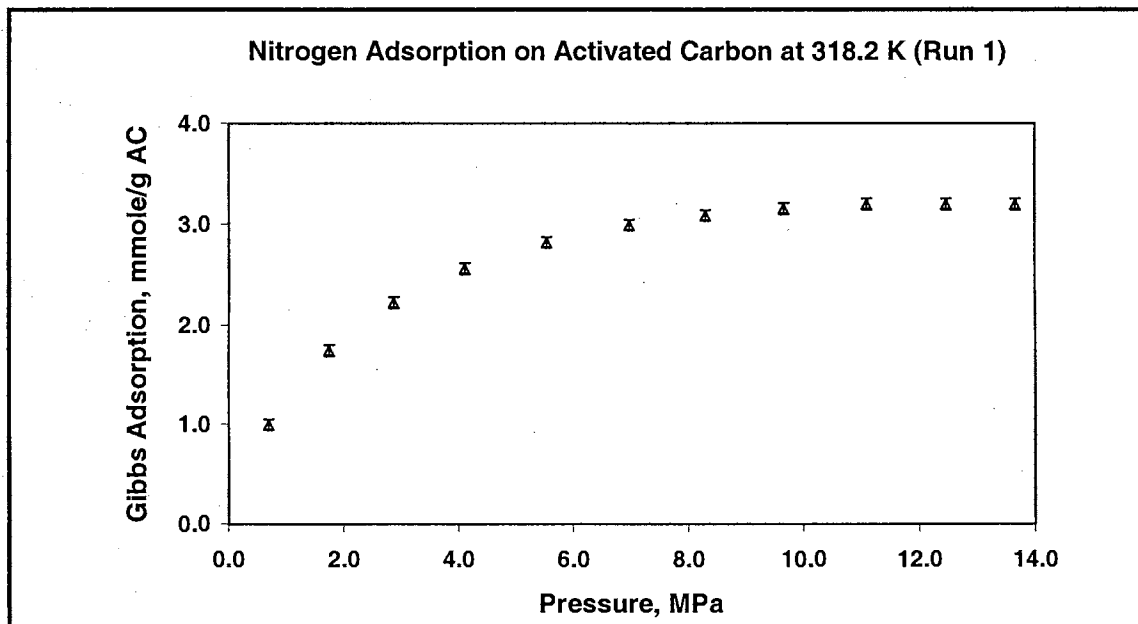
Table 7. Sample Data from the OSU Database: (b). Methane Adsorption on Activated Carbon at 318.2 K (Run 1)

SI Units

Cell T (K)	318.1
Moisture content (%)	0.0
Void volume (m^3)	0.0001003
Pump pressure (MPa)	7.2
Pump T (K)	307.8
Adsorbent mass (g)	47.1
Adsorbed phase density (g/cm^3)	0.374

Pressure (MPa)	Gibbs Ads (mmol/g)	Abs. Ads (mmol/g)	σ Gibbs (mmol/g)	σ Abs (mmol/g)
0.59	1.977	1.996	0.068	0.069
1.33	2.865	2.929	0.067	0.069
2.49	3.549	3.703	0.066	0.069
3.55	3.891	4.140	0.066	0.070
4.76	4.115	4.483	0.066	0.071
6.25	4.260	4.784	0.066	0.074
7.66	4.294	4.974	0.066	0.076
8.99	4.288	5.119	0.066	0.079
10.36	4.250	5.243	0.067	0.083
11.85	4.165	5.333	0.052	0.066
13.21	4.079	5.409	0.054	0.072

English Engineering Units

Cell T ($^{\circ}$F)	113.0
Moisture content (%)	0.0
Void volume (ft^3)	0.003542
Pump pressure (psia)	1047.3
Pump T ($^{\circ}$F)	94.4
Adsorbent mass (lb)	0.1038

Pressure (psia)	Gibbs Ads (SCF/ton)	Abs. Ads (SCF/ton)	σ Gibbs (SCF/ton)	σ Abs (SCF/ton)
85.0	1500.4	1514.9	51.9	52.4
192.9	2174.6	2223.2	51.1	52.3
361.4	2693.8	2810.9	50.5	52.6
514.7	2953.4	3142.5	50.1	53.3
689.7	3123.6	3402.2	49.8	54.3
906.2	3233.1	3631.0	49.8	55.9
1111.1	3259.4	3774.9	50.0	57.9
1303.6	3254.5	3885.4	50.4	60.1
1503.3	3225.5	3979.8	51.0	62.9
1718.6	3161.5	4047.8	39.4	50.5
1916.0	3096.1	4105.5	41.2	54.6

Methane Adsorption on Activated Carbon at 318.2 K (Run 1)
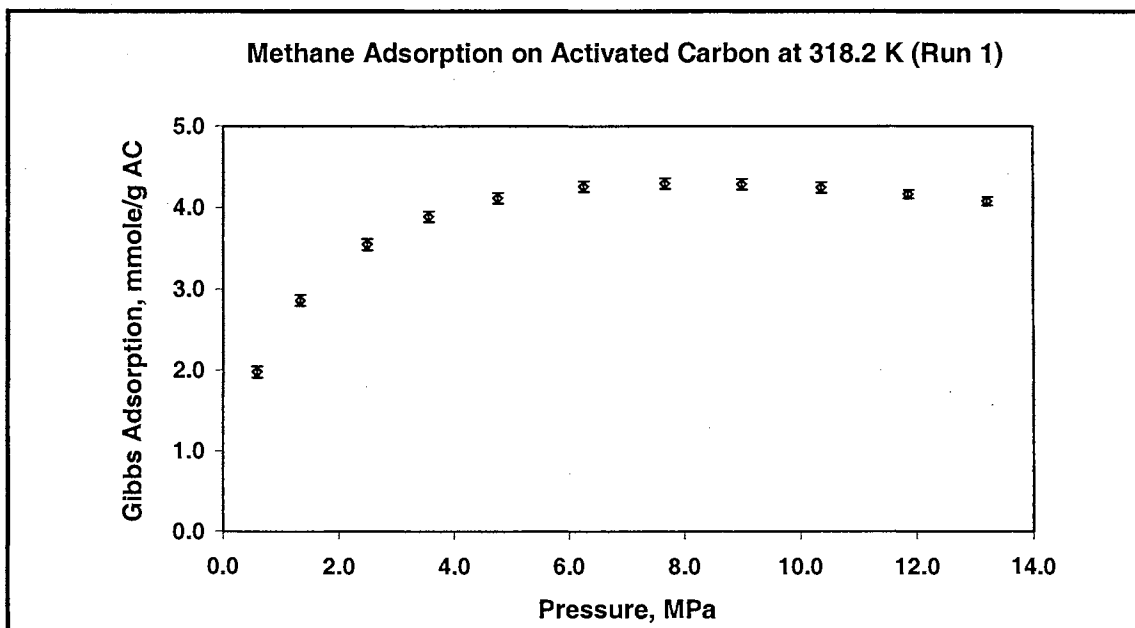
Table 7. Sample Data from the OSU Database: (c). Carbon Dioxide Adsorption on Activated Carbon at 318.2 K (Run 1)

SI Units

Cell T (K)	318.1
Moisture content (%)	0.0
Void volume (m³)	0.0001011
Pump pressure (MPa)	6.9
Pump T (K)	307.8
Adsorbent mass (g)	44.4
Adsorbed phase density (g/cm³)	1.027

Pressure (MPa)	Gibbs Ads (mmol/g)	Abs. Ads (mmol/g)	σ Gibbs (mmol/g)	σ Abs (mmol/g)
0.50	3.531	3.561	0.325	0.328
1.11	5.016	5.112	0.321	0.327
1.93	5.960	6.170	0.317	0.328
2.72	6.436	6.774	0.314	0.330
3.99	6.912	7.504	0.310	0.336
5.47	7.005	7.962	0.305	0.347
6.85	6.849	8.269	0.301	0.363
8.30	6.332	8.521	0.296	0.399
9.11	5.371	8.195	0.299	0.456
10.30	3.808	7.992	0.342	0.718
11.58	2.995	7.901	0.331	0.874
13.01	2.547	7.849	0.332	1.022

English Engineering Units

Cell T (°F)	113.0
Moisture content (%)	0.0
Void volume (ft³)	0.003570
Pump pressure (psia)	997.9
Pump T (°F)	94.4
Adsorbent mass (lb)	0.0979

Pressure (psia)	Gibbs Ads (SCF/ton)	Abs. Ads (SCF/ton)	σ Gibbs (SCF/ton)	σ Abs (SCF/ton)
72.9	2680.3	2702.8	246.9	248.9
160.4	3807.2	3880.0	243.3	248.0
279.5	4523.8	4682.8	240.3	248.8
394.1	4884.9	5141.2	238.2	250.7
579.3	5246.5	5695.8	235.0	255.1
793.7	5317.1	6043.1	231.6	263.2
993.8	5198.7	6276.2	228.3	275.6
1203.6	4806.3	6467.5	225.0	302.8
1321.9	4076.3	6219.9	227.0	346.4
1493.2	2890.1	6065.9	259.7	545.1
1678.9	2273.2	5996.5	251.6	663.7
1886.7	1933.2	5957.1	251.8	775.8

Carbon Dioxide Adsorption on Activated Carbon at 318.2 K (Run 1)
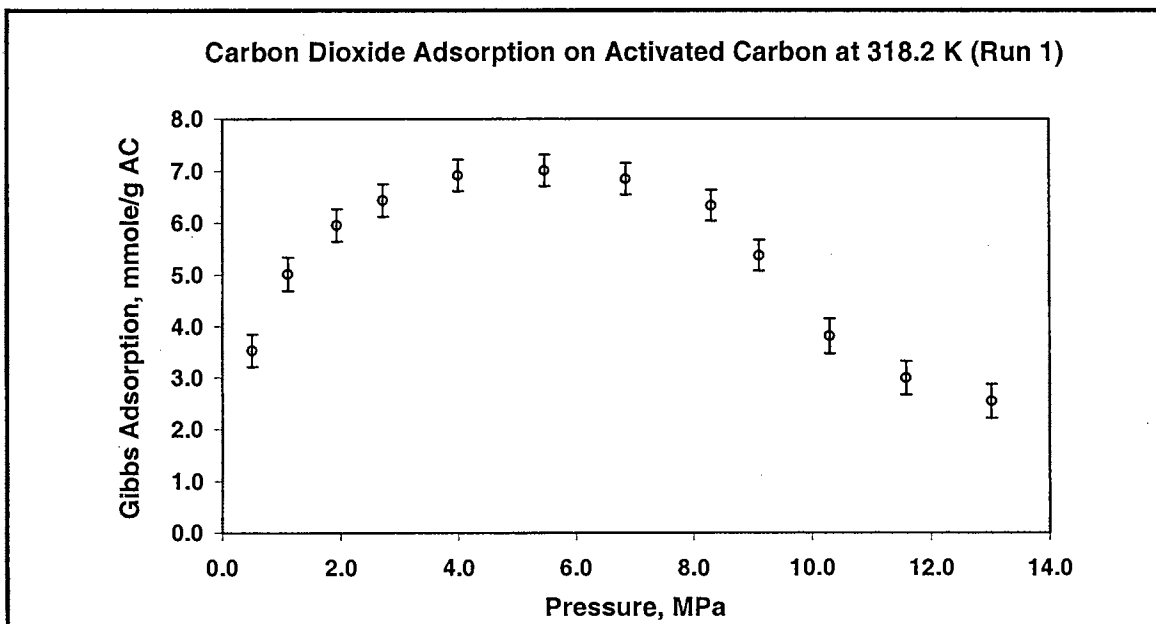
Table 7. Sample Data from the OSU Database: (d). Adsorption of a 60/40 Mole% Methane/Nitrogen Feed Mixture on Dry Activated Carbon at 318.2 K

SI Unit

Cell T (K)	318.2
Moisture content (%)	0.0
Void volume (m^3)	0.0001092
AC mass (g)	42.2
Pump T (K)	318.2

Feed Molar Composition	
Methane	0.600
Nitrogen	0.400

Pressure (MPa)	CH_4 Gas mole fraction	CH_4 Ads. (mmol/g)		N_2 Ads. (mmol/g)		Total Ads. (mmol/g)		Error in CH_4 Ads.		Error in N_2 Ads.		Error in Total Ads.	
		Gibbs	Absolute	Gibbs	Absolute	Gibbs	Absolute	σ Gibbs	σ Abs.	σ Gibbs	σ Abs.	σ Gibbs	σ Abs.
0.75	0.370	1.156	1.164	0.491	0.504	1.647	1.668	0.054	0.054	0.024	0.025	0.075	0.076
1.43	0.394	1.692	1.714	0.647	0.682	2.339	2.396	0.056	0.057	0.023	0.024	0.076	0.078
2.70	0.424	2.318	2.380	0.763	0.848	3.081	3.227	0.057	0.059	0.023	0.025	0.074	0.078
4.20	0.451	2.756	2.878	0.802	0.951	3.557	3.829	0.058	0.061	0.023	0.026	0.072	0.078
5.52	0.468	3.006	3.190	0.793	1.002	3.798	4.192	0.060	0.064	0.024	0.028	0.071	0.079
6.97	0.482	3.193	3.451	0.763	1.040	3.956	4.491	0.063	0.068	0.027	0.032	0.072	0.082
8.36	0.491	3.342	3.675	0.702	1.047	4.044	4.722	0.067	0.074	0.029	0.036	0.074	0.086
9.71	0.501	3.405	3.814	0.659	1.067	4.065	4.881	0.072	0.082	0.036	0.045	0.077	0.092
11.07	0.508	3.459	3.948	0.611	1.083	4.070	5.031	0.096	0.110	0.040	0.053	0.104	0.128
12.43	0.513	3.520	4.089	0.541	1.081	4.062	5.170	0.100	0.118	0.043	0.059	0.106	0.134

English Engineering Unit

Cell T (°F)	113.0
Void volume (ft^3)	0.003855
AC mass (lb)	0.0930
Pump T (°F)	113.0

Pressure (psia)	CH_4 Gas mole fraction	CH_4 Ads. (SCF/ton)		N_2 Ads. (SCF/ton)		Total Ads. (SCF/ton)		Error in CH_4 Ads.		Error in N_2 Ads.		Error in Total Ads.	
		Gibbs	Absolute	Gibbs	Absolute	Gibbs	Absolute	σ Gibbs	σ Abs.	σ Gibbs	σ Abs.	σ Gibbs	σ Abs.
108.8	0.370	877.5	883.4	372.4	382.3	1249.9	1265.6	40.6	40.9	18.2	18.6	57.2	57.9
207.9	0.394	1283.9	1301.0	491.0	517.3	1774.9	1818.3	42.5	43.1	17.7	18.6	57.8	59.2
391.9	0.424	1759.0	1806.1	579.5	643.5	2338.5	2449.5	43.6	44.8	17.1	18.6	56.4	59.1
609.6	0.451	2091.7	2184.8	608.3	721.8	2700.0	2906.6	44.3	46.4	17.5	19.8	54.9	59.1
800.0	0.468	2281.3	2420.9	601.7	760.7	2883.1	3181.6	45.3	48.2	18.4	21.4	54.2	59.8
1010.6	0.482	2423.6	2619.6	579.1	789.5	3002.7	3409.0	47.5	51.6	20.1	24.1	54.9	62.3
1212.3	0.491	2536.6	2789.1	532.6	794.8	3069.2	3583.8	50.5	56.0	22.2	27.4	56.1	65.6
1408.5	0.501	2584.6	2895.0	500.5	809.9	3085.1	3704.9	54.9	62.4	27.2	34.0	58.1	69.8
1605.1	0.508	2625.7	2996.3	463.7	821.9	3089.3	3818.3	72.6	83.8	30.4	40.2	78.8	97.4
1802.7	0.513	2671.9	3103.7	410.8	820.5	3082.7	3924.2	76.0	89.6	32.7	44.5	80.1	102.0

Table 7. Sample Data from the OSU Database: (e). Adsorption of a 60/40 Mole% Methane/Carbon Dioxide Feed Mixture on Dry Activated Carbon at 318.2 K

SI Unit

Cell T (K)	318.2
Moisture content (%)	0.0
Void volume (m³)	0.0001090
AC mass (g)	42.4
Pump T (K)	318.2

Feed Molar Composition	
Methane	0.600
Carbon Dioxide	0.400

Pressure (MPa)	CH₄ Gas mole fraction	CH₄ Ads. (mmol/g) Gibbs	CH₄ Ads. (mmol/g) Absolute	CO₂ Ads. (mmol/g) Gibbs	CO₂ Ads. (mmol/g) Absolute	Total Ads. (mmol/g) Gibbs	Total Ads. (mmol/g) Absolute	Error in CH₄ Ads. σ Gibbs	Error in CH₄ Ads. σ Abs.	Error in CO₂ Ads. σ Gibbs	Error in CO₂ Ads. σ Abs.	Error in Total Ads. σ Gibbs	Error in Total Ads. σ Abs.
0.68	0.777	1.475	1.500	1.182	1.189	2.657	2.689	0.083	0.085	0.067	0.067	0.150	0.151
1.42	0.775	1.938	2.009	1.705	1.726	3.642	3.735	0.080	0.083	0.071	0.072	0.150	0.154
2.77	0.766	2.240	2.418	2.275	2.329	4.515	4.748	0.074	0.080	0.075	0.077	0.145	0.153
4.17	0.755	2.306	2.614	2.667	2.766	4.972	5.380	0.069	0.077	0.078	0.082	0.140	0.152
5.56	0.744	2.267	2.717	2.949	3.103	5.216	5.820	0.066	0.078	0.082	0.087	0.137	0.153
6.95	0.727	2.215	2.810	3.099	3.323	5.315	6.132	0.065	0.081	0.086	0.093	0.136	0.157
8.30	0.720	2.063	2.810	3.252	3.543	5.315	6.353	0.072	0.093	0.097	0.108	0.137	0.164
9.66	0.707	1.946	2.848	3.310	3.683	5.256	6.531	0.091	0.126	0.135	0.154	0.197	0.245
11.04	0.700	1.788	2.859	3.377	3.838	5.165	6.697	0.091	0.135	0.143	0.167	0.198	0.257
12.41	0.688	1.674	2.908	3.344	3.903	5.017	6.811	0.093	0.146	0.149	0.180	0.200	0.272

English Engineering Unit

Void volume (ft³)	0.0038493
AC mass (lb)	0.0935
Pump T (°F)	113.0
Cell T (°F)	113.0

| Pressure (psia)	CH₄ Gas mole fraction	CH₄ Ads. (SCF/ton) Gibbs	CH₄ Ads. (SCF/ton) Absolute	CO₂ Ads. (SCF/ton) Gibbs	CO₂ Ads. (SCF/ton) Absolute	Total Ads. (SCF/ton) Gibbs	Total Ads. (SCF/ton) Absolute	Error in CH₄ Ads. σ Gibbs	Error in CH₄ Ads. σ Abs.	Error in CO₂ Ads. σ Gibbs	Error in CO₂ Ads. σ Abs.	Error in Total Ads. σ Gibbs	Error in Total Ads. σ Abs.
99.2	0.777	1119.8	1138.4	897.0	902.4	2016.8	2040.7	63.3	64.3	50.8	51.1	113.5	114.9
206.6	0.775	1470.6	1524.8	1294.0	1309.7	2764.6	2834.6	61.0	63.3	53.8	54.5	113.7	116.6
401.2	0.766	1700.1	1835.6	1726.7	1768.0	3426.7	3603.6	56.1	60.5	56.9	58.4	110.2	115.9
604.8	0.755	1749.9	1984.0	2024.0	2099.8	3773.9	4083.7	52.1	58.8	59.4	61.9	106.3	115.1
806.5	0.744	1720.9	2062.3	2238.0	2355.2	3958.9	4417.5	49.8	59.0	62.5	66.2	104.2	116.3
1007.5	0.727	1681.4	2132.5	2352.5	2521.9	4033.9	4654.4	49.4	61.4	65.0	70.5	103.5	119.5
1204.2	0.720	1565.9	2133.1	2468.0	2689.0	4033.9	4822.1	54.4	70.3	73.4	82.0	104.1	124.5
1400.6	0.707	1477.4	2161.9	2512.0	2795.1	3989.3	4957.0	68.7	95.6	102.7	116.5	149.9	186.3
1601.4	0.700	1356.9	2170.3	2563.4	2912.7	3920.3	5082.9	69.3	102.3	108.5	126.6	150.5	195.2
1800.4	0.688	1270.4	2207.2	2537.8	2962.3	3808.2	5169.5	70.9	111.0	112.8	136.2	152.0	206.5

Table 7. Sample Data from the OSU Database: (f). Adsorption of a 60/40 Mole% Nitrogen/Carbon Dioxide Feed Mixture on Dry Activated Carbon at 318.2 K

SI Unit

Cell T (K)	318.2
Moisture content (%)	0.0
Void volume (m^3)	0.0001044
AC mass (g)	51.1
Pump T (K)	318.2

Feed Molar Composition	
Nitrogen	0.581
Carbon Dioxide	0.419

Pressure	N_2 Gas	N_2 Ads. (mmol/g)		CO_2 Ads. (mmol/g)		Total Ads. (mmol/g)		Error in N_2 Ads.		Error in CO_2 Ads.		Error in Total Ads.	
(MPa)	mole fraction	Gibbs	Absolute	Gibbs	Absolute	Gibbs	Absolute	σ Gibbs	σ Abs.	σ Gibbs	σ Abs.	σ Gibbs	σ Abs.
0.90	0.888	0.808	0.831	0.949	0.952	1.757	1.783	0.055	0.056	0.064	0.064	0.115	0.116
1.54	0.880	1.042	1.095	1.365	1.373	2.407	2.468	0.053	0.056	0.068	0.068	0.116	0.119
2.74	0.872	1.234	1.363	1.957	1.976	3.191	3.339	0.049	0.053	0.073	0.073	0.112	0.118
4.26	0.866	1.265	1.511	2.543	2.581	3.808	4.092	0.046	0.053	0.078	0.080	0.109	0.117
5.56	0.853	1.222	1.578	2.926	2.987	4.148	4.564	0.046	0.054	0.081	0.084	0.105	0.116
6.96	0.843	1.121	1.603	3.278	3.368	4.399	4.970	0.047	0.058	0.087	0.091	0.104	0.118
8.31	0.831	1.011	1.618	3.552	3.675	4.563	5.293	0.066	0.080	0.103	0.111	0.106	0.123
9.67	0.817	0.897	1.631	3.766	3.930	4.663	5.562	0.073	0.096	0.143	0.154	0.157	0.187
11.12	0.808	0.740	1.616	3.988	4.197	4.728	5.813	0.077	0.104	0.151	0.165	0.156	0.192
12.54	0.795	0.603	1.615	4.137	4.397	4.740	6.012	0.080	0.111	0.157	0.175	0.156	0.198

English Engineering Unit

Cell T (°F)	113.0
Void volume (ft^3)	0.003688
AC mass (lb)	0.1127
Pump T (°F)	113.0

Pressure	N_2 Gas	N_2 Ads. (SCF/ton)		CO_2 Ads. (SCF/ton)		Total Ads. (SCF/ton)		Error in N_2 Ads.		Error in CO_2 Ads.		Error in Total Ads.	
(psia)	mole fraction	Gibbs	Absolute	Gibbs	Absolute	Gibbs	Absolute	σ Gibbs	σ Abs.	σ Gibbs	σ Abs.	σ Gibbs	σ Abs.
130.2	0.888	613.2	630.5	720.3	722.5	1333.5	1352.9	41.5	42.6	48.3	48.5	87.1	88.4
223.4	0.880	790.6	831.4	1036.2	1041.8	1826.8	1873.2	40.2	42.1	51.5	51.8	87.7	90.0
397.0	0.872	936.4	1034.3	1485.6	1499.9	2422.0	2534.2	37.1	40.5	55.1	55.8	85.4	89.3
617.2	0.866	960.3	1146.9	1930.0	1958.9	2890.3	3105.7	35.0	40.2	59.2	60.5	82.4	88.6
806.7	0.853	927.6	1197.4	2220.5	2266.9	3148.1	3464.3	34.7	41.2	61.8	63.9	79.9	87.9
1010.1	0.843	851.0	1216.6	2487.7	2556.0	3338.7	3772.5	35.9	44.0	66.0	69.1	79.1	89.4
1205.1	0.831	767.3	1227.9	2695.7	2789.6	3463.0	4017.4	50.2	61.1	78.1	84.2	80.2	93.1
1402.2	0.817	681.2	1238.2	2858.2	2983.0	3539.4	4221.2	55.4	72.7	108.5	116.7	119.0	142.0
1612.6	0.808	561.3	1226.5	3027.0	3185.5	3588.3	4412.0	58.5	78.7	114.3	125.0	118.4	145.7
1818.2	0.795	457.8	1225.6	3140.0	3337.5	3597.8	4563.1	61.0	84.3	119.1	132.5	118.5	150.4

CHAPTER 5

ONO-KONDO LATTICE MODEL FOR ADSORPTION

Lattice Model

An adsorption model based on the lattice theory was proposed first by Ono and Kondo in 1960. The more general formalism was recently developed further by Donohue and coworkers for the adsorption of solutes in liquid solutions (Aranovich et al., 1996 and 1997; Hocker et al., 1999). In the lattice model, the fluid system is assumed to be composed of layers of lattice cells that contain fluid molecules and vacancies. A configuration of molecules in a mixture fluid in its equilibrium state can be represented by a square lattice, which is shown in Figure 16. In this condition, the total number of lattice cell sites, $M = \sum_{i}^{n} N_i$, is constant. N_i is the particle numbers, including the empty cell sites. Here N_n represents the number of "holes" or empty cells present in the system. The shaded cells in Figure 16 are the primary nearest-neighbor cells around a cell filled with molecule j. Two more primary nearest-neighbor cells are on top of and under molecule j. These primary nearest-neighbor cells may be filled by other species i, or just an empty cell.

The configurational Helmholtz free energy for the system above, according to statistical thermodynamics, is defined as:

$$A = -kT \ln Q \qquad (5\text{-}1)$$
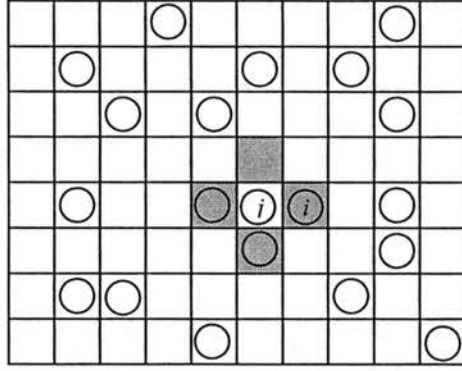
Figure 16. Fluid Mixture on a Square Lattice

with Q is the configurational partition function. A general form of this function for a mixture was derived by Hocker (1999):

$$Q = M! \prod_i^n \frac{e^{-(z_0/2)N_i\varepsilon_{ii}/kT}}{N_i!} \, exp\left[-\frac{z_0 M}{8k} \sum_i^n \sum_j^n \Delta_{ij} x_i x_j \int_0^{1/T} (\Psi_{ij} + \Psi_{ji}) d(1/T) \right] \quad (5\text{-}2)$$

which leads to the following expression for the free energy:

$$A = \frac{z_0}{2} \sum_i^n N_i \varepsilon_{ii} + kT \sum_i^n N_i \, ln \, x_i + \frac{z_0 MT}{8} \sum_i^n \sum_j^n \Delta_{ij} x_i x_j \int_0^{1/T} (\Psi_{ij} + \Psi_{ji}) d(1/T) \quad (5\text{-}3)$$

The lattice coordination number, z_0, represents the number of primary nearest-neighbor cells in the lattice system. The interaction energy between molecule i and j is expressed by ε_{ij}. Note that $z_0\Delta_{ij}/8$ is the interchange energy, i.e., the amount of energy that accompanies the exchange of molecule i (from a lattice completely filled with i's) with a molecule j (from a lattice completely filled with j), where $\Delta_{ij} \equiv 2\,\varepsilon_{ij} - (\varepsilon_{ii} + \varepsilon_{jj})$. The correlation coefficient, Ψ_{ij}, is the ratio of the probability for having a molecule i around an arbitrary molecule j, to the probability of molecule i occupies the lattice cell, $x_i = N_i/M$. Thus, this number represents the deviations of a non-random mixture from its random limit for which Ψ_{ij} is unity.

Molecules Adsorbed on a Surface

Figure 17 shows the configuration of the molecules adsorbed on a surface. To calculate the free energy of the molecules in the first adsorbed layer, we should include the contributions resulting from interactions between adsorbed molecules and the surface, and between adsorbed and bulk molecules. The contribution resulting from interactions between all the adsorbed molecules of the first layer on the surface can be written as:

$$A_{1st-s} = \sum_i^n N_i \, \varepsilon_{is} \tag{5-4}$$

where ε_{is} is the interaction energy between molecule i and the solid surface. The contribution resulting from interactions between the adsorbed molecules and the bulk molecules (or the second layer of the adsorbed molecules) is given by:

$$A_{1st-b} = \sum_i^n \sum_j^n N_i \, x_{j,2nd} \varepsilon_{ij} \tag{5-5}$$

Combining Equations (5-3), (5-4) and (5-5) results to the following expression for the configurational free energy of the adsorbed layer:

$$A_{1st} = \sum_i^n N_i \left(\tfrac{z_1}{2} \varepsilon_{ii} + \varepsilon_{is} \right) + \sum_i^n \sum_j^n N_i \, x_{j,2nd} \varepsilon_{ij} + kT \sum_i^n N_i \, ln\, x_i$$

$$+ \frac{z_1 M \, T}{8} \sum_i^n \sum_j^n \Delta_{ij} x_i \, x_j \int_0^{1/T} (\Psi_{ij} + \Psi_{ji}) d(1/T) \tag{5-6}$$

where z_1 is the parallel coordination number representing the number of primary nearest-neighbor cells in the parallel direction (or in one layer).
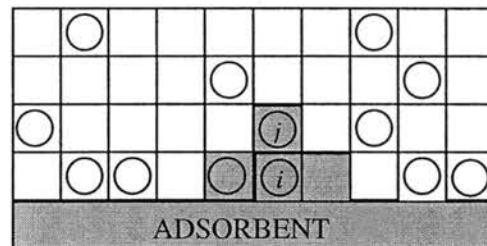
Figure 17. Configuration of Molecules Adsorbed on an Adsorbent Surface

Figure 18 presents the pictorial of multilayer pure-component adsorption; only three layers are presented in this figure. Beyond the adsorption phase is the bulk phase in which its cells are randomly filled by the gas molecules as presented in Figure 16.
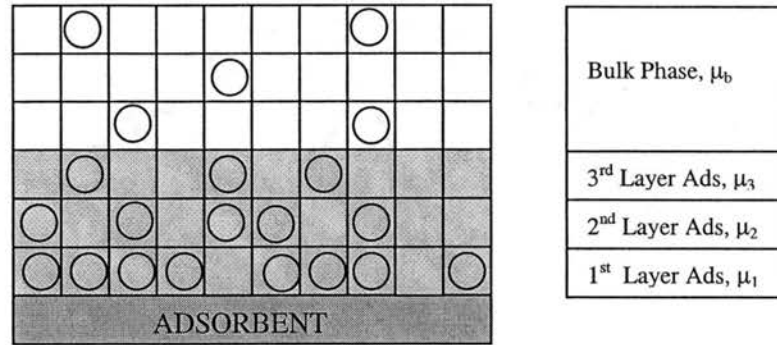
Figure 18. Pure Multilayer Adsorption

The chemical equilibrium between the adsorbed layers and the bulk is conditioned on the equality of component chemical potential in each layer and the bulk phase,

$$\mu_1 = \mu_2 = \mu_3 = ... = \mu_b \tag{5-7}$$

The chemical potential in each layer is defined as

$$\mu_i = \left(\frac{\partial A}{\partial N_i}\right)_{T,M,N_n} \tag{5-8}$$

Equation (5-3) is used to calculate the free energy for the bulk fluid, while Equation (5-6) is used to calculate the free energy for the first adsorbed layer. The empty lattice cell is treated as a second component in pure-gas adsorption modeling. Therefore, if N_i is the number of molecule in a specific layer and N_n is the number of empty cells in that layer, then $N_n = M - N_i$, or $x_n = 1 - x_i$. The chemical potential expressions for the bulk and the first adsorbed layer can be written as:

$$\mu_b = kT\left[z_0 \frac{\varepsilon_{ii}}{kT} x_b + ln\left(\frac{x_b}{1-x_b}\right)\right] \tag{5-9}$$

and

$$\mu_1 = kT\left[\frac{\varepsilon_{is}}{kT} + \frac{\varepsilon_{ii}}{kT}(x_2 + z_1 x_1) + ln\left(\frac{x_1}{1-x_1}\right)\right] \tag{5-10}$$

For a molecule which resides in the tth layer (above the first layer), its free energy depends on the interaction energy with its neighboring molecules in the same layer and the molecules in the adjacent layer. Therefore, for a random distribution, the free energy of the tth layer becomes:

$$A_{t^{th}} = \sum_i^n N_{i,t} \frac{z_1}{2} \varepsilon_{ii} + \left(\sum_i^n \sum_j^n N_{i,t} x_{j,t-1} \varepsilon_{ij} + \sum_i^n \sum_j^n N_{i,t} x_{j,t+1} \varepsilon_{ij} \right) + kT \sum_i^n N_{i,t} \, ln\, x_{i,t} \tag{5-11}$$

The chemical potential expression for the tth adsorbed layer of pure component is

$$\mu_t = kT\left[\frac{\varepsilon_{ii}}{kT}\{ z_1 x_t + (x_{t-1} + x_{t+1})\} + ln\left(\frac{x_t}{1-x_t}\right)\right] \tag{5-12}$$

The coordination number, z_0, appears in Equations (5-3) and (5-9) is related to the parallel coordination number, z_1, as $z_0 = z_1 + 2$.

Chemical potential equality between the tth adsorbed layer and the bulk phase results in the following equilibrium equation:

$$ln[x_t(1-x_b)/ x_b(1-x_t)] + z_0(x_t - x_b)\varepsilon_{ii} / kT + (x_{t+1} - 2x_t + x_{t-1})\varepsilon_{ii} / kT = 0 \tag{5-13}$$

for t = 2,3, ...m, number of layer. The chemical potential equality between the 1st adsorbed layer and the bulk phase results in:

$$ln[x_1(1-x_b)/ x_b(1-x_1)] + (z_1 x_1 + x_2 - z_0 x_b)\varepsilon_{ii} / kT + \varepsilon_{is} / kT = 0 \tag{5-14}$$

Pure Random Monolayer Adsorption

Figure 19 represents the configuration of the pure-gas molecules in the lattice cells for random monolayer adsorption. In this approach, we assume that adsorption occurs only on the adsorbent surface. Above this adsorbed layer resides the gas phase. Only one equilibrium equation is applied in this case, which is:

$$ln[x_{ads}(1-x_b)/x_b(1-x_{ads})]+(z_1 x_{ads}+x_b-z_0 x_b)\varepsilon_{ii}/kT+\varepsilon_{is}/kT=0 \qquad (5\text{-}15)$$
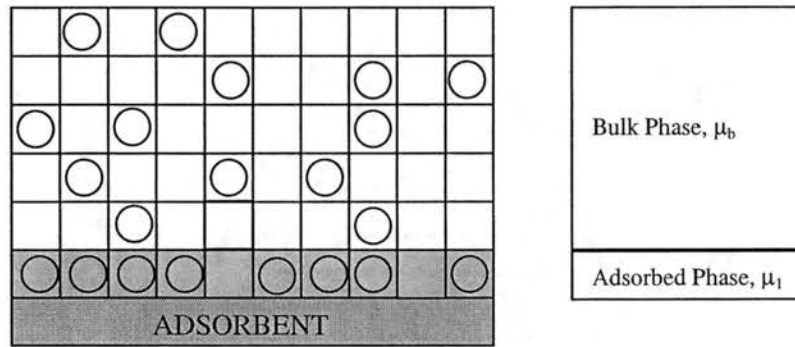
Figure 19. Pure Monolayer Adsorption

Benard and Chahine's Approach

Benard and Chahine (1997) assume that the adsorption process is directly mapped on the two parallel hexagonal graphite planes. Figure 20a shows the adsorbed molecules inside the slit, and Figure 20b shows the adsorbed molecules positioned among the carbon atoms of the graphite planes. In this approach, the equilibrium equation becomes:

$$ln[x_{ads}(1-x_b)/x_b(1-x_{ads})]+((z_1+1)x_{ads}-z_0 x_b)\varepsilon_{ii}/kT+\varepsilon_{is}/kT=0 \qquad (5\text{-}16)$$

where $z_1 = 6$ and $z_0 = 8$ for the hexagonal lattice cell.
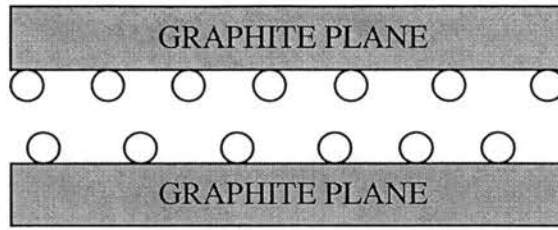
Figure 20(a). Monolayer Adsorption on Graphite Slit
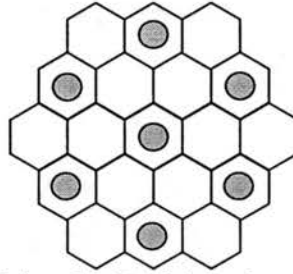
Figure 20(b). Adsorbed Molecules Positioned among the Carbon Atoms
of the Graphite Planes

Note that for $\varepsilon_{ii} = 0$, Equation (5-16) becomes equivalent to the Langmuir adsorption isotherm:

$$x_{ads} = \frac{x_b \, exp(-\varepsilon_{is} \, / \, kT)}{1 + x_b \, exp(\varepsilon_{is} \, / \, kT)} \qquad (5\text{-}17)$$

Adsorption Working Equations and the Calculation Algorithm

According to the lattice theory, the Gibbs excess adsorption is defined as

$$\Gamma_i = C_i \sum_{t=1}^{m} (x_{i,t} - x_{i,b}) \qquad (5\text{-}18)$$

where $x_{i,t}$ is the fraction of adsorbed molecules i that occupy the lattice cells at layer t ($= N_{i,t}/M_t$), and $x_{i,b}$ is the fraction of gas molecules i occupying the same number lattice cells as those at layer t ($=N_{i,b}/M_t$). This fractional coverage can also be expressed as $x_{i,t} = \rho_{i,t} / \rho_{i,mc}$ and $x_{i,b} = \rho_{i,b} / \rho_{i,mc}$, where $\rho_{i,t}$ is the adsorbed density of component i at layer t, $\rho_{i,b}$ is the adsorbed density of component i at the gas phase, and $\rho_{i,mc}$ is the

adsorbed density of component i at the maximum capacity. The prefactor C_i represents the maximum capacity of the adorbent. For pure adsorption inside the slit, according to the approach by Benard and Chahine, the number of layers, m, is equal to two, and Equation (5-18) becomes:

$$\Gamma = 2C\ (x_{ads} - x_b) = 2C\left(\frac{\rho_{ads}}{\rho_{mc}} - \frac{\rho_b}{\rho_{mc}}\right)$$ (5-19)

Here, the pre-factor C may be assumed to be a parameter taking into account the fraction of the active pores of the adsorbent and other structural properties of the adsorbent. C/ρ_{mc} in Equation (5-19) represents the specific adsorbed-phase volume for the adsorbate-adsorbent system, and the absolute adsorption can be expressed as:

$$n^{Abs} = 2C\rho_{ads} / \rho_{mc}$$ (5-20)

Equation (5-16) is used for monolayer adsorption equilibrium, and together with Equation (5-19) they can be used to correlate the experimental Gibbs adsorption isotherm to obtain four parameters, i.e., ε_{ii}/k, ε_{is}/k, ρ_{mc} and C. Figures 21 and 22 show the algorithms for monolayer and multilayer pure isotherm adsorption calculations. First, Equation (5-16), or Equations (5-13) and (5-14) for multilayer adsorption, is used to solve for x_{ads} using the Newton-Raphson method for a given initial guess of ε_{ii}/k and ε_{is}/k. The amount of adsorption is then calculated using Equation (5-19) for a given initial guess of ρ_{mc} and C. The four parameters are optimized using the objective function:

$$\sum_i^{npts}((\Gamma_{i,calc} - \Gamma_i)/\sigma_i)^2$$, where σ_i is the expected uncertainty for point i. The Marquardt method is used to regress the experimental adsorption data and generate the optimum model parameters.

71
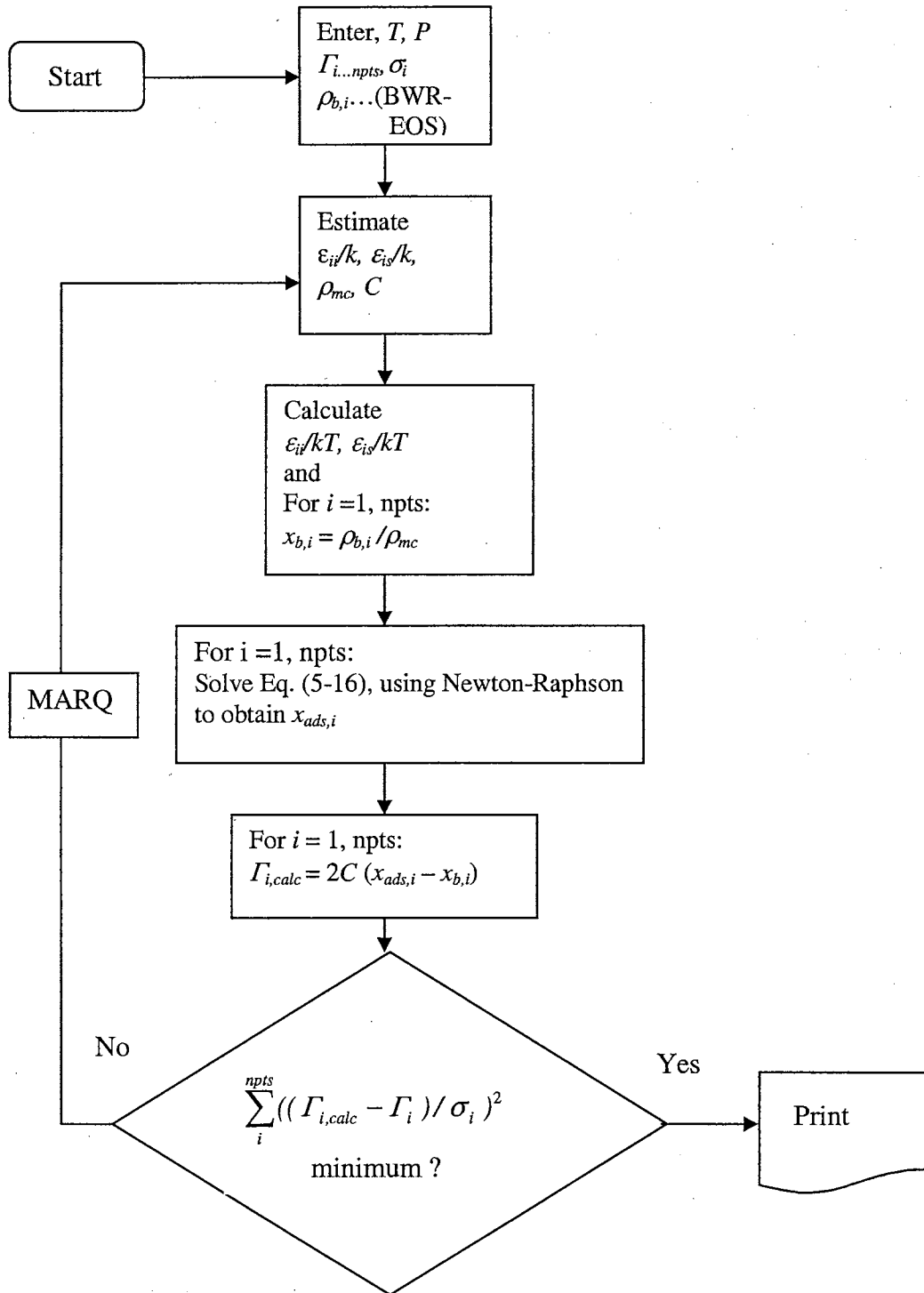
Figure 21. Algorithm for Pure-Isotherm Monolayer Adsorption
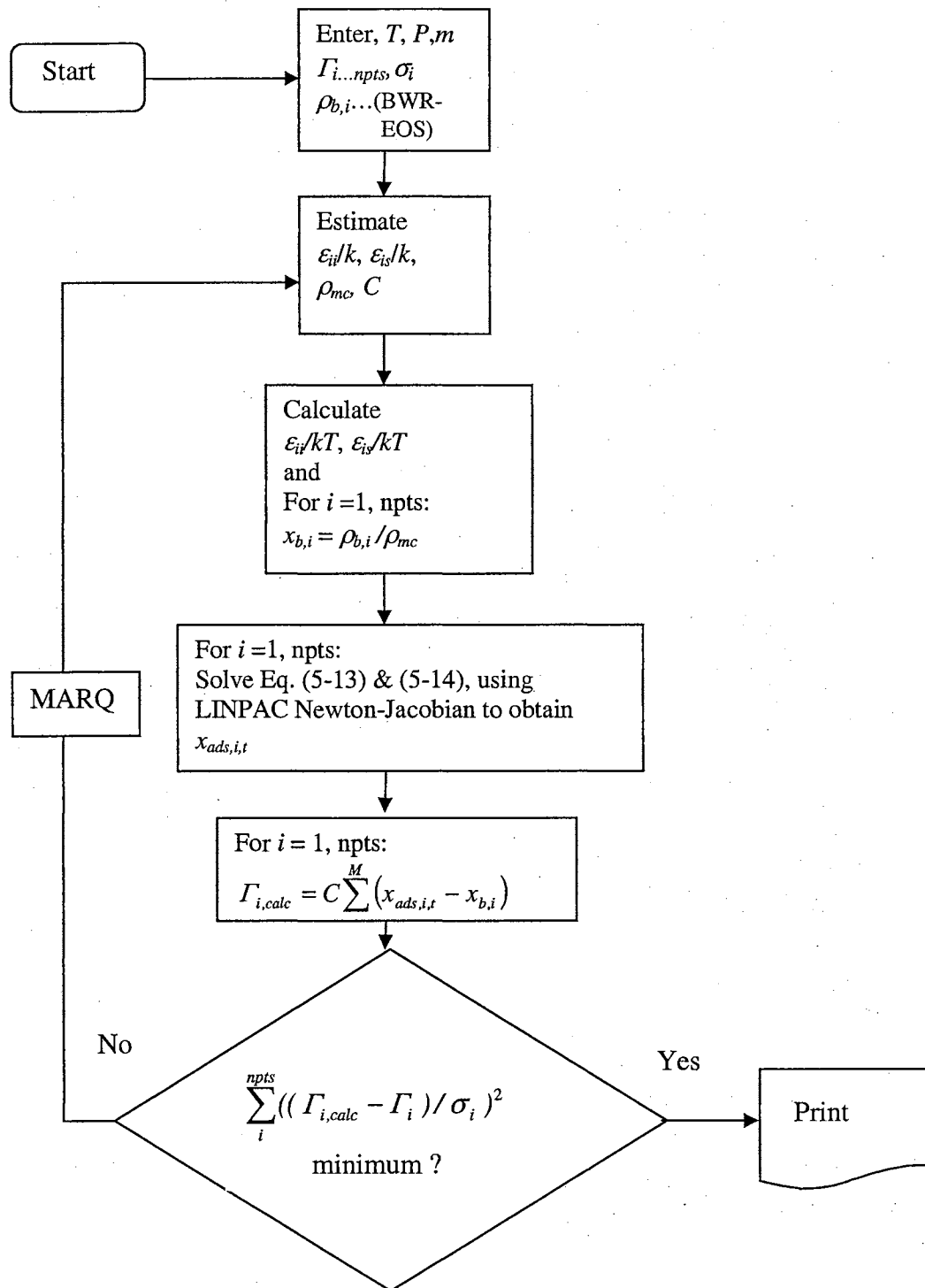
Figure 22. Algorithm for Pure-Isotherm Multilayer Adsorption

For a random binary mixed gas containing component A and B, the chemical potential for each component in the bulk can be derived using Equation (5-3) with $\psi_{ij} = \psi_{ji} = 1$ as follows:

$$A = \frac{z_0}{2}(N_A \varepsilon_{AA} + N_B \varepsilon_{BB} + N_n \varepsilon_{nn}) + kT(N_A \ln x_A + N_B \ln x_B + N_n \ln x_n)$$

$$+ \frac{z_0 M}{4}(\Delta_{AA} x_A x_A + \Delta_{AB} x_A x_B + \Delta_{An} x_A x_n + \Delta_{BA} x_B x_A + \Delta_{BB} x_B x_B + \Delta_{Bn} x_B x_n$$

$$+ \Delta_{nA} x_n x_A + \Delta_{nB} x_n x_B + \Delta_{nn} x_n x_n) \tag{5-21}$$

Subscript n represents the empty cells. Further, since $\Delta_{ij} = 2\varepsilon_{ij} - (\varepsilon_{ii} + \varepsilon_{jj})$, so $\Delta_{AA} = \Delta_{BB} = \Delta_{nn} = 0$, and because there is no interaction energy between a molecule and an empty cell and between the empty cells, then $\Delta_{An} = \Delta_{nA} = -\varepsilon_{AA}$ and $\Delta_{Bn} = \Delta_{nB} = -\varepsilon_{BB}$. Also $\varepsilon_{AB} = \varepsilon_{BA}$ implies that $\Delta_{AB} = \Delta_{BA}$. Thus, Equation (5-21) can be simplified to:

$$A = \frac{z_0}{2}(N_A \varepsilon_{AA} + N_B \varepsilon_{BB}) + kT(N_A \ln x_A + N_B \ln x_B + N_n \ln x_n)$$

$$+ \frac{z_0 M}{2} [\{ 2\varepsilon_{AB} - (\varepsilon_{AA} + \varepsilon_{BB})\} x_A x_B - \varepsilon_{AA} x_A x_n - \varepsilon_{BB} x_B x_n] \tag{5-22}$$

Noting that $x_i = N_i/M$ and $x_n = 1 - x_A - x_B$, this equation can be written as:

$$A = kT(N_A \ln x_A + N_B \ln x_B + N_n \ln x_n) + \frac{z_0 M}{2}(\varepsilon_{AA} x_A^2 + 2\varepsilon_{AB} x_A x_B + \varepsilon_{BB} x_B^2) \tag{5-23}$$

or

$$\frac{A}{MkT} = x_A \ln x_A + x_B \ln x_B + (1 - x_A - x_B) \ln(1 - x_A - x_B) + \frac{z_0}{2}(\frac{\varepsilon_{AA}}{kT} x_A^2 + \frac{2\varepsilon_{AB}}{kT} x_A x_B + \frac{\varepsilon_{BB}}{kT} x_B^2)$$

$$\tag{5-24}$$

The chemical potential for each component in the bulk can be determined using the definition on Equation (5-8):

$$\mu_i = \left(\frac{\partial A}{\partial N_i} \right)_{T,M,N_{j \neq i}} = \left(\frac{\partial A}{M \partial x_i} \right)_{T,M,N_{j \neq i}}$$

(5-25)

which leads to

$$\mu_{A,b} = kT \left[z_0 \left(\frac{\varepsilon_{AA}}{kT} x_{A,b} + \frac{\varepsilon_{AB}}{kT} x_{B,b} \right) + ln \left(\frac{x_{A,b}}{1 - x_{A,b} - x_{B,b}} \right) \right]$$

(5-26)

and

$$\mu_{B,b} = kT \left[z_0 \left(\frac{\varepsilon_{BB}}{kT} x_{B,b} + \frac{\varepsilon_{AB}}{kT} x_{A,b} \right) + ln \left(\frac{x_{B,b}}{1 - x_{A,b} - x_{B,b}} \right) \right]$$

(5-27)

Subscript b represents the bulk properties.

The chemical potential of the adsorbed component in a slit of adsorbent can be derived using Equation (5-6) (with the same assumption as in the bulk phase) as follows:

$$
\begin{aligned}
A_{1st} = & \{ N_{A,1st} (\tfrac{z_1}{2} \varepsilon_{AA} + \varepsilon_{As}) + N_{B,1st} (\tfrac{z_1}{2} \varepsilon_{BB} + \varepsilon_{Bs}) \} \\
& + N_{A,1st} x_{A,2nd} \varepsilon_{AA} + N_{A,1st} x_{B,2nd} \varepsilon_{AB} + N_{B,1st} x_{A,2nd} \varepsilon_{BA} + N_{B,1st} x_{B,2nd} \varepsilon_{BB} \\
& + kT (N_{A,1st} \ln x_{A,1st} + N_{B,1st} \ln x_{B,1st} + N_{n,1st} \ln x_{n,1st}) \\
& + \frac{z_1 M_{1st}}{2} [\{ 2\varepsilon_{AB} - (\varepsilon_{AA} + \varepsilon_{BB}) \} x_{A,1st} x_{B,1st} - \varepsilon_{AA} x_{A,1st} + \varepsilon_{AA} x^2_{A,1st} + \varepsilon_{AA} x_{A,1st} x_{B,1st} \\
& \qquad - \varepsilon_{BB} x_{B,1st} + \varepsilon_{BB} x^2_{B,1st} + \varepsilon_{BB} x_{B,1st} x_{A,1st}] \\
= & (N_{A,1st} \varepsilon_{As} + N_{B,1st} \varepsilon_{Bs}) + N_{A,1st} x_{A,2nd} \varepsilon_{AA} + N_{A,1st} x_{B,2nd} \varepsilon_{AB} \\
& + N_{B,1st} x_{A,2nd} \varepsilon_{BA} + N_{B,1st} x_{B,2nd} \varepsilon_{BB} \\
& + kT (N_{A,1st} \ln x_{A,1st} + N_{B,1st} \ln x_{B,1st} + N_{n,1st} \ln x_{n,1st}) \\
& + \frac{z_1 M_{1st}}{2} (\varepsilon_{AA} x^2_{A,1st} + 2\varepsilon_{AB} x_{A,1st} x_{B,1st} + \varepsilon_{BB} x^2_{B,1st})
\end{aligned}
$$

(5-28)

or

$$\frac{A_{1st}}{M_{1st}kT} = (\, x_{A,1st}\varepsilon_{As} + x_{B,1st}\varepsilon_{Bs}\,) + x_{A,1st}x_{A,2nd}\varepsilon_{AA} + x_{A,1st}x_{B,2nd}\varepsilon_{AB}$$

$$+ x_{B,1st}x_{A,2nd}\varepsilon_{BA} + x_{B,1st}x_{B,2nd}\varepsilon_{BB}$$

$$+ kT[(x_{A,1st}\ln x_{A,1st} + x_{B,1st}\ln x_{B,1st} + (1 - x_{A,1st} - x_{B,1st})\ln(1 - x_{A,1st} - x_{B,1st})]$$

$$+ \frac{z_1 M_{1st}}{2}(\,\varepsilon_{AA}x_{A,1st}^2 + 2\varepsilon_{AB}x_{A,1st}x_{B,1st} + \varepsilon_{BB}x_{B,1st}^2\,) \qquad (5\text{-}29)$$

The chemical potential for each component in the adsorbed phase can be determined using the definition on Equation (5-8):

$$\mu_{i,ads} = \left(\frac{\partial A_{1st}}{\partial N_{i,1st}}\right)_{T,M_{1st},N_{j\neq i,1st},N_{i,2nd}} = \left(\frac{\partial A_{1st}}{M_{1st}\partial x_{i,1st}}\right)_{T,M_{1st},N_{j\neq i,1st},N_{i,2nd}} \qquad (5\text{-}30)$$

and noting that $x_{i,1st} = x_{i,2nd}$ (we will use symbol x_i only) leads to:

$$\mu_{A,ads} = kT\left[\frac{\varepsilon_{As}}{kT} + \frac{\varepsilon_{AA}}{kT}x_A + \frac{\varepsilon_{AB}}{kT}x_B + z_1(\frac{\varepsilon_{AA}}{kT}x_A + \frac{\varepsilon_{AB}}{kT}x_B) + \ln\left(\frac{x_A}{1 - x_A - x_B}\right)\right] \qquad (5\text{-}31)$$

and

$$\mu_{B,ads} = kT\left[\frac{\varepsilon_{Bs}}{kT} + \frac{\varepsilon_{BB}}{kT}x_B + \frac{\varepsilon_{AB}}{kT}x_A + z_1(\frac{\varepsilon_{BB}}{kT}x_B + \frac{\varepsilon_{AB}}{kT}x_A) + \ln\left(\frac{x_B}{1 - x_A - x_B}\right)\right] \qquad (5\text{-}32)$$

The equality of the chemical potential in the adsorbed and the bulk phases for each component leads to the following equilibrium equations for the binary mixed-gas adsorption:

$$\ln\frac{x_A(1 - x_{A,b} - x_{B,b})}{x_{A,b}(1 - x_A - x_B)} + \frac{\varepsilon_{AA}}{kT}((\,z_1 + 1)x_A - z_0 x_{A,b}\,) + \frac{\varepsilon_{AB}}{kT}((\,z_1 + 1)x_B - z_0 x_{B,b}\,) + \frac{\varepsilon_{As}}{kT} = 0$$

$$(5\text{-}33)$$

and

$$\ln\frac{x_B(1 - x_{A,b} - x_{B,b})}{x_{B,b}(1 - x_A - x_B)} + \frac{\varepsilon_{BB}}{kT}((\,z_1 + 1)x_B - z_0 x_{B,b}\,) + \frac{\varepsilon_{AB}}{kT}((\,z_1 + 1)x_A - z_0 x_{A,b}\,) + \frac{\varepsilon_{Bs}}{kT} = 0$$

$$(5\text{-}34)$$

A general equilibrium equation for monolayer, random mixed-gas adsorption was derived to obtain the following expression:

$$\ln \frac{x_i(1-\sum_{j=1}^{n} x_{j,b})}{x_{i,b}(1-\sum_{j=1}^{n} x_j)} + \sum_{j=1}^{n} \frac{\varepsilon_{ij}}{kT}\left[(z_1+1)x_j - z_0 x_{j,b}\right] + \frac{\varepsilon_{is}}{kT} = 0 \qquad (5\text{-}35)$$

A geometric combination rule is used to evaluate the interaction energy between molecule i and j; i.e., $\varepsilon_{ij} = (1+C_{ij})\sqrt{\varepsilon_{ii}\varepsilon_{jj}}$. Here, a regressed binary interaction parameter C_{ij} was introduced to account for unlike molecular interactions, which deviate from the geometric mean relation.

The Gibbs excess adsorption for each component is calculated using the following expression:

$$\Gamma_i = 2C_i(x_i - x_{i,b}) \qquad (5\text{-}36)$$

The fractional coverage in the bulk phase, $x_{i,b}$ can be obtained from the following equation:

$$x_{i,b} = \frac{y_i \rho_b}{\rho_{mc}} \qquad (5\text{-}37)$$

where, the bulk density, ρ_b, is calculated using the Benedict-Webb-Rubin (BWR) equation of state (Pan, 2003). Since little information is known about the mixture adsorbed-phase density, the maximum density, ρ_{mc}, is estimated using the following ideal mixing rules:

$$\frac{1}{\rho_{mc}} = \frac{x_A^{Abs}}{\rho_{mc,A}} + \frac{x_B^{Abs}}{\rho_{mc,B}} \qquad (5\text{-}38)$$

The absolute adsorbed phase mole fractions, x_A^{Abs} and x_B^{Abs} are used in this equation.

A correction factor is introduced to calculate the Gibbs adsorption for each component, considering that the maximum capacity of a component may be different for pure and mixture adsorption. In this case, Equation (5-36) is modified as:

$$\Gamma_i = 2C_i(x_i - x_{i,b})C_{corr} \tag{5-39}$$

The correction factor is calculated using the following empirical expression:

$$C_{corr} = \sum_i^n \sum_j^n x_i^{Abs} x_j^{Abs} E_{ij} \tag{5-40}$$

An additional regressed binary interaction parameter, E_{ij}, is introduced in this expression, in which $E_{ii} = E_{jj} = 1$.

Iteration Function Method (IFM)

In general, the Gibbs excess adsorption can be calculated using a model if the pressure, temperature and the equilibrium composition in the gas phase are known. In our previous study (Sudibandriyo et al., 2003), the equilibrium mole fraction in the gas phase is obtained from the adsorption measurements. Even though the gas composition obtained from the experiment is adequate to calculate the individual Gibbs excess adsorption, errors in the gas composition measurement can worsen the model representation. Moreover, using the experimental gas compositions can only permit Gibbs adsorption calculations at the conditions where the experimental measurements are available. In addition, in coalbed methane production simulation, the overall gas composition information is more readily obtained than the equilibrium gas composition. To overcome these problems, an iteration function method, which is similar to flash calculation in vapor-liquid equilibrium, is used to determine the adsorption equilibrium

gas mole fractions for given pressure, temperature, feed composition and specific void volume (void volume per unit amount of adsorbent) of the system.

If z_i represents the mole fraction of each component (i) in the feed, then by a molar balance, we can express z_i in terms of the other experimentally accessible variables as:

$$z_i = \frac{\Gamma_i + \overline{V}_{void}\rho_b y_i}{\Gamma_{total} + \overline{V}_{void}\rho_b} \qquad (5\text{-}41)$$

Figure 23 shows the IFM algorithm to calculate the binary adsorption isotherm using parameters obtained from the pure adsorption. The component Gibbs adsorption is first calculated using the OK model of Equations (5-35) and (5-36). The solution, however, is contingent on *equilibrium* mole fractions, y_i, as they are needed to calculate the gas density using the BWR EOS and to calculate the fractional coverage in the bulk phase, $x_{i,b}$, as defined in Equation (5-37). The gas mole fractions were initialized with the available experimental values to speed the calculation (although any reasonable initial values could be used).

The next step is to evaluate Equation (5-41) for each component. If Equation (5-41) is not satisfied for each component, then a new set of equilibrium mole fractions is used to calculate the next trial adsorbed amount. The procedure is repeated until Equation (5-41) is satisfied. The Newton-Raphson's method with numerical derivatives is used to solve Equation (5-41).

```
Start → Data enter: P,T,
         For j component and i ...npts:
         z_{j,i}, Γ_{j,i}, σ_{j,i};
         ε_{ij}/k, ε_{js}/k, ρ_{j,mc}, C_j
         set y_{j,i,old} = y_{j,i,exp}

For component j and k
Int.Par.:C_{jk}

Calculate
ε_{ij}/kT, ε_{jk}/kT, ε_{js}/kT

For i =1, npts:
Calculate ρ_{b,i}...(using BWR-EOS)
Solve Eq. (5-35) using LINPAC, to obtain x_{j,i}
with: x_{j,b,i} = y_{j,i} ρ_{b,i} /ρ_{mc,i}

For i = 1, npts  and
For j to N component:
Γ_{j,i,calc} = 2C_{j,i} (x_{j,i} − x_{j,b,i});  Γ_{tot,i,calc} = Σ Γ_{j,i,calc}

Solve Eq.(5-41) using
Newton-Raphson to obtain y_{j,i}

|y_{j,i} - y_{j,i,old}| < ζ  ?   No → y_{j,i,old} = y_{j,i}
Yes

Prediction ?   Yes → Print
No

MARQ

For comp. j and total
Σ_{i}^{npt} [( Γ_{j,i,calc} − Γ_{j,i} )/ σ_{j,i} ]^2
Minimum ?   Yes → Print
No
```

Figure 23. Algorithm for Multicomponent Gas Adsorption Using the Iteration Function Method

CHAPTER 6

MODELING OF PURE-GAS ADSORPTION

In this Chapter, the correlative capability of the Ono-Kondo (OK) model is evaluated. Model parameters were regressed to obtain precise representations for pure-gas, high-pressure adsorption on carbon adsorbents involving adsorbates in the near critical and supercritical regions. Also, generalized model parameters were developed which can predict the adsorption equilibrium to within twice the expected experimental uncertainties.

Extending the mathematical models to describe adsorption behavior on coals is complicated by (a) the difficulty in characterizing the coal matrix adequately and (b) assessing the effect of water (found in essentially all coalbeds) on the adsorption behavior. As a result, we decided to perform initial studies (a) on a more readily characterized carbon matrix and (b) in the absence of water. This led to our choice of dry activated carbon. Our rationale is that useful models should be expected to fit data on activated carbon prior to extending them to include the effects of the complex adsorbent structure of coals and/or the presence of water.

To apply the OK model, the number of layers must be specified. Therefore, before performing model parameter evaluations, we determined the number of layers required to best describe the systems considered. The multilayer and monolayer adsorption models were compared, and the appropriate model was used for the rest of the study.

Determination of the Number of Layers

As described in the previous chapter, the OK lattice model can be applied to monolayer or multilayer adsorption. We used selected experimental data to evaluate the number layers required to adequately represent the systems considered. Specifically, our measurements at 318 K for pure adsorption of nitrogen, methane and CO_2 on activated carbon were used to represent adsorption in the supercritical region; the CO_2 adsorption data on activated carbon conducted by Humayun (2000) at 304 K were used to represent the adsorption in the near-critical region; and our CO_2 adsorption data on dry coal (Illinois #6) were used to represent an adsorbent with a wide pore-size distribution.

The modeling of monolayer and multilayer gas adsorption was done according to the algorithms described in Chapter 5. Table 8 presents a summary of our model evaluation results for the monolayer and three-layer models we used to correlate the selected data. The model parameters, given in Table 8, were determined by minimizing the sum of squares of weighted absolute deviations in the calculated adsorption, ω, for the pure gas of interest. The quality of the fit, expressed in terms of absolute average percentage deviation (%AAD) and weighted average absolute deviations (WAAD), is also given in Table 8 for both the monolayer and multilayer models. Figures 24 and 25 illustrate the quality of representation produced by the models. Both models show excellent representation within the expected experimental uncertainties; as such, comparable representation is observed for the monolayer and multilayer models. The results suggest that the simpler monolayer model is appropriate for the systems considered. The results are not surprising, considering that the adsorption of small molecules occurs mostly in the micropore structure (Gan et al., 1972; Medek et al., 1977;

Benard and Chahine, 1977). Perhaps because the size of the micropores is only several times the diameter of the molecules and the phase conditions are removed from the critical region, monolayer adsorption is adequate.

In conclusion, the monolayer model appears effective in modeling pure-gas adsorption on carbon matrices. Therefore, this approach was used for further evaluation.

Table 8. Comparison of Monolayer and Multilayer Modeling Results for Selected Systems

Model Parameters	AC (OSU, 2002)			AC (Humayun, 2000)	Dry Illinois #6 Coal
	Nitrogen	Methane	CO_2	CO_2	CO_2
Monolayer Model					
ε_{is}/k (K)	-1032	-1385	-1690	-1610	-1170
ε_{ii}/k (K)	41	64	82	100	60
ρ_{mc} (g/cc)	0.67	0.34	0.98	0.98	0.95
C (mmol/g)	2.72	3.26	4.53	5.27	1.19
NPTS	22	18	52	28	11
% AAD	**0.3**	**0.6**	**2.8**	**4.3**	**2.9**
WAAD	**0.3**	**0.6**	**0.9**	**0.8**	**0.7**
Three-layer Model					
ε_{is}/k (K)	-1020	-1380	-1650	-1570	-1160
ε_{ii}/k (K)	50	64	82	110	70
ρ_{mc} (g/cc)	0.67	0.40	1.02	0.99	0.98
C (mmol/g)	2.81	3.20	4.58	5.45	1.23
NPTS	22	18	52	28	11
% AAD	**0.3**	**0.6**	**3.4**	**4.3**	**3.0**
WAAD	**0.3**	**0.7**	**1.0**	**0.8**	**0.6**
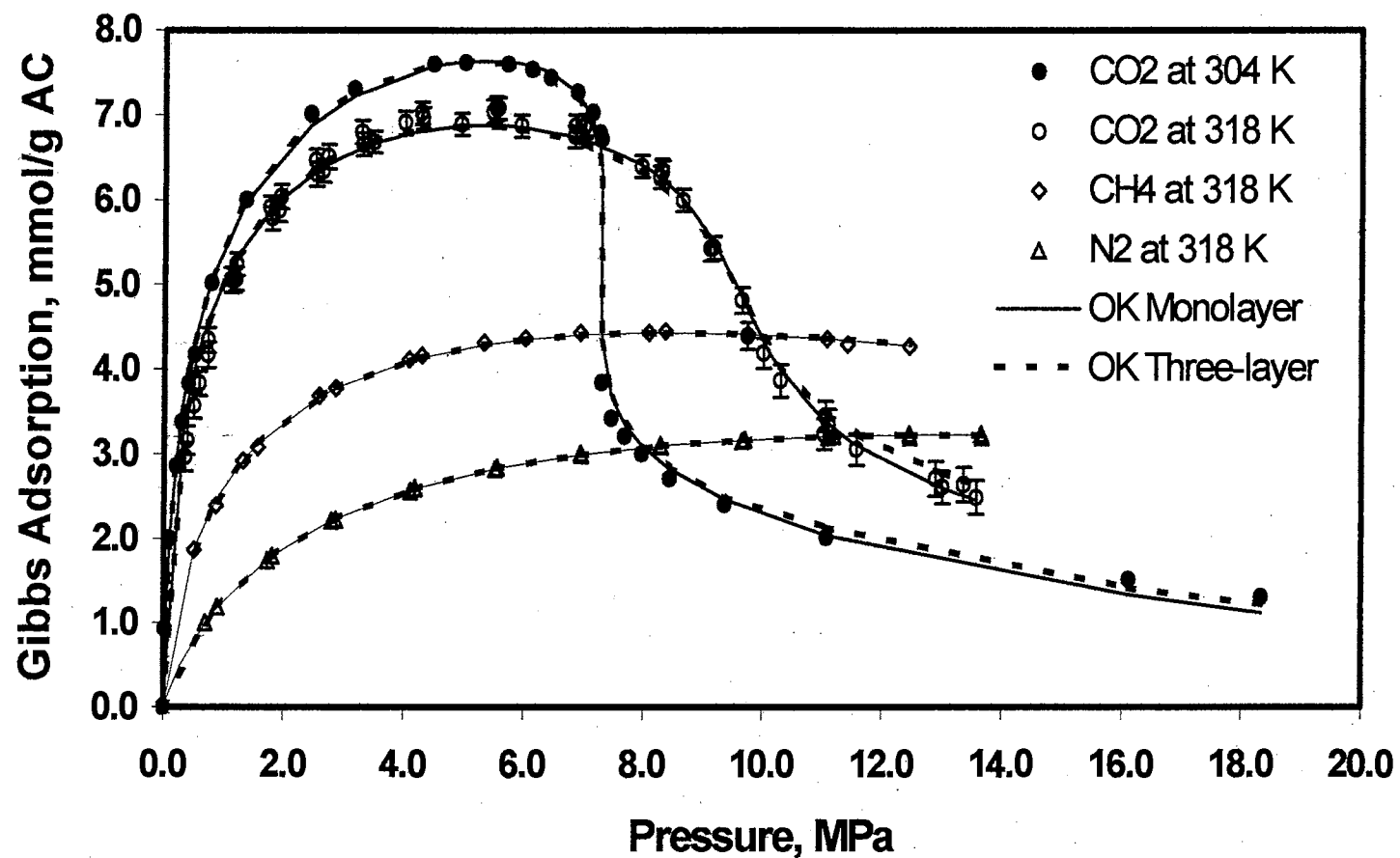
Figure 24. Comparison of Monolayer and Three-Layer OK Model Representations of Pure-Gas Adsorption on Activated Carbon
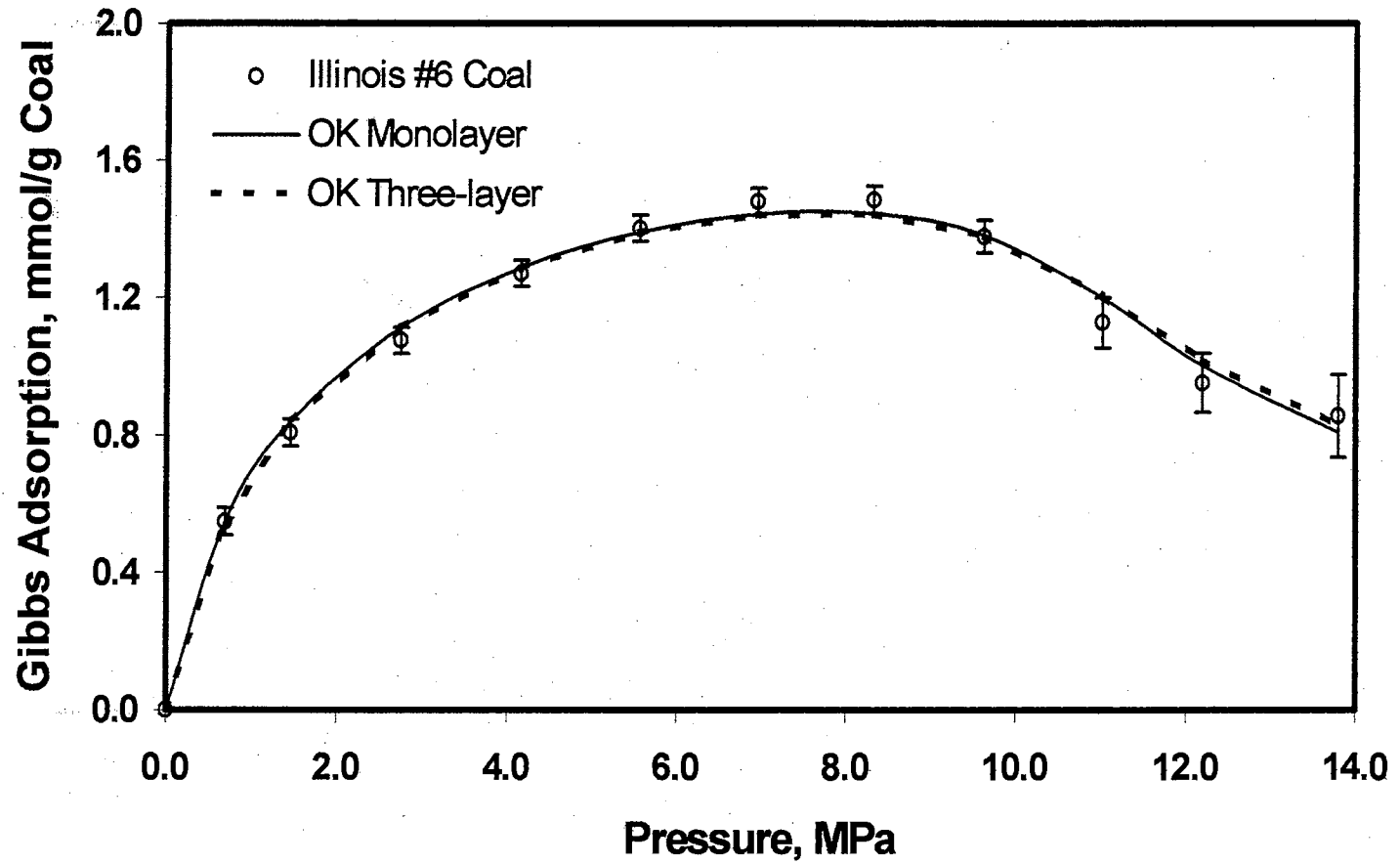
Figure 25. Comparison of Monolayer and Three-Layer OK Model Representations of Pure CO_2 Adsorption on Illinois #6 Coal

Modeling of Pure-Gas Adsorption on Activated Carbon (AC)

The Maximum Adsorbed-Phase Density Estimate

The OK model has four parameters: ρ_{mc}, ε_{ii}/k, ε_{is}/k and C. To reduce the number

of regressed parameters in the model, the maximum adsorbed-phase density, ρ_{mc}, is

usually estimated independently. A commonly used approximation is the liquid density

at the normal boiling point, as was done by Arri and Yee (1992). However, examination

of the results from the OK model reveals that the adsorbed-phase densities generated by

the OK model, as presented in Table 9, are less than the boiling point estimates and are

closer to the reciprocal van der Waals co-volume estimates. Moreover, the adsorbed-

phase densities generated by the OK model and the reciprocal van der Waals co-volume

estimates are also close to the "graphical estimates" based on the Gibbs adsorption

definition: $\Gamma = V_{ads}(\rho_{ads} - \rho_{gas})$, as illustrated by Figure 26. V_{ads} is the adsorbed-phase

volume and ρ_{ads} and ρ_{gas} are the density of the adsorbed phase and the gas phase,

respectively. As shown in the figure for CO_2, if the absolute adsorption, $V_{ads}\rho_{ads}$,

becomes constant at high pressures, then the Gibbs adsorption should show a linear

decrease with increasing ρ_{gas}. Extrapolation of this linear relation yields an x-axis

intercept where $\rho_{ads} = \rho_{gas}=\rho_{mc}$. Figure 26 indicates that $\rho_{ads} = 22.5$ mol/L or 1.02 g/cm^3.

Use of this technique requires sufficient data in the linear (high pressure) region beyond

the maximum in the Gibbs adsorption; thus, an estimate is shown in Table 9 only for

carbon dioxide. For the other adsorbates, the available data do not extend to the linear

region.

Table 9. Adsorbed-Phase Densities Estimated by Different Methods

Method	Adsorbed-Phase Density (g/cm^3)		
	Methane	Nitrogen	CO$_2$
Ono-Kondo model	0.345	0.673	0.977
Zhou-Gasem-Robinson (ZGR) EOS	0.345	0.839	0.982
Liquid density estimate	0.421	0.808	---
Solid density estimate	---	---	1.18
Reciprocal van der Waals covolume	0.374	0.725	1.03
Graphical estimate from the Gibbs adsorption	---	---	1.02
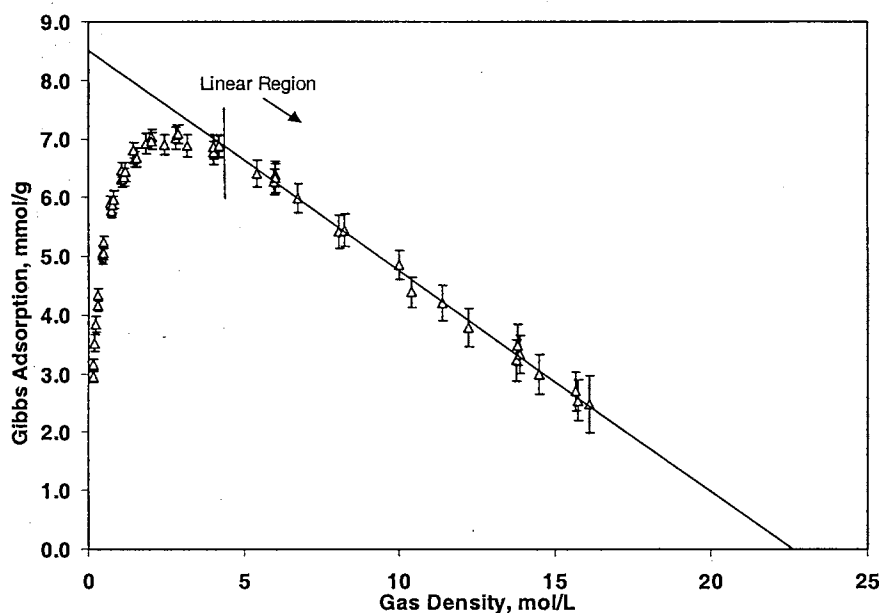
Figure 26. Graphical Method for Estimating Adsorbed-Phase Density:
CO$_2$ Adsorption on Activated Carbon at 318.2 K

In our recent publication on the simplified local density (SLD) modeling (Fitzgerald et al., 2003), a theoretical explanation was offered for why the adsorbed-phase densities are close to the equation of state (EOS) reciprocal co-volumes. The SLD model can show that, at high pressures, the adsorbed-phase density approaches the reciprocal co-volume.

87

The Fluid-Fluid Energy Parameter Estimate

In the present work, the fluid-fluid energy parameter, ε_{ii}/k, was estimated to be proportional to the Lennard-Jones well depth energy parameter. For the Lennard-Jones 12-6 potential, the pair-wise interaction between two molecules separated by a distance r is given by

$$\Phi(r) = 4\varepsilon * \left[\left(\frac{\sigma}{r} \right)^{12} - \left(\frac{\sigma}{r} \right)^{6} \right]$$ (6-1)

where $\Phi(r)$ is the potential energy, $\varepsilon*$ is the well depth of the potential, and σ is the collision diameter, which is defined as the distance at which the potential energy is zero. If the adsorbed molecules are randomly distributed, the total energy of interaction between a molecule and all the surrounding molecules is:

$$U_1 = \int_{\sigma}^{\infty} \Phi(r) \frac{N}{A} 2\pi r dr = -\frac{6\pi}{5} \varepsilon * \sigma^2 \frac{N}{A}$$ (6-2)

where N is the number of molecules on the surface and A is the surface area. The total energy due to the molecular interaction is then simply (Do, 1998):

$$U_T = \frac{N}{2} U_1 = -\frac{3\pi}{5} \varepsilon * \sigma^2 \frac{N^2}{A}$$ (6-3)

In OK model, the total energy due to molecular interactions is expressed in terms of the coordination number and the fractional coverage. Equating the two total energy expressions, for $z_0 = 8$ (hexagonal configuration), results in

$$U_T = \frac{z_0}{2} N \varepsilon_{ii} = 4 N \varepsilon_{ii} = \left| -\frac{3\pi}{5} \varepsilon * \sigma^2 \frac{N^2}{A} \right|$$ (6-4)

or

$$\varepsilon_{ii} = \frac{3\pi}{20}\varepsilon * \sigma^2 \frac{N}{A} \qquad (6\text{-}5)$$

When the spherical particles are closely packed, the fraction occupied by those particles is 0.907 (Do, 1998), and we write:

$$\frac{\pi}{4}N\frac{a^2}{A} = 0.907 \qquad (6\text{-}6)$$

Here, a is the distance between the two particles at the minimum energy potential, $a = (2)^{1/6}\sigma$. Combining Equation (6-5) and (6-6) results in the following estimate for the fluid-fluid energy parameter in the OK model:

$$\varepsilon_{ii} = 0.432\varepsilon * \qquad (6\text{-}7)$$

The fluid-fluid energy parameters obtained for the gas adsorptions on activated carbon shown in Table 8 are reasonably close to the ones obtained from the above expression; for example, the regressed value of ε_{ii}/k for CO_2 is 82 K compared to the 84.3 K value estimated using Equation (6-7). Further, the value of the calculated Gibbs excess adsorption is not highly sensitive to small deviations in ε_{ii}/k obtained from Equation (6-7); for example, a ten percent deviation in ε_{ii}/k can still produce reasonable values of the Gibbs excess adsorption. We also observed that the fluid-fluid energy parameters are positive values, which represents a repulsive energy potential. These results confirm the observations of Benard and Chahine (1997) and also agree with molecular simulation results obtained recently by Aranovich (2001). This phenomenon is similar to the negative values obtained for parameter α in two-dimensional equation of state (Zhou, 1994) and is not totally unexpected in light of the fact that surface forces are significant in the adsorbed phases. The effect of solid surface potential on adsorbed molecules may

affect the molecular energy at conditions such that the interaction between them becomes repulsive.

Because the lattice model was also assumed for the gas phase, the positive fluid-fluid energy parameter is also repulsive in the gas phase, which might be unreasonable. The use of an accurate equation of state to calculate the chemical potential in the gas phase might be more appropriate; this approach is planned for a future study.

Two-Parameter OK Model

The adsorbed-phase density and the fluid-fluid energy parameters can be estimated from the reciprocal van der Waals co-volume and from a proportional relation to the well depth of the Lennard-Jones 12-6 potential, respectively. For further generalization, the above estimates were applied for modeling of (a) selected gas adsorption on activated carbon and zeolites reported in the literature and (b) our gas adsorption measurements on activated carbon. In this case, the fluid-solid energy parameter, ε_{is}/k, was regressed for each *system* and the parameter C was regressed for each adsorption *isotherm*. Because no detailed information was given on uncertainties in the selected literature experimental data, the percentage average deviation of the Gibbs excess adsorption (% AAD) was used as the objective function to determine the two model parameters.

Table 10 presents the results of our model representation of the above selected data. Overall, for 2242 data points, the OK model with two regressed parameters (one common ε_{is}/k for each system, and individual C for each isotherm) represents the data with about 3.6% AAD. However, some significantly larger errors were observed,

Table 10. Results of Two-Parameter OK Model for Pure-Gas Adsorption

System No.	Adsorbent	Adsorbent Surface Area (m²/g)	Gas	NPTS	T (K)	Parameters		%AAD	RMSE (mmol/g)	Reference
						$-\varepsilon_{is}/k$ (K)	C (mmol/g)			
1	AC, Columbia Grade L	1152	N_2	36	310.9 338.7 366.5 394.3 422.0	1090	3.071 2.947 2.724 2.583 2.756	3.1	0.015	Ray (1950)
2	AC, Columbia Grade L	1152	CH_4	45	310.9 338.7 366.5 394.3 422.0	1410	3.692 3.546 3.217 2.847 2.737	2.6	0.049	Ray (1950)
3	AC, Columbia Grade L	1152	C_2H_6	58	310.9 338.7 366.5 394.3 422.0 449.8 477.6	2190	3.574 3.147 2.865 2.706 2.434 2.381 2.159	4.4	0.145	Ray (1950)
4	Charcoal	1157	CH_4	55	283.2 293.2 303.2 313.2 323.2	1330	5.037 4.834 4.710 4.521 4.332	1.2	0.051	Payne (1968)

Table 10. Results of Two-Parameter OK Model for Pure-Gas Adsorption (Continued)

System No.	Adsorbent	Adsorbent Surface Area (m^2/g)	Gas	NPTS	T (K)	Parameters		%AAD	RMSE (mmol/g)	Reference
						$-\varepsilon_{is}/k$ (K)	C (mmol/g)			
5	Charcoal	1157	C_3H_8	52	293.2 303.2 313.2 323.2 333.2	2490	3.774 3.662 3.592 3.486 3.375	6.7	0.200	Payne (1968)
6	AC, BPL	988	CH_4	72	212.7 260.2 301.4	1320	4.515 3.880 3.279	3.1	0.112	Reich (1980)
7	AC, BPL	988	CO_2	60	212.7 260.2 301.4	1520	9.753 6.344 5.110	4.9	0.325	Reich (1980)
8	AC, BPL	988	C_2H_6	49	212.7 260.2 301.4	2000	4.090 3.588 3.157	6.3	0.318	Reich (1980)
9	AC, BPL	988	C_2H_4	52	212.7 260.2 301.4	1935	4.387 3.758 3.281	4.5	0.234	Reich (1980)
10	AC, PCB-Calgon	1150-1250	CH_4	22	296 373 480	1380	3.994 3.191 2.547	3.2	0.066	Ritter (1987)
11	AC, PCB-Calgon	1150-1250	CO_2	12	296 373 480	1600	6.123 4.170 2.910	4.6	0.230	Ritter (1987)

Table 10. Results of Two-Parameter OK Model for Pure-Gas Adsorption (Continued)

System No.	Adsorbent	Adsorbent Surface Area (m^2/g)	Gas	NPTS	T (K)	$-\varepsilon_{is}/k$ (K)	C (mmol/g)	%AAD	RMSE (mmol/g)	Reference
12	AC, F30/470 Chemviron Carbon	993.5	CO_2	164	278 288 298 303 308 318 328	1625	5.741 5.620 5.341 5.326 5.143 4.808 4.598	1.2	0.138	Berlier (1997)
13	AC, Norit R1 Extra	1450	N_2	10	298	1050	3.409	3.3	0.021	Dreisbach (1999)
14	AC, Norit R1 Extra	1450	CH_4	12	298	1390	4.335	3.3	0.124	Dreisbach (1999)
15	AC, Norit R1 Extra	1450	CO_2	12	298	1600	6.773	9.5	0.267	Dreisbach (1999)
16	AC, Coconut Shell	3106	CH_4	122	233 253 273 293 313 333	1140	11.650 11.221 10.578 9.926 9.301 8.647	3.0	0.237	Zhou (2000)
17	AC, Calgon F-400	850	CO_2	116	303.6 305.2 309.2 313.2 318.2	1700	4.847 4.843 4.667 4.530 4.443	8.8	0.306	Humayun (2000)

Table 10. Results of Two-Parameter OK Model for Pure-Gas Adsorption (Continued)

System No.	Adsorbent	Adsorbent Surface Area (m^2/g)	Gas	NPTS	T (K)	Parameters		%AAD	RMSE (mmol/g)	Reference
						$-\varepsilon_{is}/k$ (K)	C (mmol/g)			
18	AC, Norit RB1	1100	CH_4	64	304.9 311.4 331.3 350.5	1480	3.731 3.171 3.024 2.875	1.5	0.030	Vaart (2000)
19	AC, Norit RB1	1100	CO_2	64	305.2 311.2 329.5 348.3	1655	5.839 4.788 4.301 3.884	1.7	0.060	Vaart (2000)
20	AC, Coconut Shell	3106	N_2	71	178 198 218 233 258 278 298	880	11.026 10.664 9.823 9.000 8.537 7.703 7.424	1.5	0.162	Zhou (2001)
21	AC F30/470	993.5	N_2	116	303 323 343 363 383	1135	2.617 2.457 2.284 2.134 2.008	2.0	0.044	Frére (2002)
22	AC F30/470	993.5	CH_4	122	303 323 343 362 383	1395	3.625 3.420 3.207 2.987 2.809	2.2	0.094	Frére (2002)

System No.	Adsorbent	Adsorbent Surface Area (m^2/g)	Gas	NPTS	T (K)	Parameters		%AAD	RMSE (mmol/g)	Reference
						$-\varepsilon_{is}/k$ (K)	C (mmol/g)			
23	AC F30/470	993.5	C_3H_8	102	303 323 343 363 383	2550	3.045 2.877 2.802 2.654 2.487	2.3	0.173	Frére (2002)
24	AC Norit R1	1262	N_2	31	298	1070	3.655	1.5	0.035	Beutekamp (2002)
25	AC Norit R1	1262	CO_2	29	298	1500	7.513	3.6	0.269	Beutekamp (2002)
26	Zeolite, Linde 13X	525	N_2	24	298 323 348	1185	1.627 1.480 1.329	2.2	0.042	Wakasugi (1981)
27	Zeolite, Linde 5A	~400	N_2	27	298 323 348	1310	1.525 1.403 1.284	1.3	0.032	Wakasugi (1981)
28	Zeolite, Linde 5A	~400	CH_4	28	298 323 348	1600	1.559 1.449 1.336	2.7	0.048	Wakasugi (1981)
29	Zeolite, Linde 5A	~400	CO_2	41	298 323 348	2500	2.136 2.060 1.990	5.6	0.317	Wakasugi (1981)
30	Zeolite, Linde 5A	~400	C_2H_6	27	298 323 348	2600	1.158 1.098 1.023	2.1	0.051	Wakasugi (1981)
31	H-Modernite, Z-900H	~300	CO_2	93	283 303 323	2600	1.634 1.548 1.434	11.2	0.090	Talu (1986)

95

Table 10. Results of Two-Parameter OK Model for Pure-Gas Adsorption (Continued)

System No.	Adsorbent	Adsorbent Surface Area (m^2/g)	Gas	NPTS	T (K)	$-\varepsilon_{is}/k$ (K)	C (mmol/g)	%AAD	RMSE (mmol/g)	Reference
32	H-Mordenite, Z-900H	~300	H_2S	69	283 303 338 368	3550	2.108 1.998 1.847 1.734	2.2	0.032	Talu (1986)
33	H-Mordenite, Z-900H	~300	C_3H_8	92	283 303 324	3150	0.618 0.603 0.562	7.2	0.045	Talu (1986)
34	Zeolite G5	430	CH_4	51	283 303	1200	3.352 3.100	3.9	0.055	Berlier (1995)
35	Zeolite G5	430	C_2H_6	40	283 303	2525	1.699 1.620	1.3	0.044	Berlier (1995)
36	Zeolite G5	430	C_2H_4	34	283 303	2630	1.923 1.798	1.1	0.048	Berlier (1995)
37	Zeolite 13X	383	CH_4	12	298	1500	1.699	9.8	0.131	Beutekamp (2002)
38	Zeolite 13X	383	C_2H_6	11	298	2380	1.575	2.1	0.062	Beutekamp (2002)
47	AC, Calgon F-400	850-998	N_2	22	318.2	1060	2.577	0.4	0.012	OSU (2001)
48	AC, Calgon F-400	850-998	CH_4	40	318.2	1385	3.164	1.4	0.064	OSU (2001)
49	AC, Calgon F-400	850-998	CO_2	52 10	318.2 328.2	1710	4.500 4.259	4.4 3.8	0.222 0.206	OSU (2001)
50	AC, Calgon F-400	850-998	C_2H_6	21	318.2	2135	2.835	6.4	0.153	OSU (2001)
Overall				**2242**				**3.6**		

especially for the CO_2 and propane isotherms. These larger errors are partly due to the high uncertainty in the CO_2 and propane bulk density calculation. Also, the percentage deviation is exaggerated when the Gibbs excess adsorption becomes exceedingly small; i.e. at lower pressures, at high temperatures, or at nearly full coverage adsorption at higher pressures. For the OSU adsorption data set (Systems 47-50), the OK model is capable on average of representing the data within their experimental uncertainties.

Figure 27 shows the percentage deviation plot for the OK model representation of the adsorption data on activated carbon. About 90% of the data can be represented by the model within 8.4 % AAD. As mentioned above, the large percentage deviations occurred mainly when the Gibbs excess adsorption values are small at relatively low pressures. Figure 28 illustrates the OK model representation of System 15 (CO_2 on Norit R1 Extra activated carbon), where the percentage deviations are large (9.5 % AAD). As shown in the figure, the model can actually represent the experimental data reasonably well at pressure above 0.5 MPa. The nitrogen and methane adsorption on the same activated carbon are also shown in the figure for comparison.

Figure 29 illustrates the OK model representation of a system with significant temperature range. As shown in this figure, the model is capable of describing the temperature variation.

Basis for Parameter Generalization

Based on our preliminary evaluation of the regressed parameter C presented in Table 10, it appears that, for a given adsorbate at fixed temperature, the value of C increases as the surface area of the adsorbent increases. This suggests that the maximum
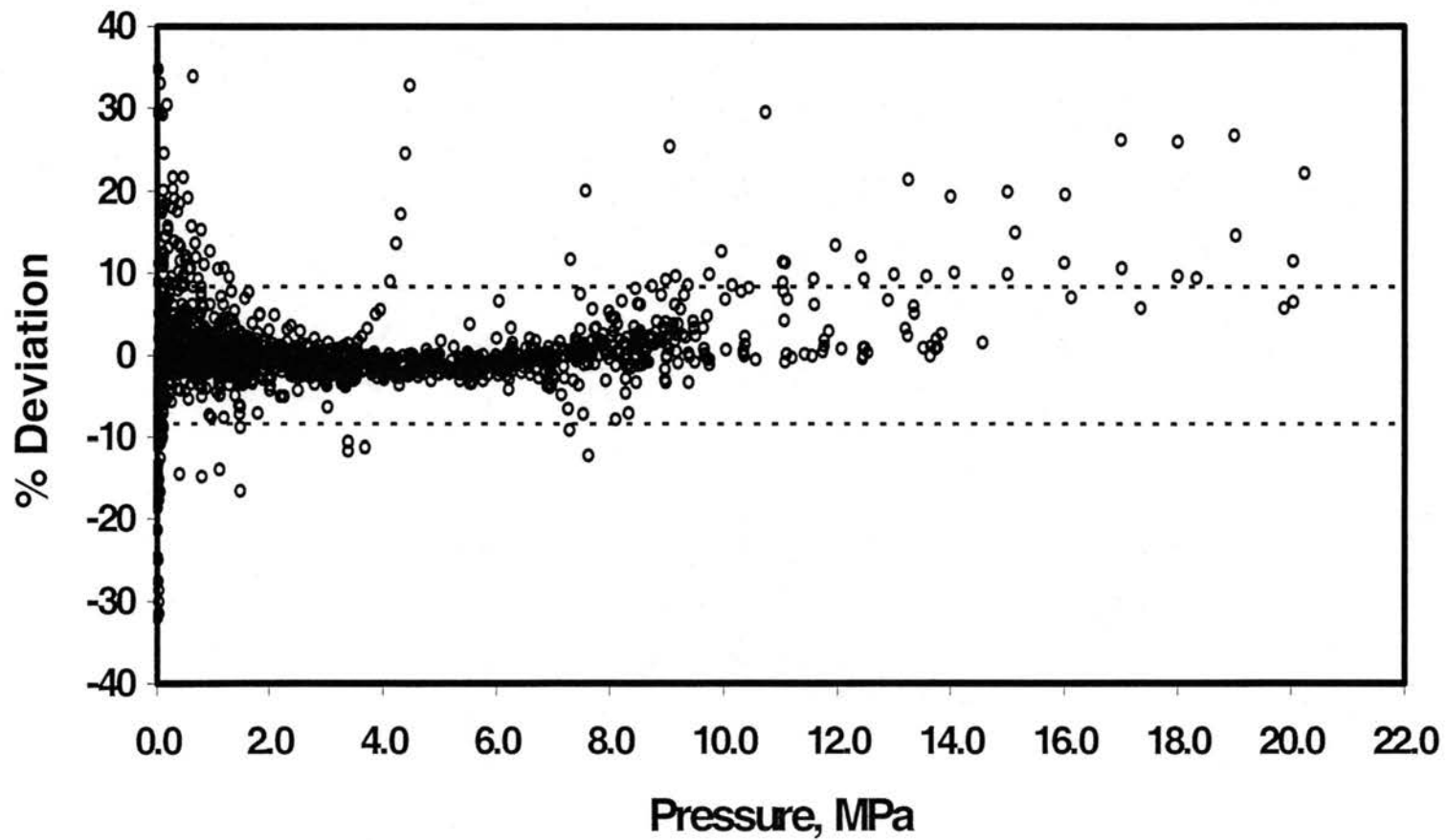
Figure 27. Deviation Plot for Two-Parameter OK Model Representations of Gas Adsorption on Activated Carbon
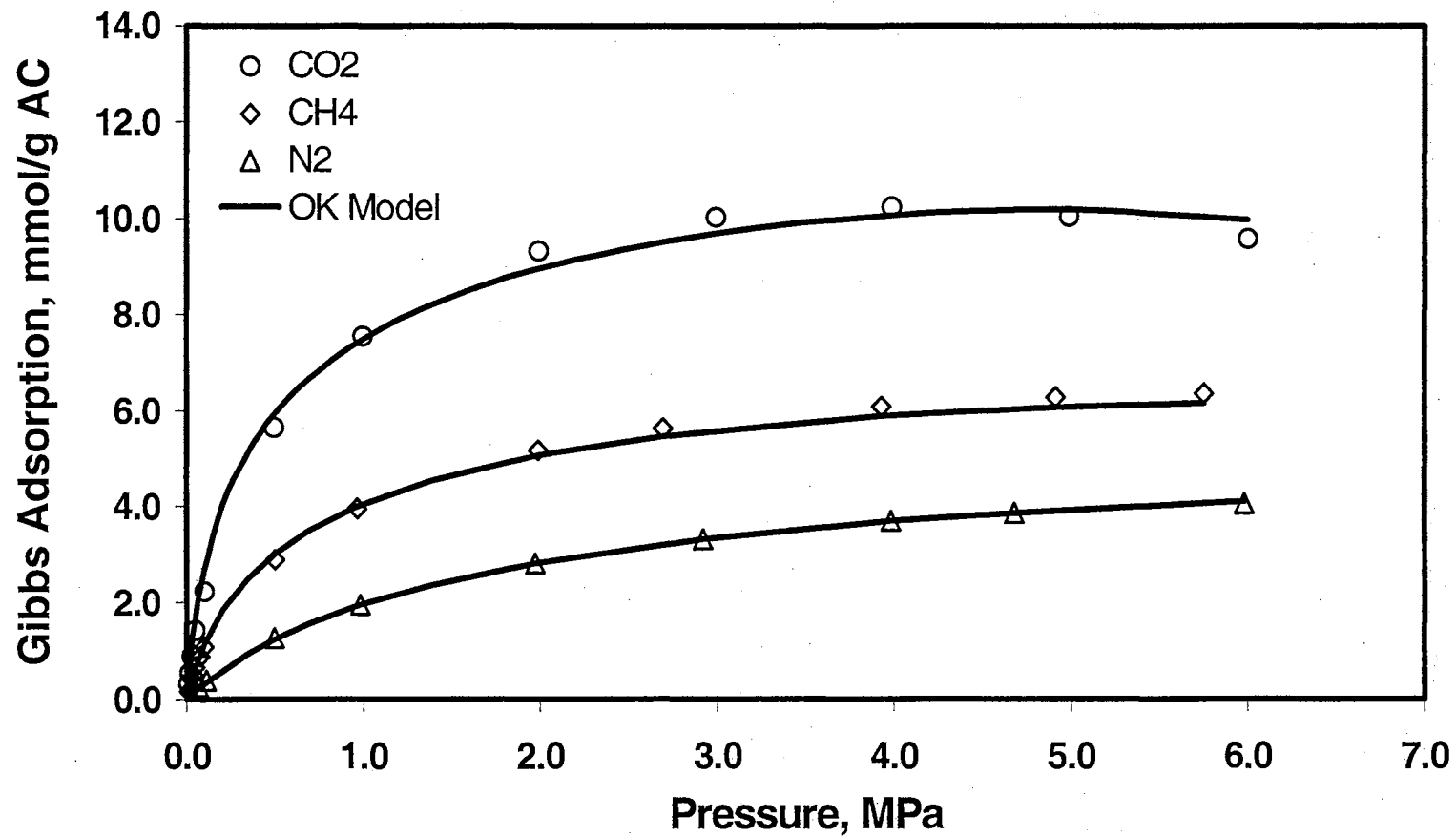
Figure 28. OK Model Representations of Gas Adsorption on Norit R1 Extra Activated Carbon at 298 K (Dreisbach, 1999)
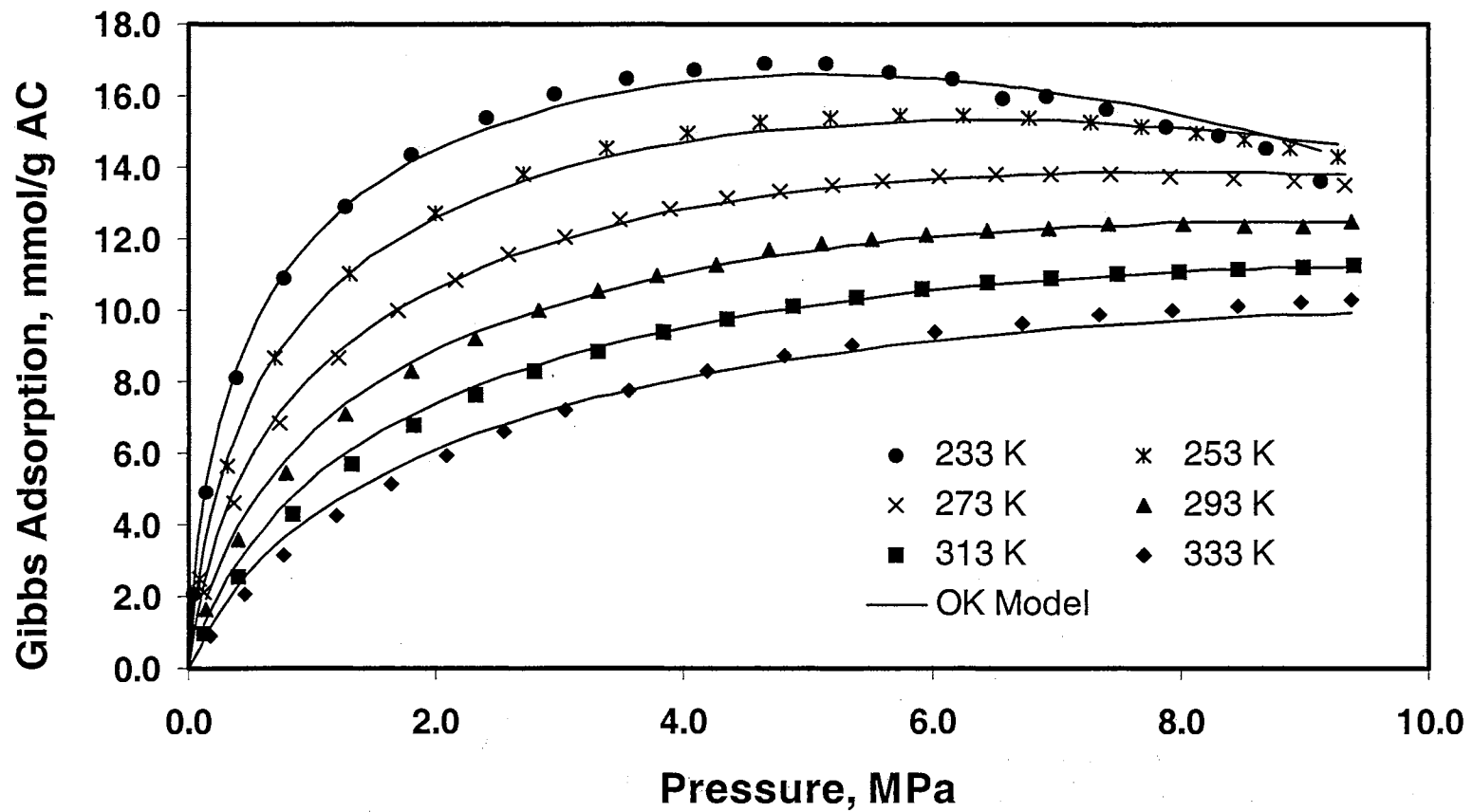
Figure 29. OK Model Representations of Methane Adsorption on Activated Carbon (Zhou, 2000)

adsorption capacity, C, can be divided into two contributions; i.e. the contribution from the adsorbent characteristics, represented by surface area (A, m^2/g), and the contribution from the adsorbate characteristic(s). In this study, we proposed the following simple relation for the maximum adsorption capacity, C:

$$C(T) = \frac{AC_a(T)}{2}$$ (6-8)

C_a is the surface adsorbed-phase density (mmol/m^2), with its value depending only on the adsorbate.

C is also temperature dependent. As reported in Table 10, the value of C increases as temperature decreases. This temperature dependence of the maximum adsorption capacity is not uncommon, based on the previous studies. Benard and Chahine (1997; 2001) reported the temperature dependence of C, and they proposed an empirical temperature relation for C. Similarly, Do (1998) asserted that the maximum adsorption capacity in the Langmuir model was a function of temperature. He described this temperature dependence as due to the thermal expansion of the adsorbed phase.

Because of its theoretical basis, we adopted Do's approach and used the following thermal expansion expression for evaluating the surface adsorbed-phase density:

$$\frac{dC_a/dT}{C_a} = -\delta$$ (6-9)

Integrating Equation (6-9) and combining with Equation (6-8) results in:

$$ln(1/C) = \delta T - [ln\,C_{a,o} + \delta T_o + ln(A/2)]$$ (6-10)

where T_o (K) is chosen at the normal boiling point of the adsorbate (triple point for CO_2), T (K) is the absolute temperature, $C_{a,o}$ is the maximum surface adsorbed-phase density at T_o, and δ is the thermal expansion coefficient of the adsorbed phase.

For a given system, Equation (6-10) yields a linear correlation if $ln(1/C)$ is plotted

against temperature, T. Figure 30 presents the correlation between $ln(1/C)$ obtained from

Table 10 for gas adsorption on BPL activated carbon (Reich, 1980) and temperature, T.
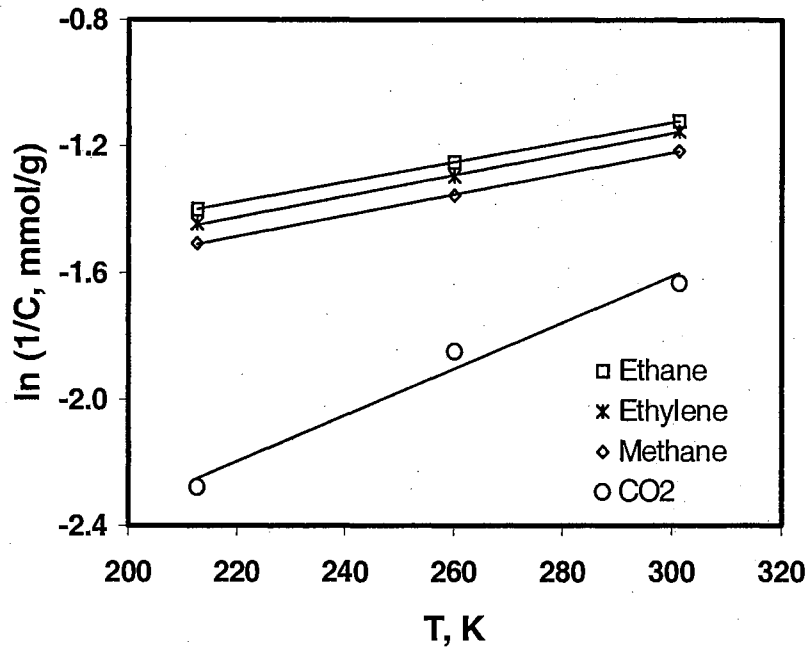
Figure 30. Temperature Dependence of the Maximum Adsorption Capacity, C,
(Reich, 1980)

The linear relationship shown in this figure suggests that Equation (6-10) provides a good

representation of the temperature dependence of the maximum adsorption capacity, C.

The values of $C_{a,o}$ and δ depend only on the adsorbate; therefore, a linear

correlation should also be obtained if C is plotted against A at constant temperature.

Figure 31 presents the plots of parameter C obtained in Table 10 against the surface area,

A. The values of the surface areas, in most cases, were reported by the investigators. In

a few cases, however, they were obtained from the information provided by the adsorbent

102
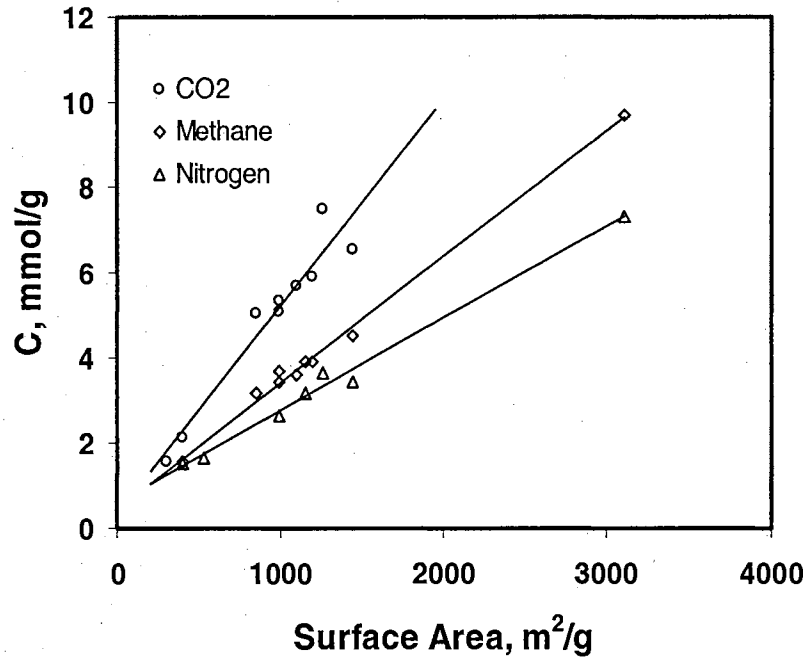
Figure 31. Correlation of the Maximum Adsorption Capacity, C, with Surface Area at Constant Temperature

production company or estimated from the literature. Although the accuracy of the reported surface areas is questionable, Figure 31 still shows a reasonable linear correlation between the parameter C and the surface area, A. This observation further supports the assumption made in Equation (6-8).

The fluid-solid energy parameter, ε_{is}/k, was generalized based on the interaction of a single molecule with a single lattice plane. If z is the distance between the adsorbate molecule i and the lattice carbon plane, the potential energy can be written as:

$$\Phi_{i,SLP} = 4\pi\rho_c\varepsilon_{iC}^*\sigma_{iC}^2\left[\frac{1}{5}\left(\frac{\sigma_{iC}}{z}\right)^{10} - \frac{1}{2}\left(\frac{\sigma_{iC}}{z}\right)^4\right] \qquad (6-11)$$

The potential energy has a minimum at a depth given by:

$$\varepsilon_{is} = -\frac{6}{5}\pi\rho_c\varepsilon_{iC}^*\sigma_{iC}^2 \qquad (6-12)$$

where ρ_c = 0.382 atom/Å^2 is the area density of carbon atoms in a graphite plane. The adsorbate-carbon collision diameter is estimated as $\sigma_{iC} = \frac{1}{2}(\sigma_{ii} + \sigma_{CC})$. The adsorbate-carbon well depth potential is estimated as $\varepsilon_{iC}^* = \sqrt{\varepsilon_{ii}^* \varepsilon_{CC}^*}$.

Generalization of the model parameters was performed by evaluating $C_{a,o}$, δ and ε_{CC}^* of the systems studied. All other physical properties of the adsorbate and carbon atom used are listed in Table 11. Five case studies described in Table 12 were explored. For each case, 1520 independent adsorption data points were employed. These data include all the activated carbon systems shown in Table 10, excluding systems that have only one adsorption isotherm. These systems were used later to validate the generalized model.

In Case 1, all the parameters, $C_{a,o}$, δ and ε_{CC}^*, were optimized simultaneously, while the surface area was taken from information provided in the literature. Table 13 shows the parameters obtained in Case 1. The regressed solid-solid energy parameter, ε_{CC}^* / k, varied from 38 to 43 K.

For all components studied, except CO_2, the mean thermal expansion coefficient of the adsorbed phase, δ, was approximately 0.0024 K^{-1}. This value is close to the 0.0025 K^{-1} value estimated by Wakasugi (1981) for all components. However, the regressed δ for CO_2 is much higher (0.0039 K^{-1}).

The maximum surface adsorbed-phase density at T_o (normal boiling point), $C_{a,o}$, obtained in Case 1 was correlated with the diameter of the adsorbed molecules. Figure 32 shows a linear correlation between $C_{a,o}$ and the reciprocal square of the molecule diameter. This finding is not unexpected since for a close-packed hard sphere molecule,

Table 11. Physical Properties of the Adsorbates[a] and Active Sites

Adsorbate	MW	Pc (MPa)	Tc (K)	Normal Boiling Point (K)	Reciprocal van der Waals co-volume (mol/L)	σ (x10^{-10} m)	ε*/k (K)
H_2	2.02	1.31	33.19	20.4	38.16	2.827	59.7
N_2	28.01	3.40	126.20	77.3	25.89	3.798	71.4
H_2S	34.08	8.96	373.53	212.8	23.08	3.623	301.1
CO_2	44.01	7.38	304.21	216.6 [b]	23.34	3.941	195.2
CH_4	16.04	4.60	190.56	111.7	23.37	3.758	148.6
C_2H_4	28.05	5.04	282.34	169.4	17.39	4.163	224.7
C_2H_6	30.07	4.87	305.32	184.6	15.41	4.443	215.7
C_3H_8	44.10	4.25	369.83	231.1	11.07	5.118	237.1
i- C_4H_{10}	58.12	3.65	408.14	261.4	8.60	5.278	330.1
C						3.4[c]	28[c]
O(Zeolite)						3.04[d]	139.96[d]

[a] Reid (1987)
[b] Triple point temperature
[c] Steele (1974)
[d] Mellot (1996)

Table 12. Description of the Cases Studied in Model Generalization

Case No	Description	Overall %AAD
1	Based on reported surface area, A $C_{a,o}$ and δ are regressed for specific adsorbate ε_{cc}/k is regressed for specific activated carbon	7.2

2	Based on reported surface area, A
	Generalized $C_{a,o}$ and δ:
	    For CO_2: $C_{a,o} = 0.0142$ mmol/m^2; $\delta = 0.0039$ (K^{-1})
	    For other component:
	        $C_{a,o} = 0.102/\sigma^2 + 0.0034$; σ in Å
	        $\delta = 0.0024$ (K^{-1})
	ε_{cc}/k (K) is obtained from Case 1 (varied from 38 to 43)
		7.3

3	Based on reported surface area, A
	Generalized $C_{a,o}$ and δ:
	    For CO_2: $C_{a,o} = 0.0142$ mmol/m^2; $\delta = 0.0039$ (K^{-1})
	    For other component:
	        $C_{a,o} = 0.102/\sigma^2 + 0.0034$; σ in Å
	        $\delta = 0.0025$ (K^{-1})
	ε_{cc}/k (K) = 40
		7.4

4	Surface area, A, is regressed
	Generalized $C_{a,o}$ and δ:
	    For CO_2: $C_{a,o} = 0.0142$ mmol/m^2; $\delta = 0.0039$ (K^{-1})
	    For other component:
	        $C_{a,o} = 0.102/\sigma^2 + 0.0034$; σ in Å
	        $\delta = 0.0023$ (K^{-1})
	ε_{cc}/k (K) is obtained from Case 1 (varied from 38 to 43)
		6.3

5	Surface area, A, is regressed
	Generalized $C_{a,o}$ and δ:
	    For CO_2: $C_{a,o} = 0.0142$ mmol/m^2; $\delta = 0.0039$ (K^{-1})
	    For other component:
	        $C_{a,o} = 0.102/\sigma^2 + 0.0034$; σ in Å
	        $\delta = 0.0023$ (K^{-1})
	ε_{cc}/k (K) = 40
		7.0

Table 13. Parameters Used in Case 1 of Model Generalization

Component	$C_{a,o}$ (mmol/m^2)	δ (K^{-1})	ε_{cc}/k (K)
N$_2$	0.0105	0.0024	
CH$_4$	0.0106	0.0024	
C$_2$H$_4$	0.00945	0.0024	
C$_2$H$_6$	0.00831	0.0024	
C$_3$H$_8$	0.00735	0.0024	
CO$_2$	0.0142	0.0039	
Activated Carbon			38 - 43
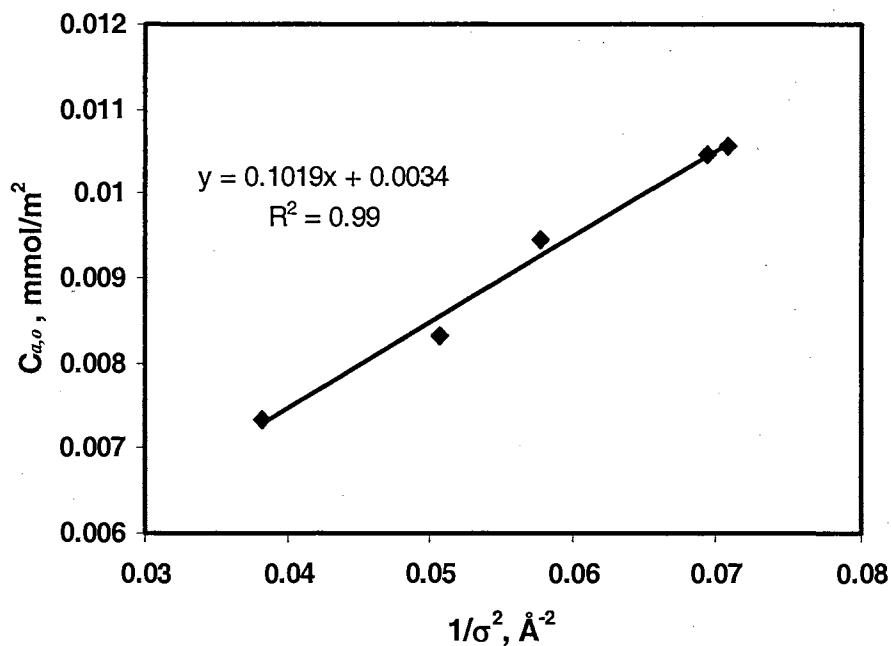
Figure 32. Variation of the Maximum Surface Adsorbed-Phase Density, $C_{a,o}$, with the Diameter of the Molecules, σ

the surface density will be equal to $\sqrt{2}/N_{av}\sigma^2$, where N_{av} is the Avogadro's number. However, $C_{a,o}$ is much higher for CO_2, and it does not follow the observed linear trend for the other adsorbates.

In Case 2, the general linear correlation for $C_{a,o}$ obtained in Case 1 was applied. A constant δ obtained in Case 1 was also used in Case 2. As shown in Table 12, the overall percentage deviations obtained in Case 1 is practically the same as for Case 2. The overall percentage deviations did not change significantly (about 7% AAD) when the solid-solid energy parameter, ε_{CC}^*/k was set constant at 40 K in Case 3.

Slightly better results were obtained when the surface area was regressed, as in Case 4 (6.4 %AAD). In this case, the regressed surface area deviated up to 8% from the reported surface area. Moreover, as shown in Case 5, using the regressed surface area and a constant solid-solid energy parameter, ε_{CC}^*/k = 40 K, the model can predict the adsorption isotherms with an AAD of 7%.

Figure 33 shows the percentage deviation plot for the generalized OK model prediction of the adsorption data on activated carbon. About 90% of the data can be predicted by the generalized model within 14.5 % AAD. Figure 34 illustrates the comparison of generalized (Case 5) and two-parameter OK model representation of methane adsorption on activated carbon (System 22). As illustrated in the figure, the generalized model can predict the adsorption isotherms about twice the error of the two-parameter OK model. The results of the five cases above suggest that the gas adsorption can be predicted using the generalized OK model with the average deviation of about 7% AAD.
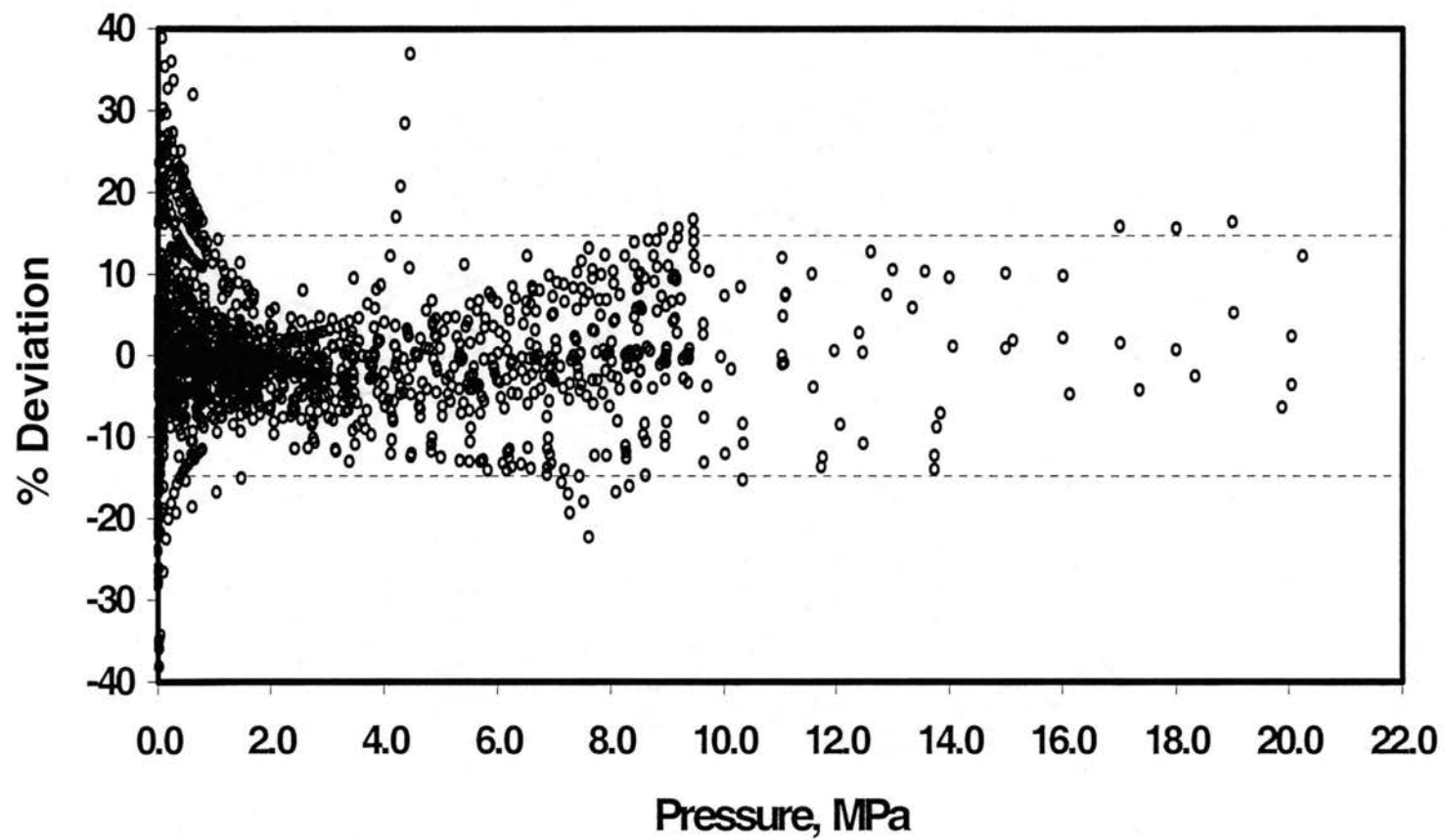
Figure 33. Deviation Plot for the Generalized OK Model Predictions of Gas Adsorption on Activated Carbon
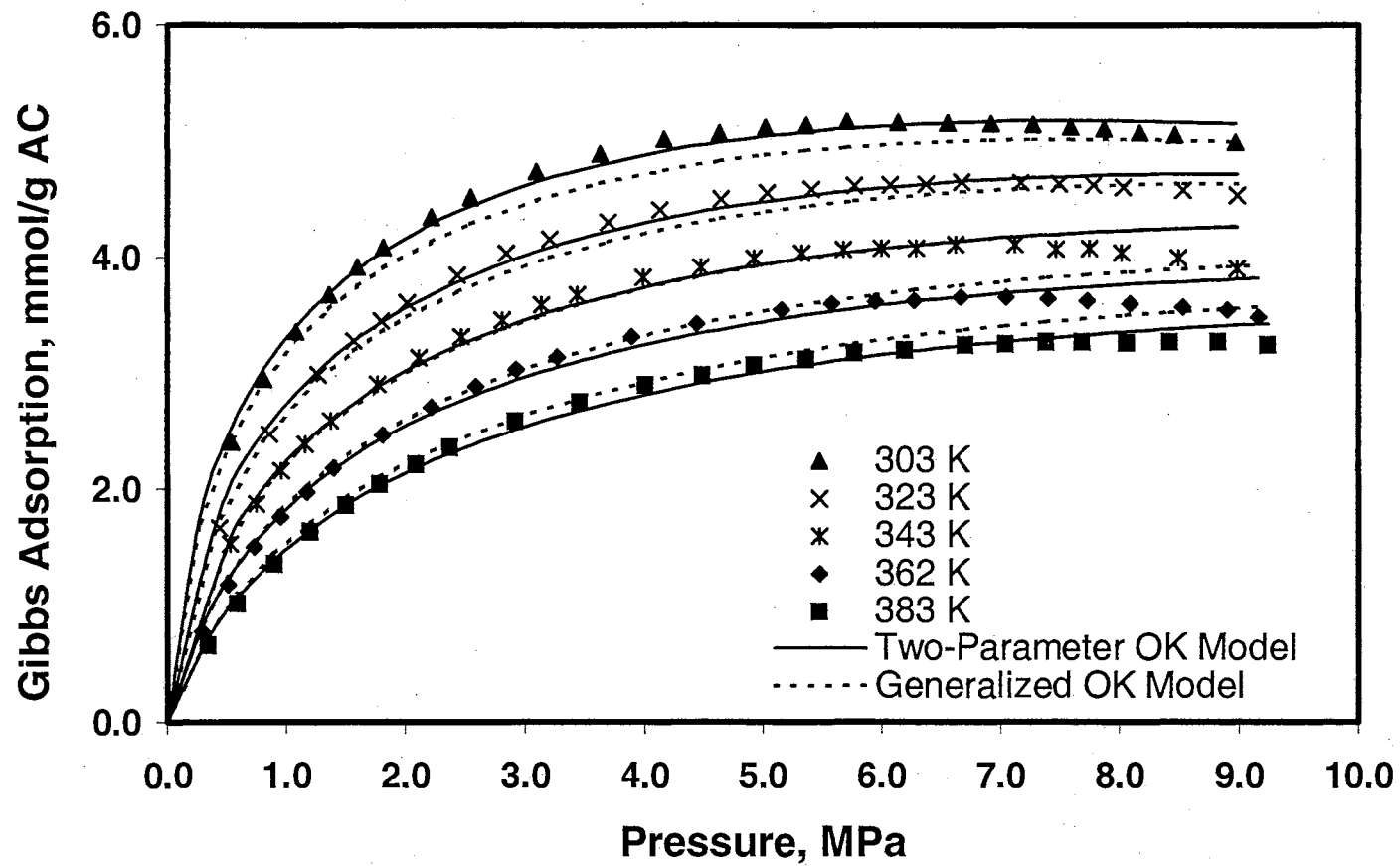
Figure 34. Comparison of the Generalized Predictions and Two-Parameter OK Model Representations of Methane Adsorption on Activated Carbon (Frere, 2000)

Several gas adsorption systems were subsequently used to validate this generalized OK model. Figure 35 shows the generalized OK model prediction of our gas adsorption measurements on activated carbon at 318.2 K. A surface area of 920 m²/g and the solid-solid energy parameter, ε_{CC}^* / k, of 39 K, were obtained from the best fit to the CO_2 adsorption data. Using this information and the generalized $C_{a,o}$ and δ, the adsorption isotherms for the other three gases were then *predicted*. A similar prediction procedure was applied for the other systems, confirming that the gas adsorption on activated carbon can be predicted using the generalized OK model with about 7% AAD or about twice the error of the two-parameter OK model.

Modeling of Pure-Gas Adsorption on Coals

Two-Parameter OK Model for Pure-Gas Adsorption on Coals

Similar to our treatment of pure-gas adsorption on activated carbon, we modeled pure-gas adsorption on coals using the adsorbed-phase density and the fluid-fluid energy parameters estimated from the reciprocal van der Waals co-volume and from the Lennard-Jones 12-6 potential, respectively. Our gas adsorption measurements on several coals were used to evaluate the fluid-solid energy parameter, ε_{is}/k, and the parameter C in the OK model. The weighted average deviation of the Gibbs excess adsorption (WAAD) was used as the objective function to determine the two model parameters.

Table 14 presents the results of our model representation of the above selected data. Overall, for 308 data points, the OK model with two regressed parameters can represent the data within the expected experimental uncertainties, which corresponds to 3.3% AAD. Specifically, the two-parameter OK model representation of gas adsorption
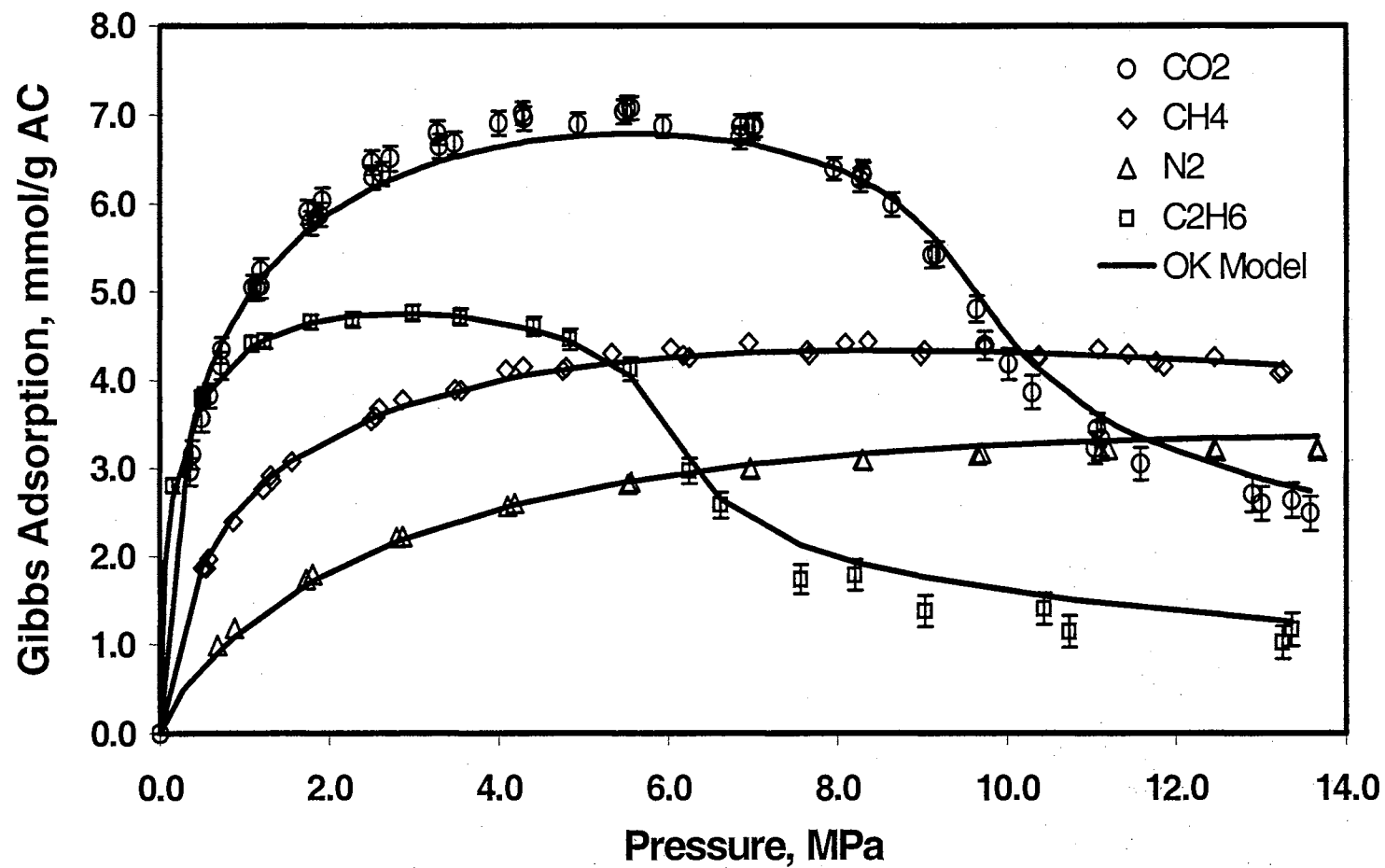
Figure 35. OK Model Predictions of Gas Adsorption on Activated Carbon at 318.2 K (OSU, 2000)

Table 14. Results of Two-Parameter OK Model for Pure-Gas Adsorption on Coals

System No.	Adsorbent	Adsorbate	NPTS	T (K)	$-\varepsilon_{is}/k$ (K)	C (mmol/g)	%AAD	RMSE (mmol/g)	WAAD
55a	Wet Fruitland Coal #1	N_2	20	319.3	610	0.572	1.3	0.005	0.2
56a	Wet Fruitland Coal #1	CH_4	20	319.3	990	0.650	0.8	0.004	0.2
57a	Wet Fruitland Coal #1	CO_2	14	319.3	1340	0.853	5.1	0.091	0.5
55b	Wet Fruitland Coal #2	N_2	20	319.3	575	0.495	1.8	0.004	0.2
56b	Wet Fruitland Coal #2	CH_4	20	319.3	960	0.663	0.8	0.005	0.4
57b	Wet Fruitland Coal #2	CO_2	20	319.3	1280	0.887	6.7	0.087	0.7
61	Wet Illinois #6 Coal	N_2	20	319.3	450	0.331	2.4	0.002	0.2
62	Wet Illinois #6 Coal	CH_4	20	319.3	780	0.468	1.7	0.005	0.3
63	Wet Illinois #6 Coal	CO_2	20	319.3	1100	0.735	3.2	0.033	0.5
67	Wet Tiffany Coal	N_2	21	327.5	530	0.287	3.3	0.003	0.4
68	Wet Tiffany Coal	CH_4	22	327.5	930	0.356	3.4	0.012	0.6
69	Wet Tiffany Coal	CO_2	16	327.5	1385	0.433	4.2	0.022	0.6
74	Wet LB Fruitland Coal	N_2	16	319.3	530	0.213	4.3	0.004	0.4
75	Wet LB Fruitland Coal	CH_4	16	319.3	815	0.327	2.6	0.007	0.5
76	Wet LB Fruitland Coal	CO_2	29	319.3	1300	0.354	5.4	0.023	0.6
77	Dry Illinois #6 Coal	CO_2	11	328	1250	1.204	5.1	0.067	0.9
78	Dry Beulah Zap Coal	CO_2	22	328	1375	1.3540	3.3	0.071	0.5
79	Dry Wyodak Coal	CO_2	11	328	1270	1.5039	2.9	0.064	0.5
80	Dry Upper Freeport Coal	CO_2	11	328	1480	0.6768	2.2	0.026	0.4
81	Dry Pocahontash Coal	CO_2	11	328	1540	0.7979	1.8	0.023	0.3
Overall			360				3.1		0.5

on wet Fruitland coal gives comparable results to three-parameter models such as LRC and 2-D EOS used by Zhou (1994).

Model Generalization for Pure-Gas Adsorption on Coals

The same approach used for activated carbon was used to determine the parameter C in the gas adsorption model on coals. Specifically, we used a generalized $C_{a,o}$ and δ obtained from the modeling on activated carbon. The surface area of the coals, however, was regressed from the experimental adsorption data, since the surface area is very specific to the coal samples and is also dependent on the wetness of the coals studied.

The fluid-solid energy parameter, ε_{is}/k, for adsorption on coals, as shown in Table 14, is much lower than that on activated carbon. This lower value might be attributed to the mean position of a molecule in the structure of the coals and the presence of water. Figure 36 illustrates the molecule positions in the slit of the activated carbon and coals. In activated carbon, the distance between a molecule and surface plane, z, is approximately equal to the collision diameter of the two atoms, i.e. $z = \sigma_{ic}$. Due to wider slit length of the coals (Gan, 1972), the distance between a molecule and surface plane of the coal might be slightly higher than σ_{ic}. Therefore, the fluid-solid energy for pure adsorption on coals was calculated according to Equation (6-11) instead of Equation (6-12). Furthermore, the chemical structure of the coal is much more complex than that of activated carbon. The wetness of the coal might also affect the regressed overall fluid-solid energy. Therefore, we proposed a modification of Equation (6-11):

$$\Phi_{i,SLP} = \varepsilon_{is} / k = 4\pi\rho_c \varepsilon_{iC}^* \sigma_{iC}^2 \varphi_c (1 + \xi_f) \left[\frac{1}{5}\left(\frac{\sigma_{iC}}{z}\right)^{10} - \frac{1}{2}\left(\frac{\sigma_{iC}}{z}\right)^4 \right] \qquad (6\text{-}13)$$

114
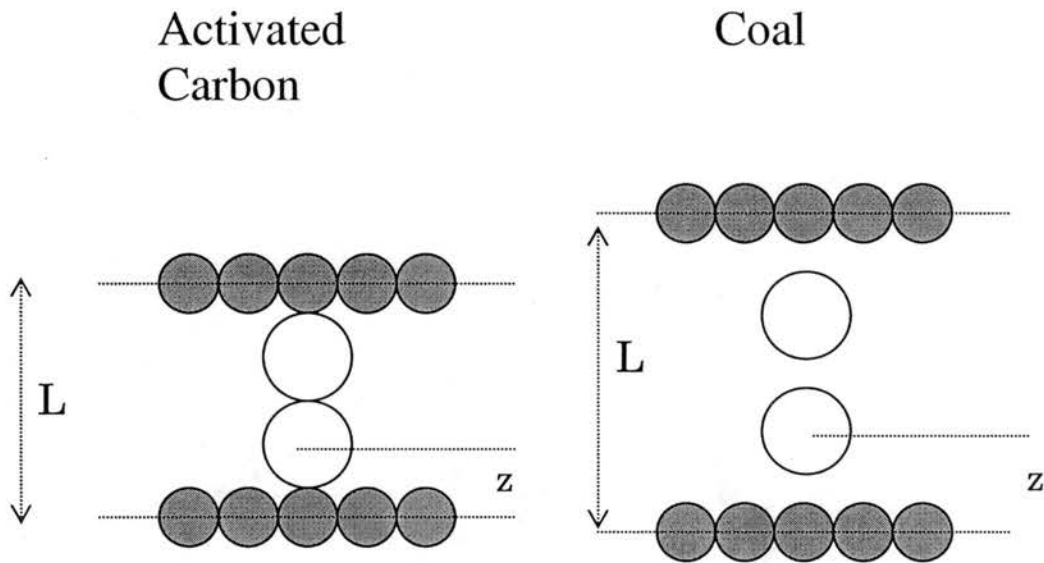
Figure 36. Molecule Positions in the Slit of the Activated Carbon and Coal

A correction, ξ_f was introduced to take into account for the effect of adsorbent chemical structure on the adsorbate. This value is close to zero for adsorption on activated carbon, and was generalized based on the chemical composition of the coals. A moisture correction effect, φ_c, was calculated as a function of the ash-free coal not occupied by equilibrium moisture content. This value of φ_c is available experimentally. A more rigorous way to handle the water effect would be to use a multicomponent model by treating the water as an additional adsorbed component. In our current stage of study, however, such a model is still under development. For simplicity, therefore, the correction above was introduced in this study.

In summary, the model generalization for gas adsorption on coals was performed in the following sequence:

1. Parameter C was calculated using Equation (6-7), where generalized $C_{a,o}$ and δ as shown in Table 12, Case 2, were applied. The surface area, A, was optimized for each coal.

2. The fluid-solid energy parameter, ε_{is}/k, was calculated using Equation (6-10), where the distance between a molecule and surface plane, z, was optimized for each coal, and the correction ξ_f was optimized for a specific adsorbate-coal system. The solid-solid energy parameter, ε_{cc}^*/k, was set 40 K.

3. The correction ξ_f was generalized by the following contribution method:

$$\xi_f = R_{VC}(ax_O + bx_H + cx_N + dx_S + e)$$ (6-14)

where R_{VC} is the ratio of the volatile to the fixed carbon contents (on dry basis) and x_O, x_H, x_N and x_S are the oxygen, hydrogen, nitrogen and sulfur contents in the coals (on dry basis), respectively.

Many researchers have tried to correlate the gas adsorption capacity in terms of the carbon content or the ratio of the volatile-to-the-fixed carbon content and the oxygen content (Moffat and Weale, 1955, Toda et al., 1970, Joubert et al., 1974, Levy et al., 1997, McCutcheon et al., 2003). Their hypothesis is that the chemical contents of the coal may produce specific available surface area of the coal. However, the chemical contents also reflect the types of functional group attached in carbon matrices, which affect the fluid-solid interaction energy. We do not evaluate the chemical contents effect on the surface area, and the surface area is regressed in this study. However, we used an

empirical correlation shown by Equation (6-14) to account for the effect of chemical contents on the fluid-solid interaction energy.

Our pure-gas adsorption data on activated carbon, Fruitland coal, Lower Basin (LB) Fruitland coal and Illinois #6 coal were employed to evaluate the correction function in Equation (6-14). Because of the limited available data, only three factors in Equation (6-14) were considered in the evaluation, i.e. the ratio of the volatile-to-the-fixed carbon contents, the oxygen content and the hydrogen content (the coefficients c and d are assumed zero). Regression results yielded the coefficients in Equation (6-14) as: $a = 0.141$, $b = 0$, $e = 0.075$ for CO_2; $a = 0$, $b = 0.166$, $e = 0.033$ for methane; and all coefficients are zero for nitrogen.

Tables 15 and 16 show the parameters used in the generalized OK model for pure-gas adsorption on wet and dry coals. The generalized OK model can represent the data with about 5.3% AAD and 3.0% AAD for gas adsorption on wet coals and dry coals, respectively. Figures 37-40 show the comparison of the two-parameter OK model representations and generalized OK model predictions for gas adsorption on wet coals (Figure 37-36) and CO_2 adsorption on dry coals (Figure 40). As shown in the figures, the generalized model can predict the data almost as well as the two-parameter model does. Larger deviations, however, are obtained for the CO_2 adsorption in the region above 8 MPa. The low-sorbing nature of coal and the high uncertainties of the CO_2 bulk density may have amplified the deviations in this region. The possibility of coal swelling when CO_2 is adsorbed at high pressure might also contribute to this large deviation.

Pure-gas adsorption on Tiffany coal at 327.6 K was used to validate the generalized OK model. Figure 41 shows the generalized OK model prediction of our gas

Table 15. Summary Results for Generalized OK Modeling of Pure-Gas Adsorption on Wet Coals

Model Parameters	Pure-Gas Adsorbed		
	Methane	Nitrogen	CO_2
Wet Fruitland Coal (φ_c=0.97)			
A (m^2/g)	194		
z	$1.296\ \sigma_{ic}$		
NPTS	20	20	20
% AAD	3.2	4.8	8.5
RMSE (mmol/g)	0.019	0.013	0.087
Wet Illinois #6 Coal (φ_c=0.97)			
A (m^2/g)	150		
z	$1.448\ \sigma_{ic}$		
NPTS	20	20	20
% AAD	2.6	4.4	3.5
RMSE (mmol/g)	0.008	0.004	0.037
Wet LB Fruitland (φ_c=0.95)			
A (m^2/g)	77		
z	$1.296\ \sigma_{ic}$		
NPTS	16	16	29
% AAD	4.9	6.4	8.3
RMSE (mmol/g)	0.019	0.007	0.036

Table 16. Summary Results for Generalized OK Modeling of CO_2 Adsorption on Dry Coals

Model Parameters	Beulah Zap	Wyodak	Illinois #6	Upper Freeport	Pocahontas
A (m^2/g)	298	332	251	149	177
z	$1.657\ \sigma_{ic}$	$1.653\ \sigma_{ic}$	$1.530\ \sigma_{ic}$	$1.277\ \sigma_{ic}$	$1.163\ \sigma_{ic}$
NPTS	22	11	11	11	11
% AAD	3.3	2.9	4.4	2.5	1.8
RMSE (mmol/g)	0.068	0.058	0.062	0.025	0.024
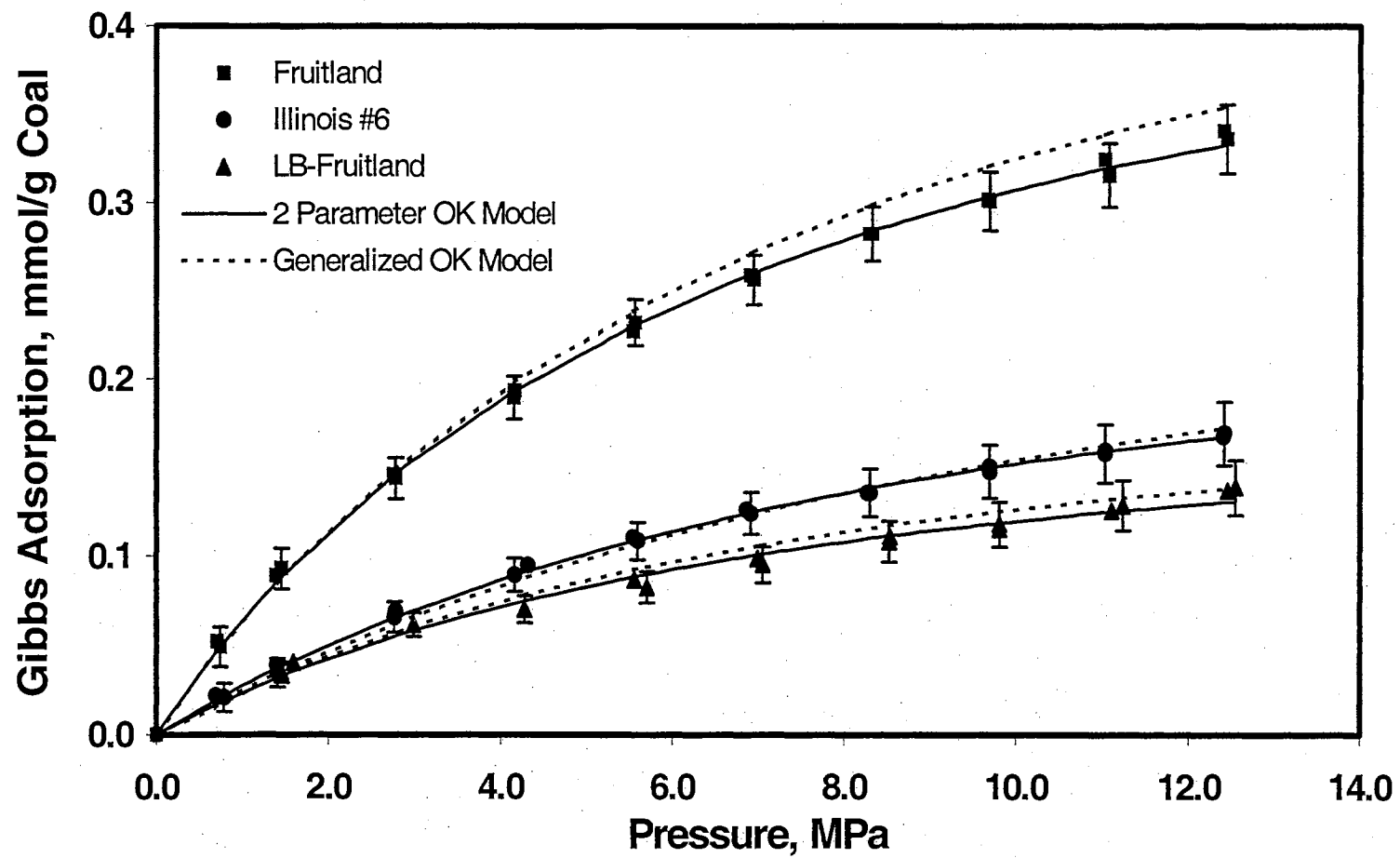
Figure 37. OK Model Representations of Nitrogen Adsorption on Wet Coals at 319. 3 K
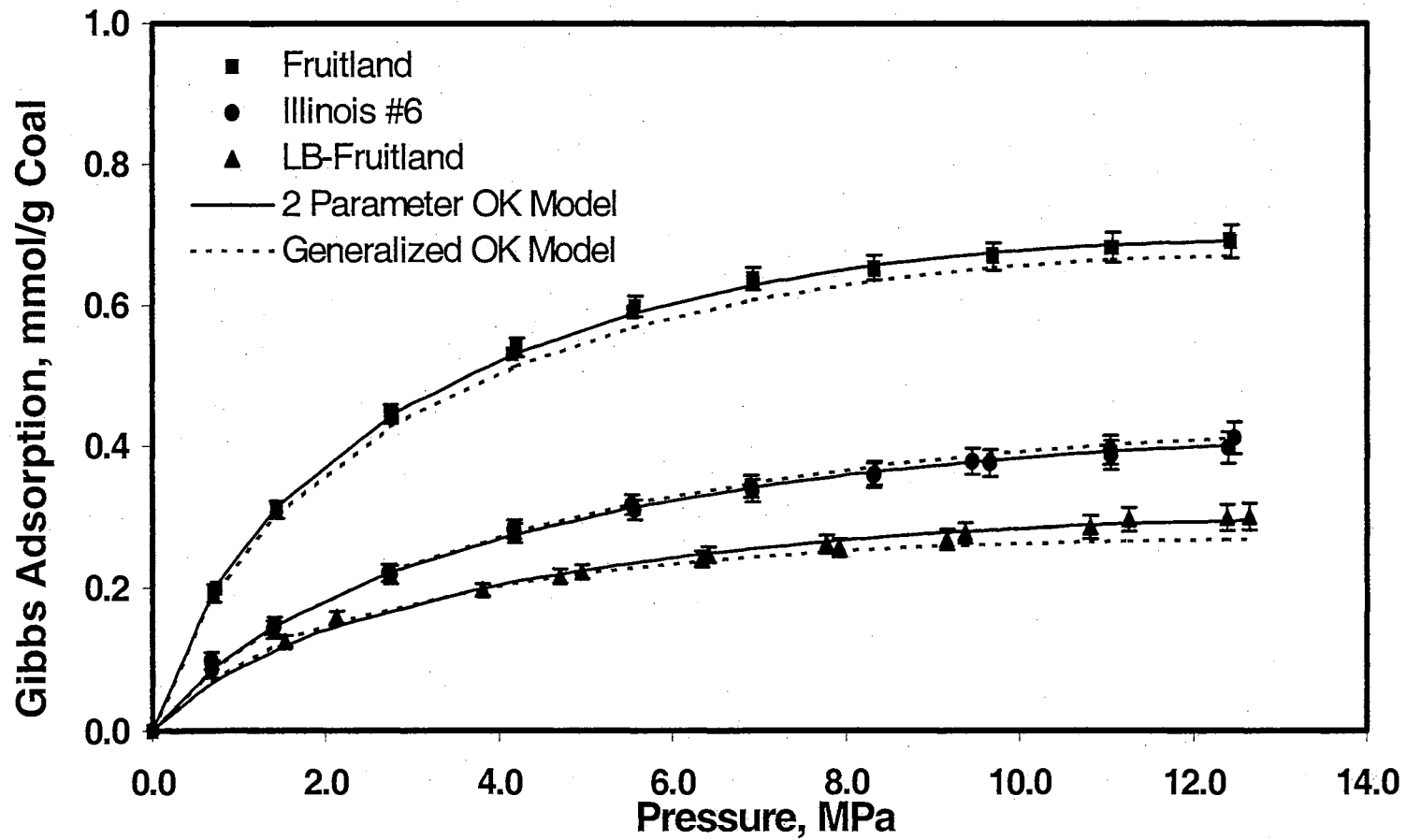
Figure 38. OK Model Representations of Methane Adsorption on Wet Coals at 319. 3 K
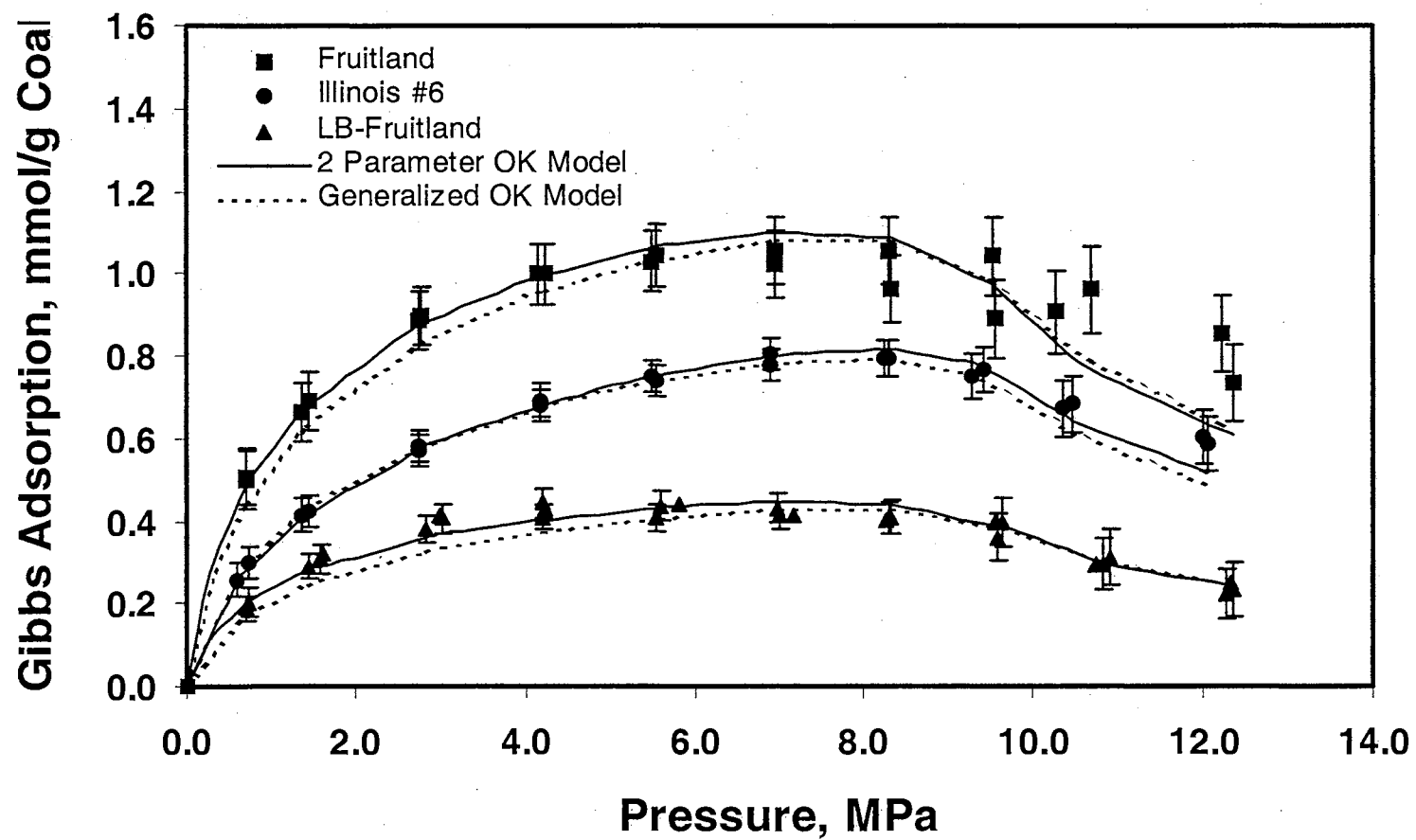
Figure 39. OK Model Representations of CO_2 Adsorption on Wet Coals at 319. 3 K
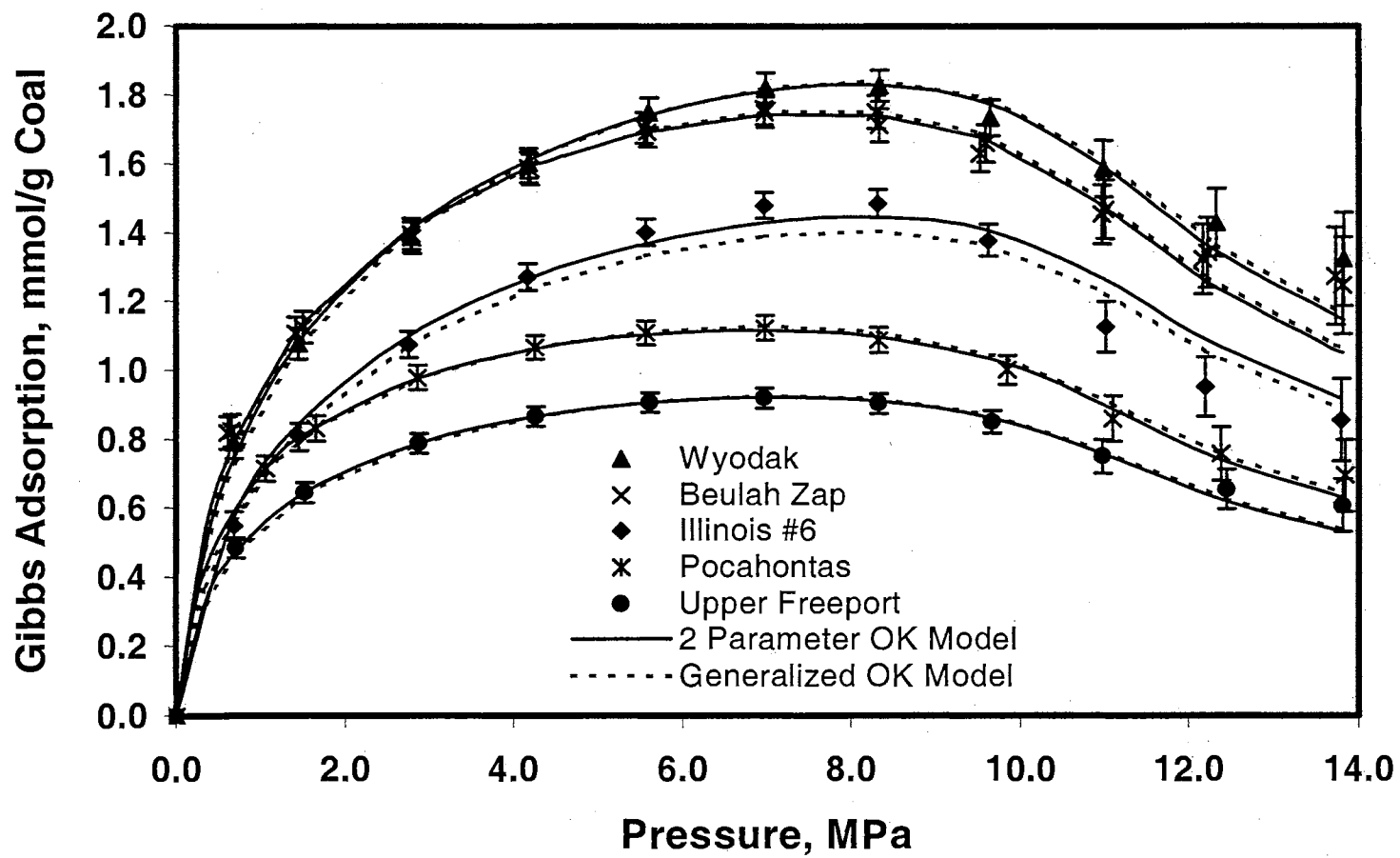
Figure 40. OK Model Representations of CO_2 Adsorption on Dry Coals at 328.2 K
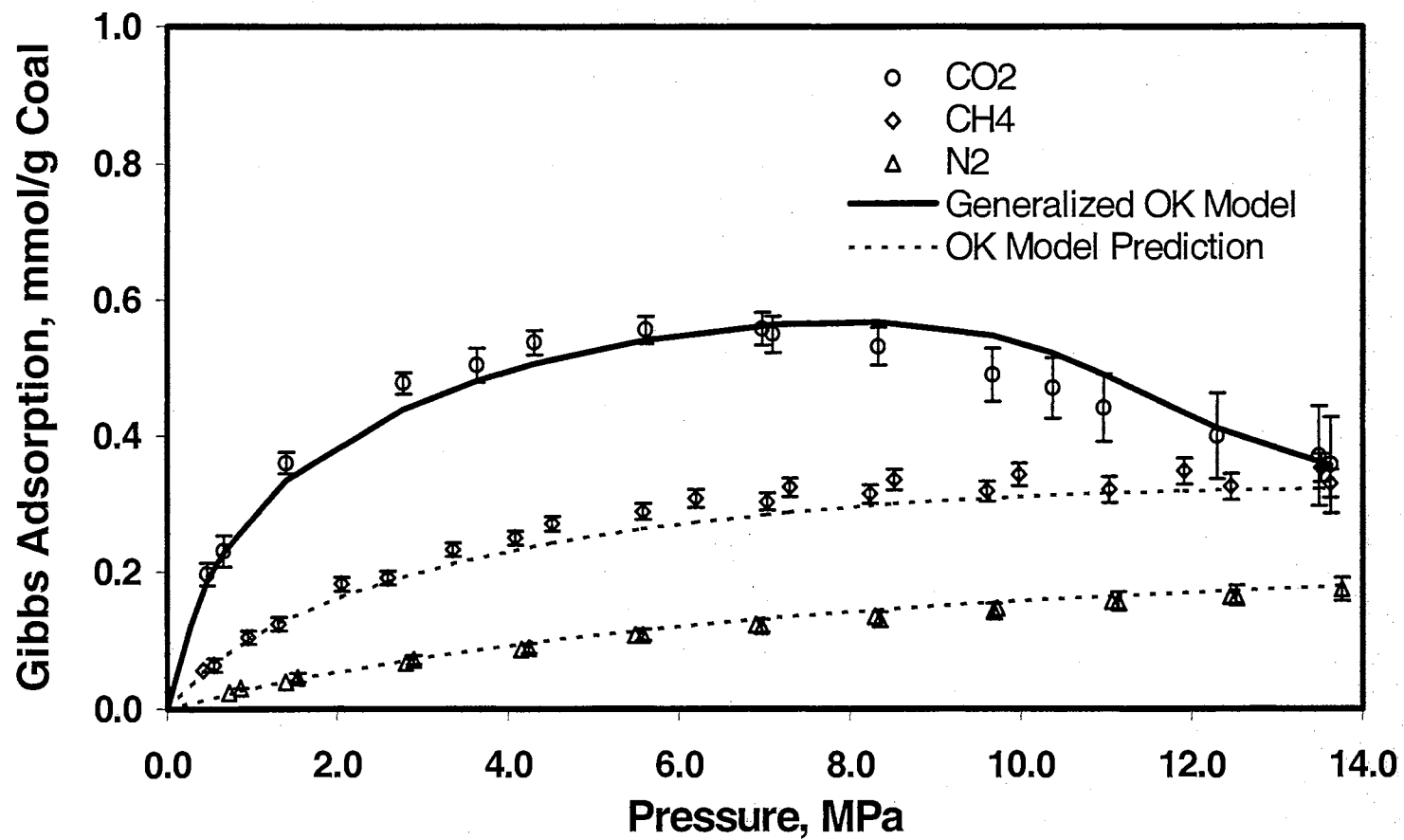
Figure 41. OK Model Predictions of Pure-Gas Adsorption on Wet Tiffany Coal at 327. 6 K

adsorption measurements on Tiffany coal. The surface area, A=100 m^2/g, and the

distance between a molecule and surface plane, $z = 1.29\sigma_{ic}$, are obtained from the best fit

for the CO$_2$ adsorption. Then, using this information and the generalized $C_{a,o}$,

δ and ξ_f, the nitrogen and methane gas adsorption isotherms were predicted. As shown in

this figure, the gas adsorption on coal can be predicted using the generalized OK model

within the expected experimental uncertainties.

Application of the generalized model to our recent CO$_2$ adsorption on wet Illinois

#6 Argonne Coal, however, gave marginal results. About 11% AAD was obtained using

this generalized model. Specifically, the generalized model over-predicted the fluid-solid

energy parameter, which resulted in high estimates for the predicted Gibbs adsorption at

lower pressures. These results suggest that the water effect on the fluid-solid energy

parameter is more complicated than that shown in Equation (6-14). As stated earlier, the

adsorption on the wet substrate should be treated as a multicomponent adsorption, where

water is an adsorbed component. Further study on the modeling of water effect on

adsorption is needed. To support such study, additional data for other adsorbates

(methane and nitrogen) on wet coals at water contents less than equilibrium moisture

value are needed. In addition, the measurement of pure-water adsorption on the dry coals

might be needed.

Summary

We have shown in this study that the OK monolayer model appears effective in

modeling pure-gas adsorption on carbon matrices. On average, the OK model with two

regressed parameters (one common ε_{is}/k for each system, and individual C for each

isotherm) can represent the adsorption on activated carbon with about 3.6% AAD. Specifically, for the OSU adsorption data set, the two-parameter OK model is capable on average of representing the data within their experimental uncertainties. The adsorbed-phase density and the fluid-fluid energy parameters in the OK model can be estimated from the reciprocal van der Waals co-volume and from a proportional relation to the well depth of the Lennard-Jones 12-6 potential, respectively.

Generalization of the model parameters was performed using adsorbent surface area and adsorbates physical properties. The results show that the generalized OK model can predict the adsorption isotherms on activated carbon with about 7% AAD or twice the deviation of the two-parameter OK model. Moreover, the model can also predict other gases adsorption isotherms based on the parameters (surface area and the solid-solid energy, ε_{CC}^* / k) obtained from one gas at given temperature.

The generalized OK model also appears effective for pure-gas adsorption on wet coals when the moisture content in the coal is above its equilibrium moisture content (EMC). The model parameters in this condition, however, are affected by the presence of water. Moreover, the generalized model was unable to predict the adsorption on wet coal, which has moisture content less than its EMC. These results suggest that the water effect on the fluid-solid energy parameter is more complicated than that shown in the generalized model. Furthermore, the adsorption on the wet substrate should be treated as a multicomponent adsorption, where water is recognized as one of the adsorbed components. Further study on the modeling of water effect on adsorption, however, needs additional data for other adsorbates (methane and nitrogen) on dry coals and wet coals with water contents less than their equilibrium moisture value.

CHAPTER 7

MODELING OF MULTICOMPONENT GAS ADSORPTION

The results shown in Chapter 6 have indicated that the Ono-Kondo (OK) lattice model has the capability to represent high-pressure, pure-gas adsorption data. Based on these results, the OK framework is extended to mixture predictions. Specifically, we have:

1. Evaluated the predictive capability, where the OK model parameters obtained from pure-gas adsorption are used to predict gas mixture adsorption for selected multicomponent adsorption systems.

2. Evaluated the predictive capability of the model, where binary interaction parameters (BIP) are used to examine the model representation of the mixture data.

The model development/evaluation was conducted using our newly-acquired data and data from the literature.

As in the modeling of pure-gas adsorption, we first performed studies on dry activated carbon matrices, followed by studies on wet coals. Data in the literature on high-pressure multicomponent gas adsorption, however, are not as plentiful as for pure fluids. Thus, the following mixture adsorption data on activated carbon were selected for the model evaluation:

1. Mixture adsorption of methane, nitrogen and CO_2 on Calgon F-400 activated carbon at 318.2 K (OSU, 2002).

2. Mixture adsorption of methane, nitrogen and CO_2 on Norit R1-Extra activated carbon at 298 K (Dreisbach et al., 1999).

3. Mixture adsorption of methane, ethane, and ethylene on BPL activated carbon at 301.4 K (Reich et al., 1980).

A few experimental studies have examined high-pressure multicomponent gas adsorption on coals (Arri et al., 1992; DeGance, 1992; Harpalani and Pariti, 1993; Greaves et al., 1993; Clarkson and Bustin, 2000). Limited information, however, was given on the experimental data in most of those references. Therefore, we decided to use only OSU mixture adsorption measurements on various wet coals for model evaluation.

Modeling Mixed-Gas Adsorption on Dry Activated Carbon

Methane, Nitrogen and CO_2 Mixture Adsorption on Calgon F-400 (OSU Data)

Our measurements on pure and mixture adsorption of methane, nitrogen and CO_2 on activated carbon at 318.2 K and pressures to 13.6 MPa were used to evaluate the OK modeling capability. The experimental data are given in a recent publication (Sudibandriyo et al., 2003) and also documented in a DOE Report (Gasem et al., 2002). The binary mixture adsorption includes methane/CO_2, nitrogen/CO_2, and methane/nitrogen at nominal molar feed gas compositions of 20, 40, 60 and 80% with a specific void volume ranging from 2.04-2.57 cm^3/g. Adsorption isotherms were also measured for a single methane/nitrogen/CO_2 ternary mixture at the nominal molar feed composition of 10/40/50 with a specific void volume of 2.10 cm^3/g.

Because adsorption calculations are very sensitive to inaccuracies in experimental mole fraction, in general, using the "iteration function method" (IFM) to predict the gas composition, gives better results than using the experimental gas compositions. Therefore, in this study, we only present the results based on the iteration function method. The sum of squares of weighted absolute errors in the calculated adsorption was selected for the objective function to determine the binary interaction parameters.

Evaluation of the pure adsorption is reported in Chapter 6, and the OK model parameters used to fit the pure adsorption data are given in that chapter.

Table 17 presents the results of the OK model predictions for binary mixture adsorption on dry activated carbon. The results are based solely on parameters from fits to pure component data (C_{ij}=0). On average, the OK model can predict the binary adsorption data with about 1.6 times the expected experimental uncertainties. The OK model can predict the total and the more-adsorbed component adsorptions within 7.5% AAD. Although the RMSE is small, the percentage deviation for the lesser-adsorbed component adsorptions is large as the Gibbs excess adsorption becomes exceedingly small. For example, in the nitrogen/CO_2 system, 81% AAD and 0.20 mmol/g RMSE were obtained for nitrogen adsorption, compared to 7.5% AAD and 0.33 mmol/g RMSE for total adsorption in the same system. However, worse results were generally obtained for the predictions of the lesser-adsorbed component adsorptions, as indicated by larger WAAD (up to 3.5 for nitrogen adsorption in nitrogen/CO_2 system).

Here, we evaluate the capability of the generalized pure-adsorption model described in the previous chapter to predict mixture adsorption. Accordingly, pure-adsorption model parameters based on the generalized model were used for mixture

Table 17. OK Model Predictions of Binary Mixture Adsorption on Dry Activated Carbon at 318.2 K (OSU, 2002)

Systems	NPTS	%AAD	RMSE (mmol/g)	WAAD
Based on Parameters from the Pure-Adsorption Model				
CH$_4$-N$_2$				
Methane	40	2.5	0.080	1.0
Nitrogen	40	11.7	0.064	1.7
Total	40	0.7	0.029	0.3
CH$_4$-CO$_2$				
Methane	40	17.8	0.132	2.1
CO$_2$	40	4.1	0.113	1.0
Total	40	4.0	0.206	1.1
N$_2$-CO$_2$				
Nitrogen	40	81.1	0.199	3.5
CO$_2$	40	4.6	0.152	1.2
Total	40	7.5	0.335	2.4
Based on Generalized Pure-Adsorption Model				
CH$_4$-N$_2$				
Methane	40	3.3	0.096	1.2
Nitrogen	40	6.9	0.070	1.5
Total	40	2.9	0.098	1.2
CH$_4$-CO$_2$				
Methane	40	18.7	0.126	1.9
CO$_2$	40	3.1	0.130	0.8
Total	40	1.5	0.087	0.4
N$_2$-CO$_2$				
Nitrogen	40	71.0	0.164	2.6
CO$_2$	40	3.8	0.127	1.0
Total	40	5.6	0.277	1.8

adsorption predictions. The results presented in Table 17 show that slightly better predictions are obtained than those based on the pure-adsorption model regressions. On average, the generalized OK model can predict the binary adsorption data with about 1.4 times the experimental uncertainties. However, using the generalized pure-component parameters results in poor predictions for the pure-component adsorption (up to three times the experimental uncertainties for methane adsorption).

Figures 42 and 43 show the OK model predictions of the individual component adsorption of methane/CO_2 system. As shown in these figures, on average, the OK model can predict the binary mixture adsorptions within twice the experimental uncertainties. In addition, the model can also predict a maximum in the Gibbs adsorption as experimentally observed for the lesser-adsorbed component.

Table 18 presents the OK model representation of binary mixture adsorption based on only one binary interaction parameter, C_{ij}, in the fluid-fluid energy parameter, ε_{ij}. Significant improvement has been obtained, especially for the nitrogen component adsorption in the nitrogen/CO_2 system; specifically, a reduction in WAAD from 3.5 to 0.6 is observed with the use of one binary interaction parameter. On average, the OK model can represent the binary adsorption data with about 0.8 times the experimental uncertainties with the maximum error obtained for representing the CO_2 component adsorption in the nitrogen/CO_2 mixture, which yielded 1.4 times the expected experimental uncertainties.
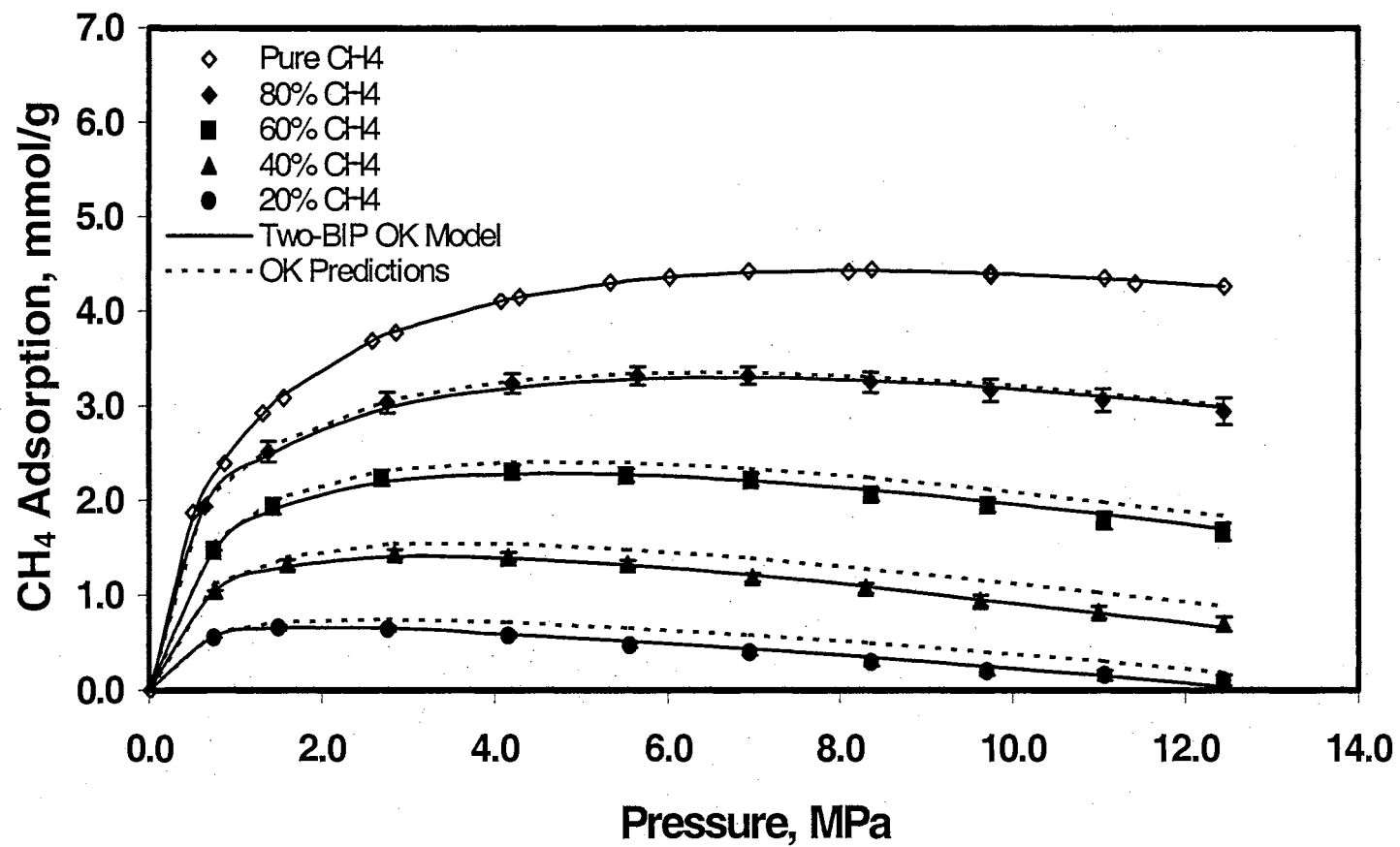
Figure 42. CH$_4$ Gibbs Adsorption from CH$_4$/CO$_2$ Mixture on Dry Activated Carbon at 318.2 K and Various Feed Gas Composition (OSU Data)
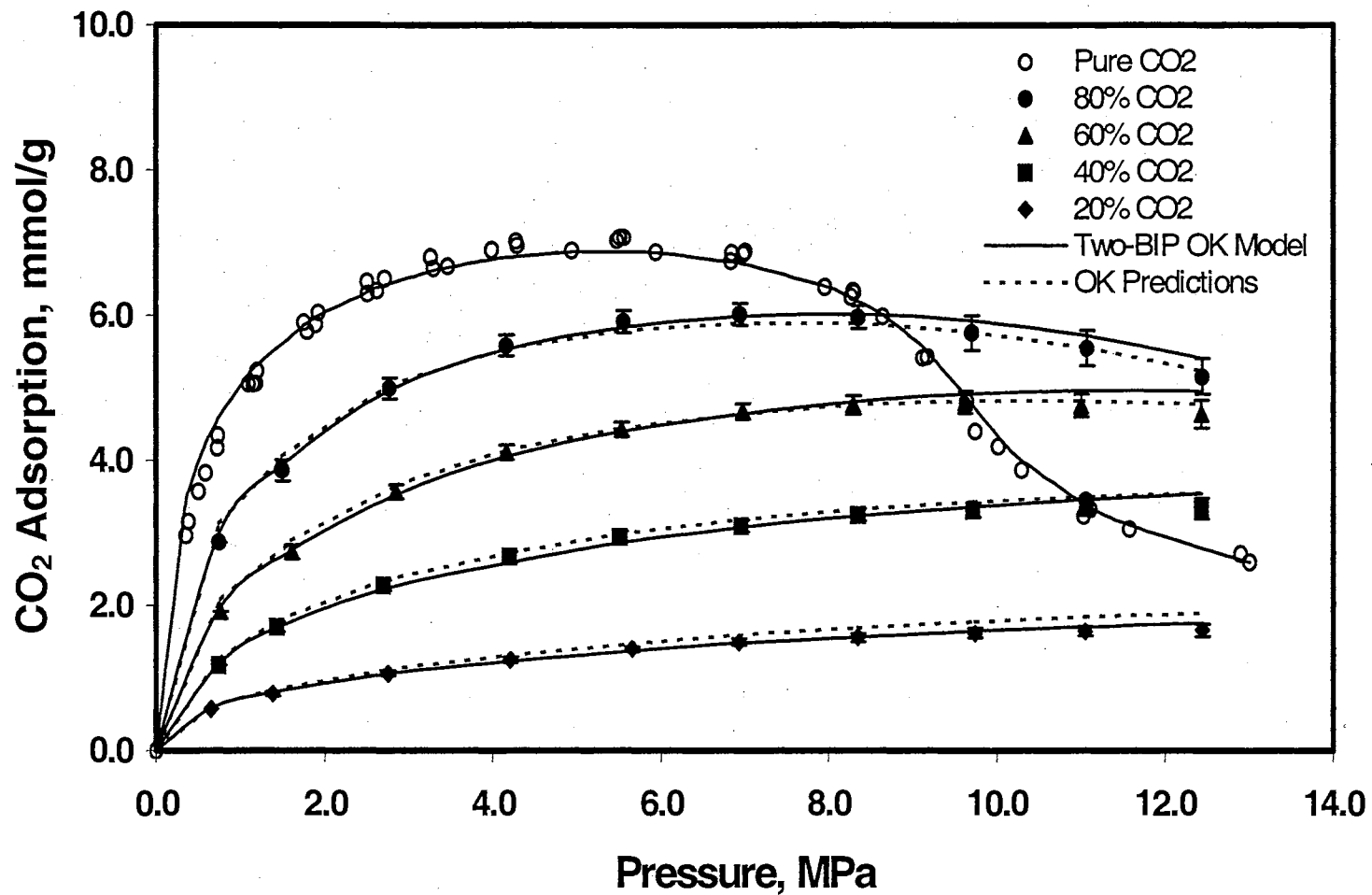
Figure 43. CO_2 Gibbs Adsorption from CH_4/CO_2 Mixture on Dry Activated Carbon at 318.2 K and Various Feed Gas Composition (OSU Data)

Table 18. OK Model Representations of Binary Mixture Adsorption on Dry Activated Carbon at 318.2 K (OSU, 2002)

Systems	NPTS	%AAD	RMSE (mmol/g)	WAAD	C_{ij}	E_{ij}
Based on One Regressed Parameter (C_{ij})						
CH$_4$-N$_2$						
Methane	40	2.8	0.073	1.1	0.198	1.0
Nitrogen	40	5.0	0.032	0.7		
Total	40	1.8	0.065	0.8		
CH$_4$-CO$_2$						
Methane	40	4.8	0.047	0.4	0.335	1.0
CO$_2$	40	2.7	0.147	0.7		
Total	40	2.2	0.152	0.6		
N$_2$-CO$_2$						
Nitrogen	40	8.2	0.045	0.6	0.658	1.0
CO$_2$	40	4.4	0.255	1.4		
Total	40	4.1	0.262	1.4		
Based on Two Regressed Parameters						
CH$_4$-N$_2$						
Methane	40	1.5	0.036	0.6	0.351	1.078
Nitrogen	40	2.0	0.020	0.5		
Total	40	0.7	0.033	0.3		
CH$_4$-CO$_2$						
Methane	40	4.2	0.033	0.4	0.280	0.956
CO$_2$	40	2.1	0.101	0.5		
Total	40	1.7	0.107	0.5		
N$_2$-CO$_2$						
Nitrogen	40	17.6	0.044	0.7	0.446	0.871
CO$_2$	40	2.3	0.130	0.7		
Total	40	2.6	0.162	0.8		

133

The binary interaction parameters obtained, however, are relatively large ($C_{ij} =$ 0.658, 0.335 and 0.198 for nitrogen/CO_2, methane/CO_2 and methane/nitrogen system, respectively). This is, at least in part, due to influence of the quadrupole moment of the CO_2 affected by the fluid-solid interaction energy. Exact calculations of this effect are complicated, but it appears that the nitrogen/CO_2 system shows more non-ideality than the other systems. Other reasons for the large C_{ij} include the inadequacy of the mixing/combining rules applied in OK model to predict binary adsorption.

The relatively large values of C_{ij} also suggest that the correlative burden of the binary adsorption modeling has mainly rested on the correction in the fluid-fluid interaction energy. In future studies, application of the surface heterogeneity through the fluid-solid energy distribution should be considered, while the chemical potential in the gas phase should be calculated using an accurate equation of state.

Table 18 also presents the results when two binary interaction parameters are regressed to represent the binary mixture adsorption. As presented in Table 18, on average, the deviation obtained is about 0.5 times the experimental uncertainties. The second binary interaction parameters, E_{ij}, for methane/CO_2 and methane/nitrogen system are close to the nominal one; for nitrogen/CO_2 system, however, significant correction is needed (E_{ij}=0.871).

Figures 42 and 43 also show the OK representations of the individual component adsorption of methane/CO_2 system. For completeness, pure-substance adsorption is included in each figure. As shown in these figures, the OK model can represent the binary mixture adsorptions very well within the experimental uncertainties, as indicated by the error bars in the figures.

Figure 44 presents an example for a comparison between the gas compositions obtained from experimental measurements and the ones obtained from the IFM calculations. The figure shows that the gas compositions obtained from IFM calculations produce an excellent fit to the experimental values. Slight deviations, however, occur at lower pressures. This might be due to a modeling deficiency or an experimental error, where the equilibrium condition may have not been reached in the earlier stages of adsorption even though the system had been allowed 24 hours to reach equilibrium.

Table 19 presents the model predictions for the ternary mixture adsorption on dry activated carbon at 318.2 K. The predictions based on pure adsorption parameters produce deviations of about 1.8 times the experimental uncertainties, on average. Larger deviations are seen for the lesser-adsorbed component adsorption; i.e. nitrogen (about three times the experimental uncertainties). Table 19 also presents the component adsorption predictions of the ternary mixture based on the pure and the binary interaction parameters (BIP) obtained from binary adsorption data. As expected, the use of binary interaction parameters not only reduces the calculated deviations for the binary systems, but also improves the predictions for the component ternary adsorption. The prediction based on pure and binary adsorption parameters produce errors of about 0.8 and 0.7 times the experimental uncertainties when using one and two binary interaction parameters, respectively. The slight difference from the two results indicates that using only one binary interaction parameter may be sufficient to represent the mixture adsorption.
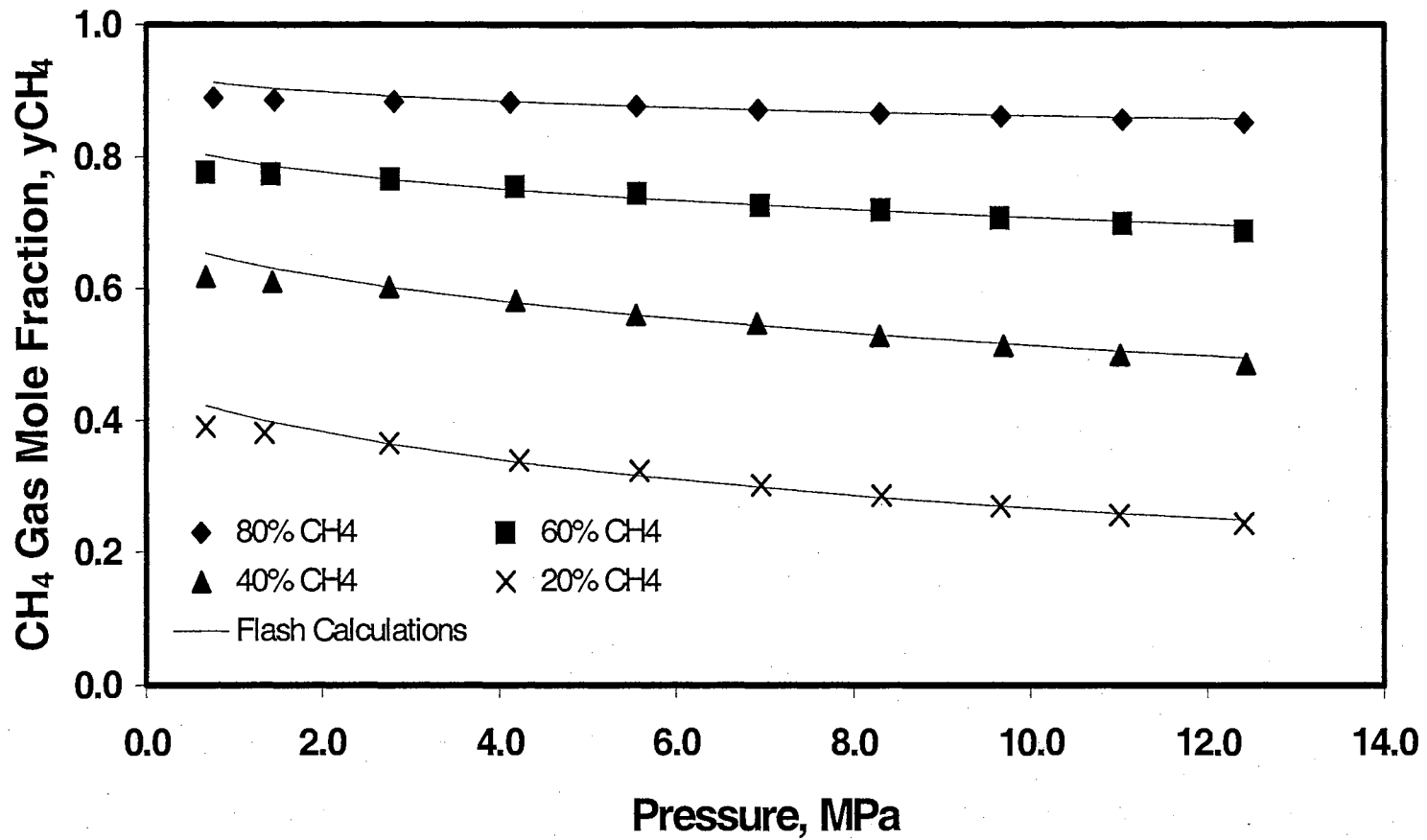
Figure 44. Comparison between the Gas Compositions Obtained from Experimental Measurements and from Iteration Function Method Calculations

Table 19. OK Model Predictions of Ternary Mixture Adsorption on Dry Activated Carbon at 318.2 K

Systems	NPTS	%AAD	RMSE (mmol/g)	WAAD
Based on Parameters from the Pure-Adsorption Model				
Methane	11	8.9	0.040	0.7
Nitrogen	11	540	0.201	3.3
CO_2	11	3.1	0.107	0.9
Total	11	6.8	0.335	2.2
Based on Generalized Pure-Adsorption Model				
Methane	11	11.4	0.054	0.9
Nitrogen	11	474	0.158	2.3
CO_2	11	1.7	0.077	0.5
Total	11	4.9	0.275	1.6
Based on Pure and One Binary Interaction Parameter (C_{ij})				
Methane	11	2.6	0.012	0.2
Nitrogen	11	37.6	0.022	0.4
CO_2	11	4.3	0.290	1.2
Total	11	4.2	0.299	1.3
Based on Pure and Two Binary Interaction Parameters				
Methane	11	4.2	0.017	0.5
Nitrogen	11	121	0.052	0.9
CO_2	11	2.5	0.139	0.7
Total	11	3.2	0.177	0.9

Figures 45 shows the OK model predictions for the ternary mixture adsorption on activated carbon, based on pure-component data and with two binary interaction parameters from the binary adsorption data. As shown in the figure, the OK model can predict all the ternary mixture adsorptions well and within the experimental uncertainties (represented by the error bars in the figures) when the binary interaction parameters are included.

137
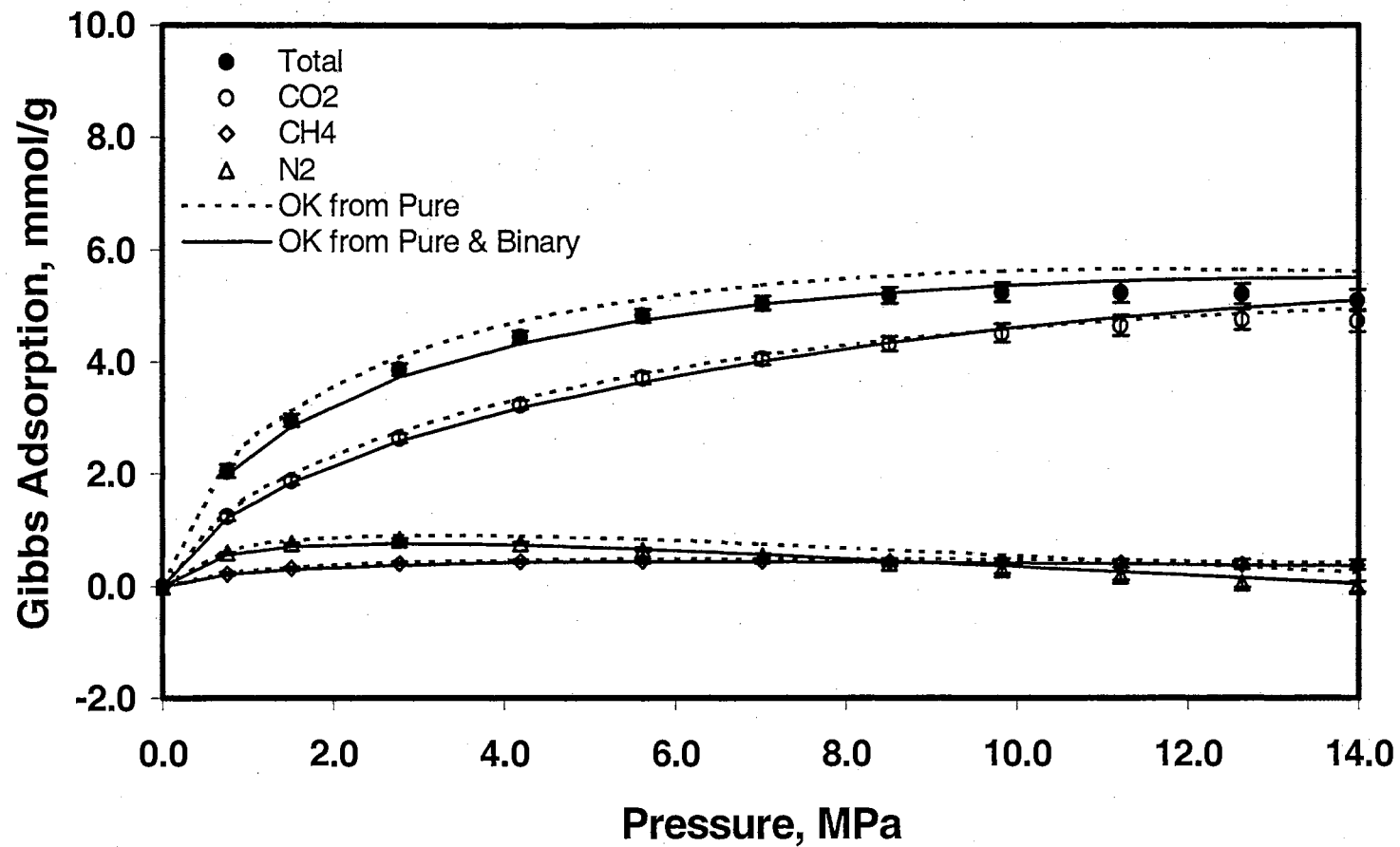
Figure 45. OK Model Predictions from a $CH_4/N_2/CO_2$ Feed Mixture Adsorption on Dry Activated Carbon at 318.2 K (OSU Data)

Methane, Nitrogen and CO_2 Mixture Adsorption on Norit R1-Extra (Dreisbach, 1999)

The measurements from other investigators were used to validate the mixture adsorption model. Pure and mixture adsorption of methane, nitrogen and CO_2 on Norit R1-Extra activated carbon at 298 K (Dreisbach, 1999) were used to evaluate the OK modeling capability. Because no detailed information was given on the uncertainties of the experimental data selected, the percentage average error of the Gibbs excess adsorption (%AAD) was used for the objective function to determine the model parameters. Evaluation of the pure adsorption has been conducted in the previous chapter, where the OK model parameters used to fit the pure adsorption data were reported.

Also, because no detailed information was given on the feed composition and the specific void volume of the system, the IFM procedure cannot be employed in the modeling effort. In this case, the gas-phase equilibrium mole fractions obtained from the adsorption measurements were smoothed using a regressed logarithmic function, before they were used to calculate the individual Gibbs excess adsorption.

Table 20 presents the prediction of binary mixture adsorption on dry Norit R1-Extra activated carbon at 298 K based on pure component parameters. As presented in the table, the OK model can predict the total adsorption data within 6% AAD (about 0.4 mmol/g in RMSE). However, the prediction for individual component adsorption produces only mediocre results (12 to 139% AAD or 0.18 to 0.57 mmol/g in RMSE). These unsatisfactory prediction results are, in part, due to the large uncertainties in the equilibrium mole fractions in the gas phase data obtained from the adsorption measurements. Not unexpectedly, the worst predictions are for the nitrogen adsorption in

Table 20. OK Model Predictions of Binary Mixture Adsorption on Dry Activated Carbon at 298 K (Dreisbach, 1999)

Systems	NPTS	%AAD	RMSE (mmol/g)
Based on Two-Parameter Pure-Adsorption Model			
CH_4-N_2			
Methane	24	12.2	0.352
Nitrogen	24	22.3	0.181
Total	24	4.3	0.197
CH_4-CO_2			
Methane	24	13.4	0.207
CO_2	24	18.8	0.569
Total	24	5.8	0.487
N_2-CO_2			
Nitrogen	24	139	0.317
CO_2	24	7.6	0.483
Total	24	6.0	0.364
Based on Generalized Pure-Adsorption Model			
CH_4-N_2			
Methane	24	7.4	0.240
Nitrogen	24	12.8	0.113
Total	24	4.6	0.192
CH_4-CO_2			
Methane	24	10.2	0.319
CO_2	24	31.3	0.571
Total	24	8.3	0.584
N_2-CO_2			
Nitrogen	24	38.2	0.100
CO_2	24	13.2	0.597
Total	24	11.9	0.609

nitrogen/CO_2 system (139% AAD). For this system, the RMSE of the nitrogen adsorption is 0.32 mmol/g, which is actually smaller than the RMSE of the total adsorption (0.36 mmol/g) with only 6% AAD. The higher %AAD in nitrogen adsorption is mainly due to its lower adsorption in this mixture.

Using the parameters based on the generalized pure-adsorption model improves the individual adsorption predictions, especially the nitrogen adsorption in nitrogen/CO_2 system (38% AAD). As in the case of OSU data, however, using these generalized pure component parameters results in unsatisfactory predictions for the pure-component adsorption.

Table 21 presents the OK model representation of binary mixture adsorption based on only one binary interaction parameter, C_{ij}, in the fluid-fluid energy parameter, ε_{ij}. Significant improvement from the predictive case has been obtained. The total adsorption can be represented within 6.4% AAD and the individual component adsorption can be represented with deviations from 5.7 to 17.8% AAD.

Table 21 also presents the results when two binary interaction parameters are applied to represent the binary mixture adsorption. As presented in Table 21, only slight improvement is obtained compared to the results obtained by using only one binary interaction parameter. The total adsorption can be represented with AAD from 3 to 5% and the individual component adsorption can be represented from 6 to 17% AAD.

Table 22 presents the model prediction results for the ternary mixture adsorption on dry Norit R1-Extra activated carbon. The total adsorption can be predicted based on pure adsorption parameters to within 12% AAD. The OK model can predict the more-adsorbed component adsorptions within 18% AAD. The percentage deviations for the

141

Table 21. OK Model Representations of Binary Mixture Adsorption on Dry Activated Carbon at 298 K (Dreisbach, 1999)

Systems	NPTS	%AAD	RMSE (mmol/g)	C_{ij}	E_{ij}
Based on One Regressed Parameter (C_{ij})					
CH$_4$-N$_2$				0.610	1.0
Methane	24	14.8	0.345		
Nitrogen	24	5.8	0.119		
Total	24	6.4	0.291		
CH$_4$-CO$_2$				0.294	1.0
Methane	24	6.8	0.182		
CO$_2$	24	10.1	0.451		
Total	24	6.2	0.540		
N$_2$-CO$_2$				0.832	1.0
Nitrogen	24	17.8	0.087		
CO$_2$	24	5.7	0.344		
Total	24	4.8	0.327		
Based on Two Regressed Parameters					
CH$_4$-N$_2$				0.665	1.197
Methane	24	11.0	0.214		
Nitrogen	24	8.2	0.204		
Total	24	2.9	0.100		
CH$_4$-CO$_2$				0.319	1.206
Methane	24	3.7	0.097		
CO$_2$	24	9.4	0.257		
Total	24	4.8	0.276		
N$_2$-CO$_2$				0.832	0.971
Nitrogen	24	17.2	0.079		
CO$_2$	24	5.9	0.363		
Total	24	4.9	0.342		

Table 22. OK Model Predictions of Ternary Mixture Adsorption on Dry Activated Carbon at 298 K (Dreisbach, 1999)

Systems	NPTS	%AAD	RMSE (mmol/g)
Based on Parameters from the Pure-Adsorption Model			
Methane	40	13.4	0.514
Nitrogen	40	45.0	0.446
CO_2	40	12.5	0.261
Total	40	8.7	0.794
Based on Pure and One Binary Interaction Parameter (C_{ij})			
Methane	40	17.2	0.661
Nitrogen	40	48.5	0.5
CO_2	40	14.2	0.34
Total	40	11.9	1.09
Based on Pure and Two Binary Interaction Parameters			
Methane	40	17.9	0.638
Nitrogen	40	47.2	0.473
CO_2	40	14.9	0.393
Total	40	9.1	0.731

lesser-adsorbed component adsorptions, however, are large as the Gibbs excess adsorption becomes very small. Application of the binary interaction parameters does not appear to improve the predictions for this adsorption system. In fact, about the same magnitude of deviations were also obtained by Dreisbach (1999) for ternary adsorption predictions using a dual-site Langmuir model.

Inaccuracy in experimental gas mole fractions may have contributed to the larger deviations in the mixture adsorption predictions. In his study, Dreisbach used two different methods to obtain the bulk-phase compositions. For binary adsorption, he used an equation of state to infer both the bulk-phase composition and density from P-T

measurements and system volume calibrations, while for ternary adsorption he used a gas chromatograph to measure the bulk-phase composition.

Methane, Ethane, and Ethylene Mixture Adsorption (Reich, 1980)

Zhou (1994) used data for methane, ethane, and ethylene on activated carbon at 301.4 K (Reich et al., 1980) for model comparisons. For the same reason, the OK model was also used to represent those data and compared with the modeling results obtained by Zhou.

Because no detailed information was given on the uncertainties of the experimental data selected, the percentage average absolute error of the adsorption (%AAD) was used for the objective function to determine the model parameters. Also, because no detailed information was given on the specific void volume of the system, the IFM calculation procedure could not be employed in the modeling effort. The feed compositions are the same as the gas-phase equilibrium mole fractions in their adsorption measurements. These experimental equilibrium gas mole fractions were used to calculate the individual Gibbs excess adsorption.

Table 23 presents the comparison of model predictions and representations for mixture adsorption of methane, ethane and ethylene on dry BPL activated carbon at 301.4 K. As exhibited in the table, on average, the OK model predicts the total and more-adsorbed component adsorption very well (with 4% AAD). The model, however, is unable to provide good estimates for the lesser-adsorbed component (up to 35% AAD). For individual adsorption, the OK model prediction gives better results compared to the Langmuir model and gives results comparable to the 2-D EOS model. In addition, for total adsorption predictions, the OK model has better performance than the

Table 23. Comparison of Model Predictions and Representations for CH$_4$, C$_2$H$_6$ and C$_2$H$_4$ Mixture Adsorption on Dry Activated Carbon at 301.4 K (Reich, 1980)

Systems	NPTS	% AAD						RMSE (mmol/g)		
		Lang-muir	2-D EOS	2-D EOS (C_{ij})	OK	OK (C_{ij})	OK (C_{ij} & E_{ij})	OK	OK (C_{ij})	OK (C_{ij} & E_{ij})
CH$_4$-C$_2$H$_6$										
Methane	14	36.7	39.8	19.5	35.2	23.8	23.7	0.329	0.169	0.168
Ethane	14	4.4	2.4	2.3	3.8	2.5	2.4	0.142	0.086	0.084
Total	14	5.8	7.2	3.5	4.5	2.3	2.2	0.226	0.125	0.153
CH$_4$-C$_2$H$_4$										
Methane	15	28.9	33.9	8.8	29.9	15.2	14.0	0.297	0.110	0.104
Ethylene	15	5.4	2.9	3.3	3.8	3.2	1.9	0.148	0.113	0.088
Total	15	5.8	6.3	2.7	3.1	2.8	2.2	0.172	0.126	0.141
C$_2$H$_6$-C$_2$H$_4$										
Ethane	12	5.2	4.6	5.0	4.3	5.1	4.1	0.099	0.110	0.084
Ethylene	12	8.3	6.8	5.7	5.7	5.0	3.3	0.187	0.185	0.116
Total	12	6.4	5.6	5.1	3.8	3.3	1.3	0.193	0.176	0.080
CH$_4$-C$_2$H$_6$-C$_2$H$_4$										
Methane	14	59.3	51.2	33.5	52.2	39.1	38.1	0.486	0.303	0.285
Ethane	14	3.7	3.5	4.8	5.6	4.7	5.4	0.122	0.093	0.102
Ethylene	14	4.9	4.4	5.5	4.9	4.9	5.5	0.133	0.154	0.131
Total	14	9.5	8.4	5.5	5.7	3.9	3.9	0.420	0.334	0.287

* The results presented in the third to fifth columns are taken from Zhou (1994).

other models (on average, the %AAD are 3.8, 6.0, and 6.4 for the OK, Langmuir and EOS-S model, respectively).

As other models do, the OK model can also predict the ethane/ethylene adsorptions very well, within 6% AAD. Pure ethane and ethylene have very similar adsorption on activated carbon. Therefore, the adsorbed phase is expected to form an ideal mixture.

The use of optimum interaction parameters significantly improves the predictions of methane adsorption in the binary and ternary systems. The average deviations for methane adsorption were reduced from 35.2% to 23.8% for methane/ethane and from 33.9% to 15.2% for methane/ethylene. For the ternary system, using the binary interaction parameter obtained from binary data, the OK model reduced average deviations in predicting the amount of methane adsorbed from 52.2 % to 39.1%. However, application of the second binary interaction parameters (E_{ij}) in these systems does not improve the mixture adsorption representations.

The binary interaction parameters for the OK model are reported in Table 24. Interestingly, negative values of C_{ij} were also obtained for these systems, as was the case of interaction parameters obtained by Zhou using a two-dimensional equation of state model (2-D EOS). As expected, only small C_{ij} (= -0.037) was obtained for the ethane/ ethylene system.

Figures 46 and 47 show the OK model predictions and representations of the methane/ethane mixture adsorption on dry BPL activated carbon. For completeness, pure adsorption is also included in each figure. As shown in the figures, using the binary interaction parameters improves the model in representing the methane adsorption data.

However, the model always underestimates the methane adsorption in the methane/ethane and methane/ethylene systems, especially at higher pressures.

Table 24. Binary Interaction Parameters Used in OK Model for CH_4, C_2H_6 and C_2H_4 Mixture Adsorption on Dry AC at 301.4 K (Reich, 1980)

Systems	C_{ij}	E_{ij}
One Binary Interaction Parameter		
CH_4-C_2H_6	-0.569	-
CH_4-C_2H_4	-0.550	-
C_2H_6-C_2H_4	-0.037	-
Two Binary Interaction Parameters		
CH_4-C_2H_6	-0.577	0.972
CH_4-C_2H_4	-0.642	0.890
C_2H_6-C_2H_4	-0.037	1.088

Modeling of Mixed-Gas Adsorption on Coals

Data Employed

Pure and binary mixture adsorption of methane, nitrogen and CO_2 on wet Fruitland coal at 319.3 K and pressures to 12.4 MPa have been measured at OSU as documented by Hall (1993). The mixture data include methane/CO_2, nitrogen/CO_2, and methane/nitrogen adsorption isotherms at nominal molar feed gas compositions of 20, 40, 60 and 80% with a specific void volume ranging from 1.22-1.29 cm^3/g and moisture content ranging from 8% to 14%.

147
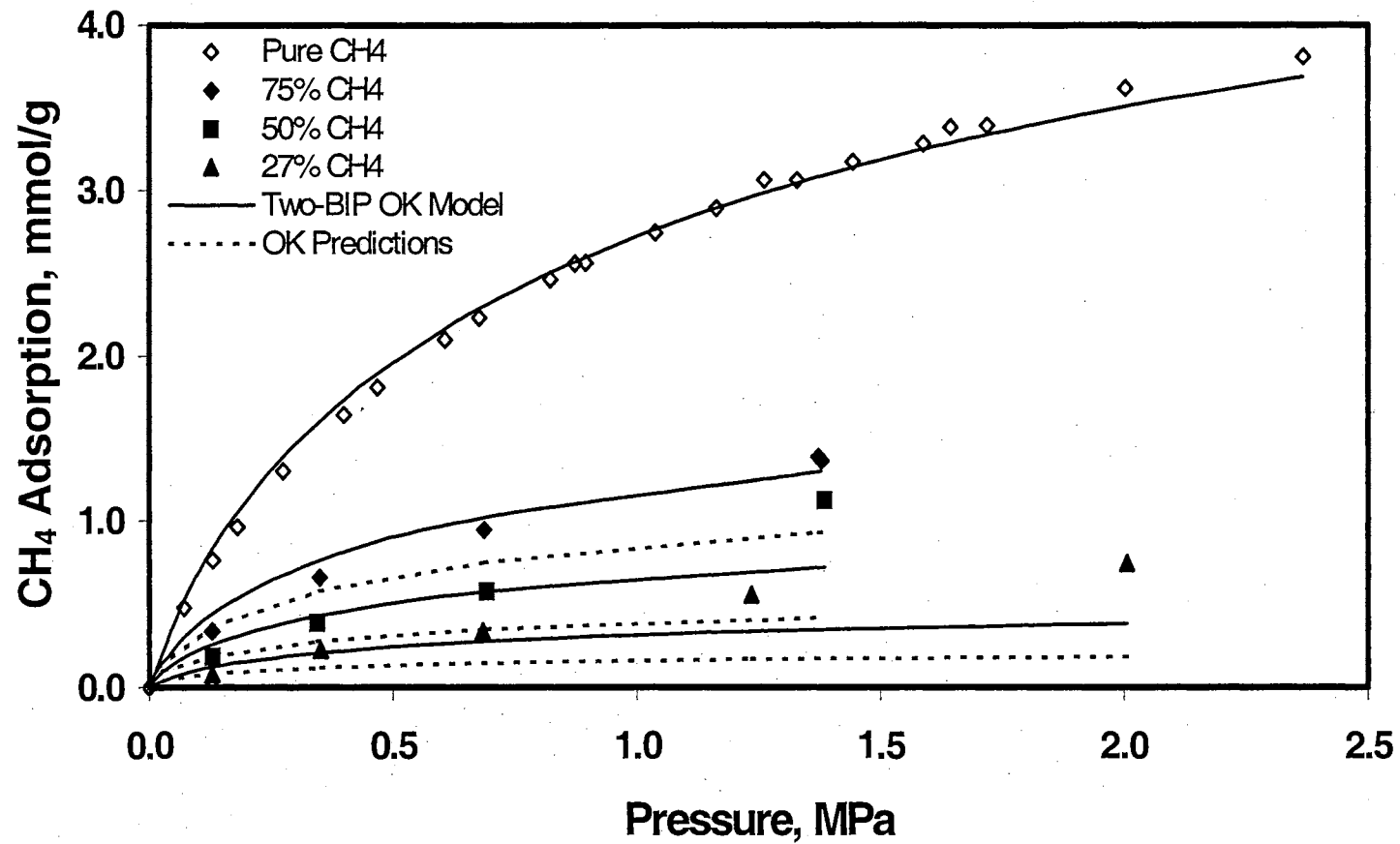
Figure 46. CH$_4$ Adsorption from CH$_4$/C$_2$H$_6$ Mixture on Dry Activated Carbon at 301.4 K and Various Feed Gas Composition (Reich)
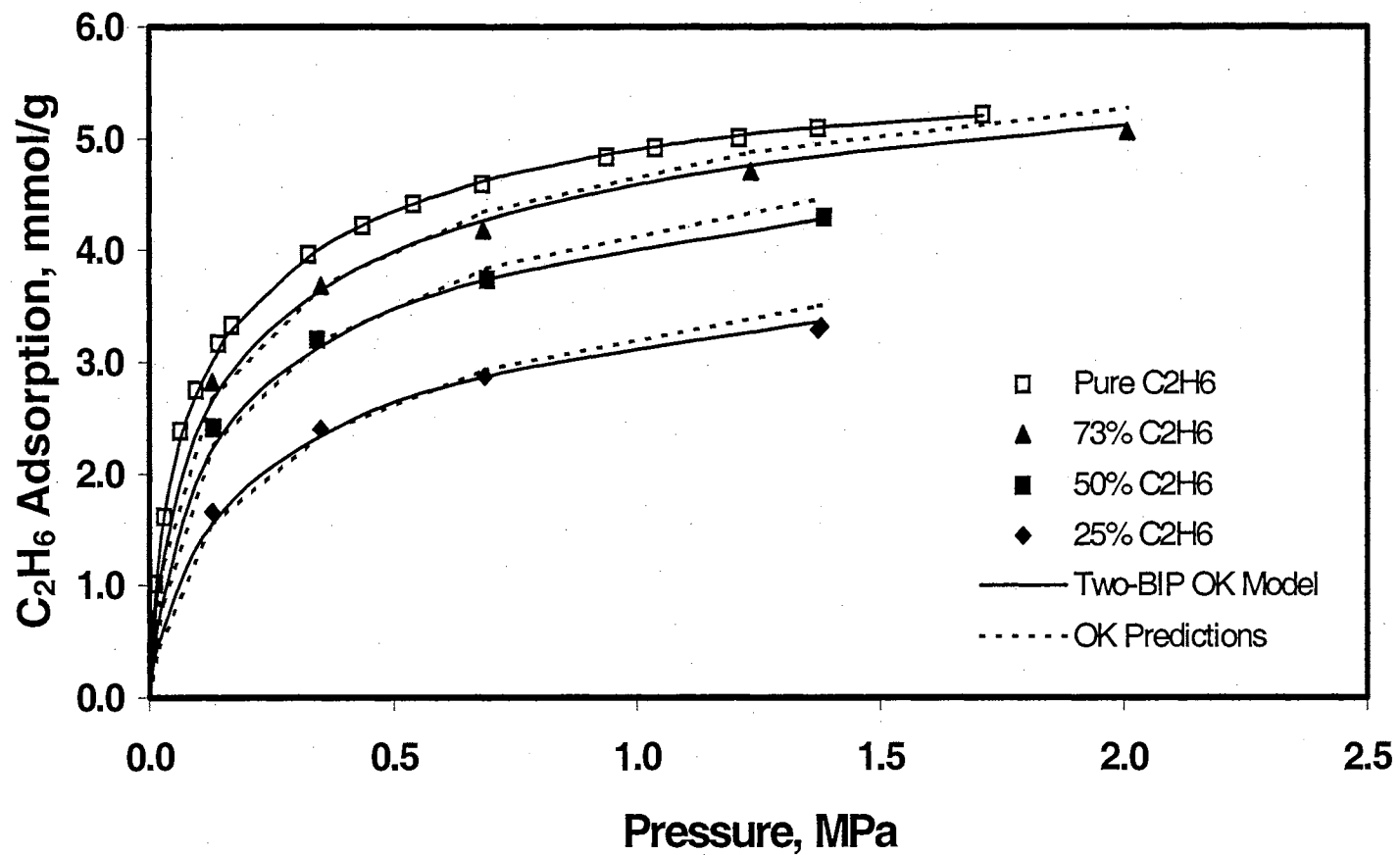
Figure 47. C_2H_6 Adsorption from CH_4/C_2H_6 Mixture on Dry Activated Carbon at 301.4 K and Various Feed Gas Composition (Reich)

The adsorption data on Fruitland coal reported by Hall were reanalyzed from primary PVTy measurements since the Redlich-Kwong (RK) equation of state was used to determine the gas compressibility factors. The RK predictions are inadequate in this near-critical portion of the CO_2 phase diagram. Therefore, in the present data-reduction calculations, the raw measurements were reprocessed using highly-precise equations of state (Span and Wagner, 1996; Pan, 2003) to obtain the Gibbs excess adsorptions, which were used for this model evaluation.

The adsorption of pure and binary mixture adsorption of methane, nitrogen and CO_2 on wet Illinois #6 at 319.3 K and pressures to 12.4 MPa have been measured at OSU and documented in a DOE Report (Gasem et al., 2001). The mixture data include methane/CO_2, nitrogen/CO_2, and methane/nitrogen adsorption isotherms at nominal molar feed gas compositions of 20, 40, 60 and 80% with a specific void volume ranging from 1.00-1.69 cm^3/g and moisture content ranging from 5% to 23%.

The low-adsorptive nature of the Illinois #6 coal makes the adsorption measurement very sensitive to the bulk-gas composition measurement, especially for the methane/CO_2, nitrogen/CO_2 systems. In this case, the gas-phase equilibrium mole fractions obtained from the adsorption measurements were smoothed using a regressed logarithmic function for methane/CO_2 system and using IFM procedure for the nitrogen /CO_2 system. The smoothed gas-phase equilibrium mole fractions were then used to reprocess the data-reduction calculations for the earlier reported data (Gasem et al., 2001) to obtain Gibbs excess adsorption isotherms.

Adsorption isotherms were measured at OSU for the methane/nitrogen, methane/CO_2 and nitrogen/CO_2 binary mixtures on wet, mixed Tiffany coal at 327.6 K

and pressures to 13.8 MPa. The coal sample was from an equal-mass mixture of coals from BP Amoco Tiffany Injection Wells #1 and #10. These measurements were conducted for a single molar feed composition for each mixture with specific void volume about 0.89 cm^3/g and moisture content about 11%. Adsorption isotherms were also measured for a single methane/nitrogen/CO_2 ternary mixture on wet, mixed Tiffany coal at 327.6 K and pressures to 13.8 MPa. The nominal molar feed composition was 10/40/50 with specific void volume of 0.89 cm^3/g and moisture content of 10%. The adsorption data for those measurements were documented in a DOE report (Gasem et al., 2000) and also in a topical report (Gasem et al., 2002).

Results

The IFM procedure was used for the model evaluation, and the sum of squares of weighted absolute errors in the calculated adsorption was selected for the objective function to determine the binary interaction parameters.

The model evaluation for the pure adsorptions and the corresponding OK model parameters, are presented in Chapter 6.

Tables 25-27 present the results of the OK model adsorption predictions for the binary mixtures on the selected wet coals. On average, the OK model can predict the binary adsorption data within twice the expected experimental uncertainties. However, high WAAD of 4.5 was observed for methane adsorption in the methane/CO_2 adsorption on wet Tiffany coal. It appears that the model underestimates the methane adsorption in this system, especially at higher pressures.

The OK model can predict the total and the more-adsorbed component adsorptions within 17% AAD. However, the percentage deviation for the lesser-adsorbed

151

component adsorptions is large as the Gibbs excess adsorption becomes exceedingly small. For example, the %AAD of the nitrogen adsorption in the nitrogen/CO_2 adsorption on wet Tiffany coal reaches 156, although the RMSE is only 0.015 mmol/g.

Tables 25 and 26 also present the results when the parameters based on a generalized pure-adsorption model were used to predict the mixture adsorption. Comparable statistical results to the case without generalization were obtained.

Tables 28-30 present the OK model representation of binary mixture adsorption using binary interaction parameters. Significant improvement has been obtained, especially for the lesser-adsorbed component adsorptions. For example, a reduction in WAAD from 4.5 to 1.0 is observed for methane component adsorption in the methane/CO_2 adsorption on wet Tiffany coal with the use of one binary interaction parameter, C_{ij}. Also, a reduction from 152 to 67 %AAD is observed for nitrogen component adsorption in nitrogen/CO_2 adsorption on wet Fruitland coal. On average, the OK model can represent the binary adsorption on wet coals data with about 0.8 times the expected experimental uncertainties. Better representations were further obtained when two binary interaction parameters were applied, as indicated by a WAAD of about 0.5.

The binary interaction parameters obtained from the adsorption on Fruitland coal are similar in order to those obtained from the adsorption on dry activated carbon, i.e., C_{ij} = 0.438, 0.126 and 0.099 for nitrogen/CO_2, methane/CO_2 and methane/nitrogen system, respectively. But the binary interaction parameters obtained from the adsorption on Illinois #6 and Tiffany coals do not show similar trend to those obtained from the adsorption on dry activated carbon.

Table 25. OK Model Predictions of Binary Mixture Adsorption on Wet Fruitland Coal at 319.3 K (OSU, 2000)

Systems	NPTS	%AAD	RMSE (mmol/g)	WAAD
Based on Two-Parameter Pure-Adsorption Model				
CH4-N2				
Methane	40	3.1	0.014	0.3
Nitrogen	40	16.4	0.019	0.9
Total	40	5.1	0.023	0.6
CH4-CO2				
Methane	40	8.9	0.012	0.5
CO2	40	5.7	0.036	0.8
Total	40	4.7	0.040	0.7
N2-CO2				
Nitrogen	40	152	0.026	1.0
CO2	40	7.1	0.059	0.9
Total	40	11.3	0.078	1.2
Based on the Generalized Pure-Adsorption Model				
CH4-N2				
Methane	40	3.1	0.012	0.3
Nitrogen	40	29.4	0.023	1.5
Total	40	4.0	0.016	0.4
CH4-CO2				
Methane	40	29.5	0.036	1.3
CO2	40	9.5	0.049	1.2
Total	40	4.2	0.034	0.6
N2-CO2				
Nitrogen	40	130	0.016	0.6
CO2	40	6.2	0.045	0.6
Total	40	5.9	0.053	0.6

Table 26. OK Model Predictions of Binary Mixture Adsorption on Wet Illinois #6 Coal at 319.3 K (OSU, 2001)

Systems	NPTS	%AAD	RMSE (mmol/g)	WAAD
Based on Two-Parameter Pure-Adsorption Model				
CH4-N2				
Methane	40	12.6	0.018	1.0
Nitrogen	40	85.2	0.013	0.8
Total	40	13.5	0.030	1.2
CH4-CO2				
Methane	40	17.6	0.017	1.1
CO2	40	9.8	0.054	1.2
Total	40	8.7	0.058	1.3
N2-CO2				
Nitrogen	40	44.3	0.004	0.5
CO2	40	9.5	0.045	1.6
Total	40	7.6	0.042	1.3
Based on the Generalized Pure-Adsorption Model				
CH4-N2				
Methane	40	26.5	0.039	2.0
Nitrogen	40	31.9	0.005	0.6
Total	40	16.8	0.038	1.5
CH4-CO2				
Methane	40	21.2	0.021	1.5
CO2	40	8.3	0.045	1.0
Total	40	8.0	0.053	1.2
N2-CO2				
Nitrogen	40	207	0.018	1.6
CO2	40	11.9	0.054	1.9
Total	40	6.8	0.036	1.1

Table 27. OK Model Predictions of Binary Mixture Adsorption on Wet Tiffany Coal at 327.6 K (OSU, 2002)

Systems	NPTS	%AAD	RMSE (mmol/g)	WAAD
CH$_4$-N$_2$				
Methane	11	6.9	0.018	1.0
Nitrogen	11	5.3	0.003	0.3
Total	11	6.5	0.020	1.0
CH$_4$-CO$_2$				
Methane	11	45.7	0.055	4.5
CO$_2$	11	16.9	0.072	2.5
Total	11	3.5	0.020	0.6
N$_2$-CO$_2$				
Nitrogen	11	156	0.015	1.5
CO$_2$	11	7.8	0.049	1.0
Total	11	5.9	0.036	0.9

Table 28. OK Model Representations of Binary Mixture Adsorption on Wet Fruitland Coal at 319.3 K (OSU, 2000)

Systems	NPTS	%AAD	RMSE (mmol/g)	WAAD	C_{ij}	E_{ij}
Based on One Regressed Parameter (C_{ij})						
CH4-N2						
Methane	40	3.1	0.015	0.3	0.099	1.0
Nitrogen	40	17.7	0.018	1.0		
Total	40	4.6	0.020	0.5		
CH4-CO2						
Methane	40	8.8	0.013	0.4	0.126	1.0
CO2	40	5.6	0.040	0.7		
Total	40	3.8	0.035	0.6		
N2-CO2						
Nitrogen	40	67.1	0.014	0.6	0.438	1.0
CO2	40	8.1	0.073	1.0		
Total	40	9.9	0.073	1.1		
Based on Two Regressed Parameters						
CH4-N2						
Methane	40	3.4	0.011	0.3	-0.241	0.825
Nitrogen	40	10.5	0.012	0.6		
Total	40	1.7	0.011	0.2		
CH4-CO2						
Methane	40	7.8	0.017	0.5	0.012	0.891
CO2	40	2.7	0.017	0.3		
Total	40	2.1	0.018	0.3		
N2-CO2						
Nitrogen	40	82.3	0.010	0.4	0.152	0.681
CO2	40	4.3	0.034	0.5		
Total	40	3.5	0.035	0.4		

156

Table 29. OK Model Representations of Binary Mixture Adsorption on Wet Illinois #6 Coal at 319.3 K (OSU, 2001)

Systems	NPTS	%AAD	RMSE (mmol/g)	WAAD	C_{ij}	E_{ij}
Based on One Regressed Parameter (C_{ij})						
CH_4-N_2					1.094	1.0
Methane	40	11.1	0.021	0.9		
Nitrogen	40	27.3	0.005	0.5		
Total	40	9.4	0.023	0.8		
CH_4-CO_2					0.180	1.0
Methane	40	18.7	0.015	0.9		
CO_2	40	10.4	0.060	1.2		
Total	40	8.0	0.055	1.1		
N_2-CO_2					-0.306	1.0
Nitrogen	40	34.1	0.003	0.4		
CO_2	40	9.2	0.040	1.5		
Total	40	8.3	0.042	1.4		
Based on Two Regressed Parameters						
CH_4-N_2					0.403	0.740
Methane	40	3.2	0.006	0.2		
Nitrogen	40	54.5	0.007	0.6		
Total	40	4.2	0.010	0.4		
CH_4-CO_2					-0.104	0.799
Methane	40	12.0	0.010	0.6		
CO_2	40	7.9	0.034	0.9		
Total	40	5.7	0.032	0.8		
N_2-CO_2					-0.618	0.715
Nitrogen	40	86.0	0.006	0.5		
CO_2	40	1.3	0.009	0.2		
Total	40	1.4	0.010	0.2		

Table 30. OK Model Representations of Binary Mixture Adsorption on Wet Tiffany Coal at 327.6 K (OSU, 2002)

Systems	NPTS	%AAD	RMSE (mmol/g)	WAAD	C_{ij}	E_{ij}
Based on One Regressed Parameter (C_{ij})						
CH$_4$-N$_2$					-0.364	1.0
Methane	11	7.0	0.019	1.0		
Nitrogen	11	8.1	0.004	0.4		
Total	11	5.0	0.016	0.8		
CH$_4$-CO$_2$					-0.692	1.0
Methane	11	12.5	0.021	1.0		
CO$_2$	11	12.9	0.049	2.0		
Total	11	7.0	0.030	1.2		
N$_2$-CO$_2$					-1.239	1.0
Nitrogen	11	52.5	0.005	0.5		
CO$_2$	11	6.0	0.036	0.8		
Total	11	5.1	0.031	0.7		
Based on Two Regressed Parameters						
CH$_4$-N$_2$					0.108	1.179
Methane	11	2.7	0.005	0.2		
Nitrogen	11	6.6	0.003	0.3		
Total	11	2.6	0.006	0.4		
CH$_4$-CO$_2$					-1.074	0.764
Methane	11	8.9	0.015	0.7		
CO$_2$	11	4.4	0.017	0.7		
Total	11	1.8	0.007	0.4		
N$_2$-CO$_2$					-1.230	1.036
Nitrogen	11	53.1	0.005	0.5		
CO$_2$	11	6.1	0.037	0.8		
Total	11	5.2	0.032	0.7		

The second binary interaction parameters, E_{ij}, for most of the systems are less than the values obtained from the adsorption on dry activated carbon. This indicates that the model without interaction parameters overestimates the individual component adsorption on the wet coals. The chemical structure of the coal and the presence of water in the coal affect the predictive capability of the model. Further, separating the two factors affecting the mixture adsorption modeling would require additional data, especially mixture adsorption data on dry coals.

Figure 48 shows an example of the OK predictions and representations for the binary mixture adsorption on wet coal. For completeness, the corresponding pure-substance adsorption isotherms are included in the figure. As shown in the figure, the OK model can represent all the binary mixture adsorptions within the experimental uncertainties (represented by the error bars in the figures) when two binary interaction parameters are used.

Table 31 presents the model predictions for the ternary mixture adsorption on wet Tiffany coal. For the total adsorption in this system, the OK model can predict data within the expected experimental uncertainties (within 8.5% AAD). The predictions based on pure-adsorption parameters produce deviations about 1.5 times the expected experimental uncertainties, on average. The larger deviations are exhibited by the lesser-adsorbed component adsorption; i.e., nitrogen (about 2.6 times the experimental uncertainties). The ternary mixture adsorption predictions based on the pure and the binary interaction parameters (BIP) obtained from binary adsorption data were also presented in Table 31. As in the case for adsorption on dry activated carbon, the use of binary interaction parameters not only reduces the observed deviations for the binary
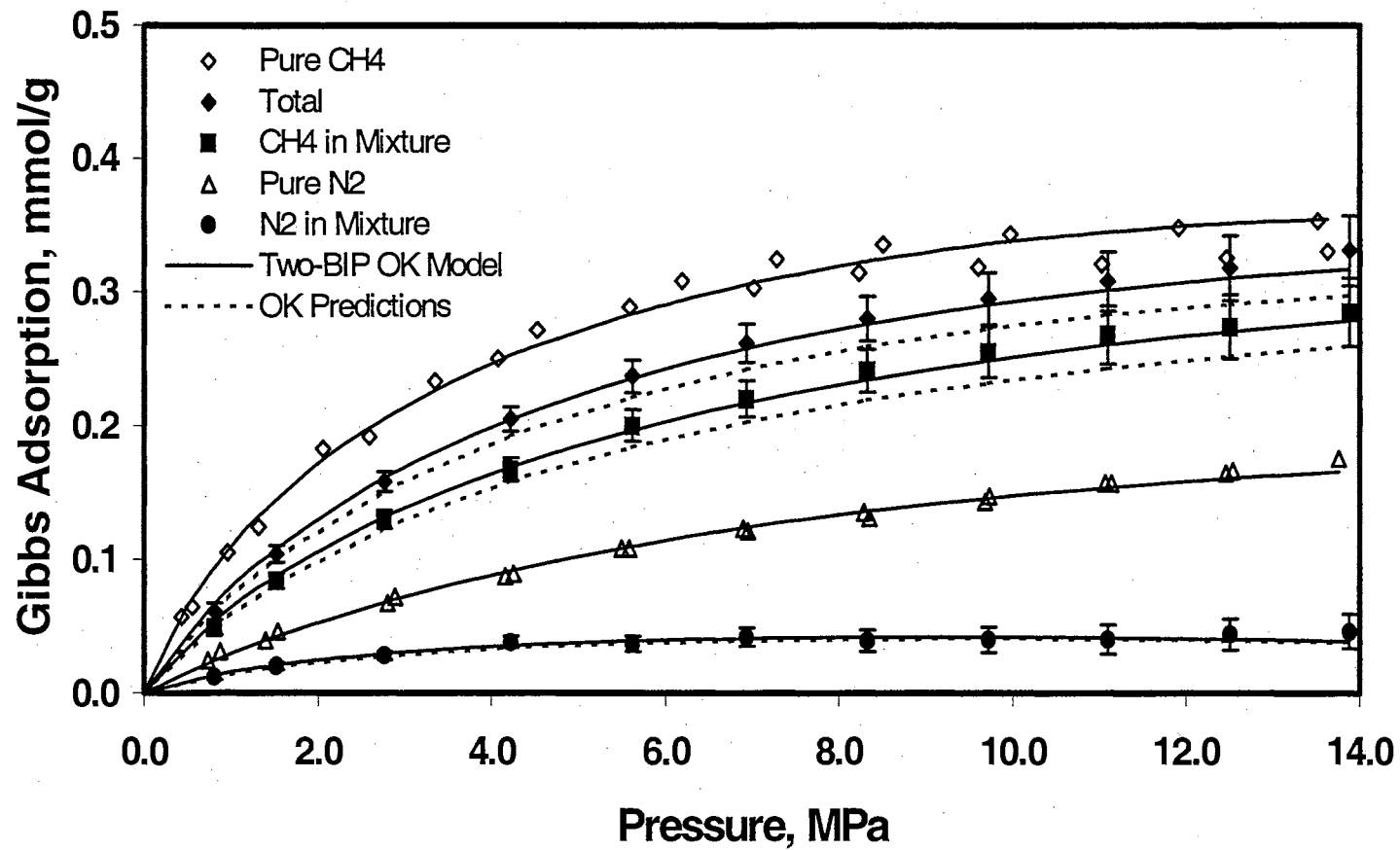
Figure 48. Gibbs Adsorption from an Equimolar CH_4/N_2 Feed Mixture on Wet Tiffany Coal at 327.6 K (OSU Data)

systems, but they also improve the predictions for the ternary adsorption systems. On average, the use of both one and two binary interaction parameters in the model can predict the ternary adsorption within the expected experimental uncertainties.

Table 31. OK Model Predictions of Ternary Mixture Adsorption on Wet Tiffany Coal at 327.6 K

Systems	NPTS	%AAD	RMSE (mmol/g)	WAAD
Based on Parameters from Pure-Adsorption Model				
Methane	11	34.0	0.010	0.7
Nitrogen	11	85.8	0.037	2.6
CO_2	11	19.3	0.073	2.1
Total	11	5.1	0.028	0.6
Based on Pure and One Binary Interaction Parameters (C_{ij})				
Methane	11	7.0	0.002	0.1
Nitrogen	11	40.7	0.017	1.2
CO_2	11	15.3	0.051	1.6
Total	11	8.5	0.034	1.0
Based on Pure and Two Binary Interaction Parameters				
Methane	11	29.2	0.010	0.6
Nitrogen	11	48.4	0.021	1.4
CO_2	11	13.1	0.042	1.4
Total	11	7.5	0.030	0.9

Figure 49 shows the OK model predictions for the ternary mixture adsorption on wet Tiffany coal, based on pure-component data and with two binary interaction parameters from the binary adsorption data. As shown in the figure, the OK model can predict almost all total and individual component adsorptions in the ternary mixture system within the experimental uncertainties when the binary interaction parameters are included.
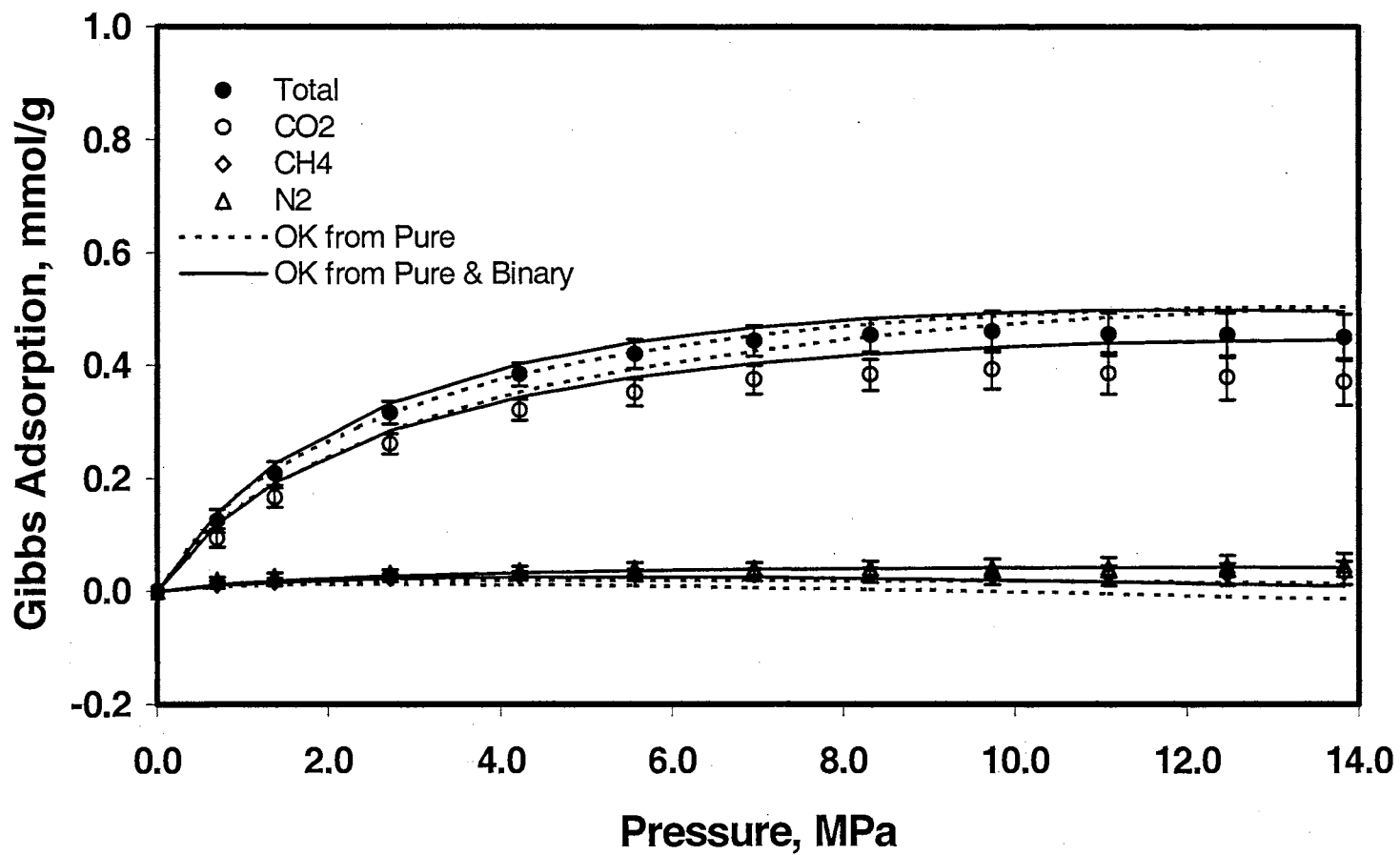
161

Figure 49. OK Model Predictions from a $CH_4/N_2/CO_2$ Feed Mixture Adsorption on Wet Tiffany Coal at 327.6 K (OSU Data)

Summary

The OK model can be used to predict individual component adsorption in the binary and ternary system within twice the experimental uncertainties, on average. In general, the model can also predict the total adsorption in the binary system within the expected experimental uncertainties. Worse results were generally obtained for the predictions of the lesser-adsorbed component adsorptions, as indicated by larger WAAD (3.5 for nitrogen adsorption in the nitrogen/CO_2 adsorption on activated carbon, and 4.5 for methane adsorption in the methane/CO_2 adsorption on wet Tiffany coal).

The predictions of the binary adsorption on the dry activated carbon systems based on the generalized pure-adsorption model produced slightly better results than those based on the correlative pure-adsorption model. In the wet coal systems, comparable results were obtained for both cases.

In general, the use of one binary interaction parameter, C_{ij}, significantly improved the binary mixture adsorption representation. Specifically, the lesser-adsorbed components can be represented to within the expected experimental uncertainties with the use of C_{ij}. Better representations were further obtained when two binary interaction parameters (C_{ij} and E_{ij}) were applied, as indicated by a WAAD of about 0.5.

Relatively large values of C_{ij} in some system suggests that the correlative burden of the binary adsorption modeling has mainly rested on correcting values for the fluid-fluid interaction energy. Application of the surface heterogeneity, such as the fluid-solid energy distribution, and application of an accurate equation of state with adequate mixing rules to calculate the chemical potential in the gas phase, should be considered in future studies.

The second binary interaction parameter, E_{ij}, for most of the wet coal systems are less than the values obtained from the adsorption on dry activated carbon. This indicates that the model without interaction parameters overestimates the individual component adsorptions on the wet coals. The chemical structure of the coal and the presence of water in the coal affect the predictive capability of the model. Further, separating the two factors affecting the mixture adsorption modeling would require additional data, especially mixture adsorption data on dry coals.

Comparison of the OK model to the other models in mixture adsorption on BPL activated carbon (Reich, 1980) shows that the OK model produced better predictions, for individual adsorption, compared to Langmuir model and gave comparable results to the 2-D EOS model. For the total adsorption predictions, the OK model has a better performance than the other models.

CHAPTER 8

CONCLUSIONS AND RECOMENDATIONS

This study was an investigation of the efficacy of the Ono-Kondo (OK) lattice model for correlating and predicting high-pressure, supercritical adsorption isotherms encountered in CBM recovery and CO_2 sequestration. Specifically, the parameters of the Ono-Kondo (OK) model were evaluated to obtain precise representation of pure-gas, high-pressure adsorption on carbon adsorbents for adsorbates in the near critical and supercritical regions. Generalized model parameters determined by accessible adsorbate and adsorbent characterizations were developed, and the model was extended to mixture adsorption. Following are specific conclusions and recommendations based on this work.

Conclusions

Pure-Gas Adsorption Modeling

1. The OK monolayer model appears effective in modeling gas adsorption on carbon matrices at supercritical and near critical region.

2. On average, the OK model with two regressed parameters for each system can *correlate* pure adsorption isotherms within the expected experimental uncertainties (3.6% AAD).

3. The generalized OK model *predicts* the adsorption on activated carbon with 8% AAD or twice the error of the two-parameter OK model.

4. A high potential exists for developing *a priori* predictive model using fully-generalized parameters that provides reasonably accurate predictions (within twice the experimental uncertainties) for the adsorption isotherms of various gases based on the adsorption isotherm of one gas on the same matrix. This includes the prediction of a maximum in the pure component excess adsorption at high pressures.

Mixed-Gas Adsorption Modeling

The OK model:

5. Correlates the *total* and *individual component* adsorption in the binary systems within the expected experimental uncertainties.

6. Predicts *total* adsorption for the *binary* systems studied within the expected experimental uncertainties.

7. Predicts *individual component* adsorption in the *binary* systems within twice the expected experimental uncertainties.

8. Predicts the *total* and *individual component* adsorption in the *ternary* systems within the expected experimental uncertainties, if the information obtained from binary adsorption is utilized.

9. Produces better prediction, for *individual component* adsorption, than the Langmuir model and gives comparable results to the 2-D EOS model.

166

Recommendations

To fully exploit the potential of the OK model, the following developments are needed:

1. Develop improved mixing/combining rules, and apply an accurate equation of state to calculate the chemical potential of the gas phase.

2. Develop a more rigorous approach to account for the effect of water on CBM adsorption systems.

3. Include the effect of the surface heterogeneity by using descriptions, which include fluid-solid energy and/or pore size distributions.

REFERENCES

1. Angus, S., Armstrong, B., de Reuck, K.M., "International Thermodynamic Tables of the Fluid State-5: Methane," IUPAC Chemical Data Series No.16, Pergamon Press, New York, (1978).

2. Angus, S., de Reuck, K.M., Armstrong, B., "International Thermodynamic Tables of the Fluid State-6: Nitrogen," IUPAC Chemical Data Series No.20, Pergamon Press, New York, (1979).

3. Aranovich, G.L., Donohue, M.D., *Adsorption of Supercritical Fluids*, J. Colloid and Interface Sci. 180 537-541 (1996).

4. Aranovich, G.L., Donohue, M.D., *Predictions of Multilayer Adsorption Using Lattice Theory*, J. Colloid and Interface Sci. 189 101-108 (1997).

5. Aranovich, G.L., Donohue, M.D., *Surface Compression in Adsorption Systems*, Colloid and Surfaces A. 187-188 95-108 (2001).

6. Aranovich, G.L., Hocker, T., Wu, D.W., Donohue, M.D., *Nonrandom Behavior in Multicomponent Lattice Mixture: Effects of Solute Size and Shape*, J. Chem. Phys. 106 (24) 10282-10291 (1997).

7. Arri, L. E., Yee, D., *Modeling Coalbed Methane Production With Binary Gas Sorption*, SPE Paper 24363, presented at the SPE Rocky Mountain Regional Meeting, Casper, Wyoming, May 18-21, (1992).

8. Benard, P., Chahine, R., *Modelling of High-Pressure Adsorption Isotherms above the Critical Temperature on Microporous Adsorbents: Application to Methane*, Langmuir, 13 808-813 (1997).

9. Benard, P., Chahine, R., *High-Pressure Adsorption Isotherms of Hydrogen*, Langmuir, 13 808-813 (2001).

10. Berlier, K., Frere, M., *Adsorption of CO_2 on Microporous Materials. 1. On Activated Carbon and Silica Gel*, J. Chem. Eng. Data, 42 533-537 (1997).

11. Berlier, K., Olivier, M-G., Jadot, R., *Adsorption of Methane, Ethane, and Ethylene on Zeolite*, J. Chem. Eng. Data, 40 1206-1208 (1995).

12. Beutekamp, S., Harting, P., *Experimental Determination and Analysis of High Pressure Adsorption Data of Pure Gases and Gas Mixture*, Adsorption, 8 255-269 (2002).

13. Bishnoi, P.R., Robinson, D.B., *Mixing rules improve BWR use*, Hydrocarbon Processing, 11 152-156 (1972)

14. Brunauer, S., Emmet, P.H., Teller, E. J., *Adsorption of Gases in Multimolecular layers*, Am.Chem.Soc. 60 309-319 (1938).

15. Brunauer, S., Deming, L.S., Deming, E., Teller, E., J., *On A Theory of the van der Waals Adsorption of Gases*, Am.Chem.Soc. 62 1723-1732 (1940).

16. Callen, H.B., "Thermodynamics and an Introduction to Thermostatistics 2nd Ed.," Wiley, New York, (1985).

17. Camp, R.W., Stanley, H.D., American Laboratory, September, p.34. (1991).

18. Chen, J. H., Wong, D. S. H., Tan, C. S., Subramanian, R., Lira, C. T., Orth, M., *Adsorption and Desorption of Carbon Dioxide onto and from Activated Carbon at High Pressures,* I&EC Research 36 2808-2815 (1997).

19. Clarkson, C.R, Bustin, R.M., Levy, J.H., *Application of the Mono/multilayer and Adsorption Potential Theories to Coal Methane Adsorption Isotherms at Elevated Temperature and pressure*, Carbon 35(12) 1689-1705 (1997).

20. Clarkson, C.R, Bustin, R.M., *Binary Gas Adsorption/Desorption Isotherms: Effect of Moisture and Coal Composition upon Carbon Dioxide Selectivity over Methane*, International Journal of Coal Geology 42 241-271 (2000).

21. Cochran, T. W., Kabel, R. L., Danner, R. P., *Vacancy Solution Theory of Adsorption Using Flory-Huggins Activity Coefficient Equations,* AIChE J 31 268-277 (1985).

22. Cranston, R.W., Inkey, F.A., "Advance in Catalysis, Vol. 9," Academic Press, New York, (1957).

23. de Boer, J. H., "The Dynamical Character of Adsorption 2nd Ed.," Oxford at The Clarendon Press, London, (1968).

24. DeGance, A. E., *Multicomponent High-Pressure Adsorption Equilibria on Carbon Substrates: Theory and Data,* Fluid Phase Equilib. 78 99-137 (1992).

25. Dhima, A., de Hemptinne, J., Moracchini, G., *Solubility of Light Hydrocarbons and Their Mixtures in Pure Water Under High Pressure*, Fluid Phase Equilib. 145 129-150 (1998).

26. Do, D.D., "Adsorption Analysis: Equilibria and Kinetics," Imperial College Press, London, (1998).

27. Dreisbach, F., Staudt, R., Keller, J.U., *High Pressure Adsorption Data of Methane, Nitrogen, Carbon Dioxide and Their Binary and Ternary Mixtures on Activated Carbon.* Adsorption, 5 215-227 (1999).

28. Dubinin, M. M., "Chemistry and Physics of Carbon Vol. 2.," Walker, P. L., Eds., Jr. Edward Arnold Ltd., New York, (1966).

29. Ergun, S., Tiensuu, V.H., *Tetrahedral Structures in Amorphous Carbon*, Acta Crystallogr., 12 1050-1051 (1959).

30. Fitzgerald, J. E., Sudibandriyo, M., Pan, Z., Robinson, Jr., R. L., Gasem, K. A. M., *Modeling the Adsorption of Methane, Carbon Dioxide, Nitrogen and their Binary Mixtures on Activated Carbon Using the Simplified Local Density Model*, Proceedings of the AIChE Spring National Meeting, New Orleans, Louisiana, March 31-April 3, (2003).

31. Fitzgerald, J. E., Sudibandriyo, M., Pan, Z., Robinson, Jr., R. L., Gasem, K. A. M., *Modeling the Adsorption of Pure Gases on Coals with The SLD Model*, Carbon 41 2203-2216 (2003).

32. Frére, M.G., De Weireld, G.F., *High-Pressure and High-Temperature Excess Adsorption Isotherms of N_2, CH_4, and C_3H_8 on Activated Carbon*, J. Chem. Eng. Data, 47 823-829 (2002).

33. Gan, H., Nandi, S.P., Walker, P.L., Jr., *Nature of the Porosity in American Coals*, Fuel, 51 272-277 (1972).

34. Gasem, K.A.M., Robinson, Jr., R. L., Radovic, L.R., *Sequestering Carbon Dioxide in Coalbeds*, Grant Continuation Report: Volume I, 1999-2000, prepared for the U.S. Department of Energy, (2000).

35. Gasem, K.A.M., Robinson, Jr., R. L., Radovic, L.R., *Sequestering Carbon Dioxide in Coalbeds*, Grant Continuation Report: Volume I, 2000-2001, prepared for the U.S. Department of Energy, (2001).

36. Gasem, K.A.M., Robinson, Jr., R. L., Radovic, L.R., *Sequestering Carbon Dioxide in Coalbeds*, Grant Continuation Report: Volume I, 2001-2002, Prepared for the U.S. Department of Energy, (2002).

37. Gasem, K.A.M., Robinson, Jr., R. L., *Adsorption of Pure Methane, Nitrogen, and Carbon Dioxide and Their Mixtures on Wet Tiffany Coal*, Prepared for Advanced Resources International, (2002).

38. Gasem, K.A.M., Robinson, Jr., R. L., Sudibandriyo, M., Pan, Z., Fitzgerald, J. E., *CO₂ Adsorption on Selected Coals*, Prepared for The Department of Energy - National Energy Technology Laboratory (NETL), (2003).

39. Greaves, K.H., Owen, L.B., McLennan, J.D., *Multi-component Gas Adsorption-Desorption Behavior of Coal*, Proc. of the Int. Coalbed Methane Symp., Tuscaloosa, AL, (1993).

40. Hall, F.E., Jr.,"Adsorption of Pure and Multicomponent Gases on Wet Fruitland Coal," M.S. Thesis, Oklahoma State University, Stillwater, Oklahoma (1993).

41. Hall, F., Zhou, C., Gasem, K. A. M., Robinson, Jr., R. L., *Adsorption of Pure Methane, Nitrogen, and Carbon Dioxide and Their Binary Mixtures on Wet Fruitland Coal*, presented at the Eastern Regional Conference & Exhibition, Charleston, November 8-10, (1994).

42. Harpalani, S., Pariti, U.M., in Preceedings of the 1993 International Coalbed Methane Symposium. The University of Alabama/Tuscaloosa, p. 151, May 17-21, (1993).

43. Haydel, J.J., Kobayashi, R., *Adsorption Equilibria in the Methane-Propane-Silica Gel System at High Pressures*, I&EC Fundamentals, 6 546-554 (1967).

44. Hocker, T., Aranovich, G.L., Donohue, M.D., *Monolayer Adsorption for The Subcritical Lattice Gas and Partially Miscible Binary Mixture*, J. Colloid and Interface Sci. 211 61-80 (1999).

45. Hocker, T., Aranovich, G.L., Donohue, M.D., *Monolayer Adsorption of Nonrandom Mixtures*, J. Chem. Phys. 111 (3) 1240-1254 (1999).

46. Hoory, S. E., Prausnitz, J. M., *Monolayer Adsorption of Gas Mixtures on Homogeneous and Heterogeneous Solids,* Chemical Engineering Science 22 1025-1033 (1967).

47. Humayun, R., Tomasko, D L., *High-Resolution Adsorption Isotherms of Supercritical Carbon Dioxide on Activated Carbon*, AIChE J., 46 2065-2075 (2000).

48. Jankowska, H., Swiatkowski, A., Choma, J., "Active Carbon," Kemp, T.J., Editor, Ellis Horwood Ltd., New York, (1991).

49. Joubert, J.I., Grein, C.T., Bienstock, D., *Sorption of Methane in Moist Coal*, Fuel 52 181-185 (1973).

50. Kadlec, O., Choma, J., Jankowska, H., *Analysis of the Pore Structure of Adsorbents and Its Characterization by a Numerical Method*, Chem. Comm., 49 (12) 2721-2738 (1984).

51. Katsuyuki, K., Mustapha, El-M., Katsumi, K., *A New Determination Method of Absolute Adsorption Isotherm of Supercritical Gases Under High Pressure with a Special Relevance to Density-Functional Theory Study*. J. Chem. Phys., 114 4196-4205 (2001).

52. King, M.B., Mubarak, A., Kim, J.D., Bott, T.R., *The Mutual Solubilities of Water with Supercritical and Liquid Carbon Dioxide*, J. Supercritical Fluids 5 296-302 (1992).

53. Krim, J., Watts, E.T., "Third International Conference on Fundamentals of Adsorption," Mersmann, A.B., Scholl, S.E., Eds., Engineering Foundation, New York, (1991).

54. Krooss, B.M., van Bergen, F., Gensterblum, Y., Siemons, N., Pagnier, H.J.M., David, P., *High-pressure Methane and Carbon Dioxide Adsorption on Dry and Moisture-equilibrated Pennsylvanian Coals*, International Journal of Coal Geology, 51 69-92 (2002).

55. Langmuir, I., *The Adsorption of Gases on Plane Surfaces of Glass, Mica, and Platinum*, J. Am. Chem. Soc. 40 1361 (1918).

56. Levy J.H, Day S.J, Killingley J.S., *Methane capasities of Bowen Basin coals related to coal properties*, Fuel 76 (9) 813-819 (1997).

57. Lewis, W.K., Gilliland, E.R., Chertow, B., Cadogan, W.P., *Pure Gas Isotherms*, I&EC 42 1326-1332 (1950).

58. Malbrunot, P., Vidal, D., Vermesse, J., Chahine, R., Bose, T.K., *Adsorption Measurements of Argon, Neon, Krypton, Nitrogen, and Methane on Activated Carbon up to 650 MPa*. Langmuir, 8 77-580 (1992).

59. Masel, R.I., "Principles of Adsorption and Reaction on Solid Surfaces," John Wiley & Sons, Inc., New York, (1996).

60. McCutcheon, A.L., Barton, W.A., Wilson, M.A., *Characterization of Water Adsorbed on Bituminous Coals*, Energy & Fuels, 17 107-112 (2003).

61. Medek, J., *Possibility of Micropore Analysis of Coal and Coke from the Carbon Dioxide Isotherm*, Fuel, 56 131-133 (1977).

62. Mellot, C., Lignieres, J., *Molecular Modeling As a Complement to Experiment; Application to the Separation of Nitrogen and Oxygen*, in "Physical Adsorption: Experiment, Theory and Applications," Fraissard, J., Ed., Kluwer Academic Publisher, Netherlands, (1997).

63. Meyers, R.A., "Coal Structure," Academic Press, New York, (1982).

64. Moffat, D.H., Weale, K.E., *Sorption By Coal of Methane at High Pressure*, Fuel, <u>34</u> 449-462 (1955).

65. Myers, A.L., *Molecular Thermodynamics of Adsorption of Gas and liquid Mixtures* in "Fundamentals of Adsorption," Liapis, A.I., Eds., Engineering Foundation, New York, (1987).

66. Myers, A.L., Prausnitz, J.M., *Thermodynamics of Mixed-Gas Adsorption*, AIChE J <u>11</u> 121-129 (1965).

67. Myers, A.L., *Thermodynamics of Adsorption in Porous Materials*, AIChE J <u>48</u> 145-160 (2002).

68. Nelsen, F.M., Eggertsen, F.T., *Determination of Surface Area. Adsorption Measurements by a Continuous Flow Methods*, Anal. Chem. <u>30</u> 1387 (1958).

69. Ono, S., Kondo, S., *Molecular Theory of Surface Tension in Liquids*, in "Encyclopedia of Physics (S. Flugge, Ed.), Vol. X.," Springer-Verlag, Gottingen, (1960).

70. Pan, Z., "Modeling of Gas Adsorption Using Two-Dimensional Equations of State," Ph.D. Dissertation, Oklahoma State University, Stillwater, Oklahoma (2003).

71. Payne, H. K., Sturdevant, G. A., Leland, T. W., *Improved Two-Dimensional Equation of State to Predict Adsorption of Pure and Mixed Hydrocarbons*, I&EC Fundamentals, <u>7</u> 363-374 (1968).

72. Pieters, W.J.M., Gates, W.E., US Patent 4 489 593 (1984).

73. Pray, H.A., Schweickert, C.E., Minnich, B.H., *Solubility of Hydrogen, Oxygen, Nitrogen, and Helium in Water at Elevated Temperatures*, I&EC <u>44</u> 1146-1151 (1952).

74. Ray, G.C., Box, E.O., *Adsorption of Gases on Activated Carbon. I&EC* <u>42</u> 1315-1318 (1950).

75. Reich, R., Ziegler, W.T., Rogers, K.A., *Adsorption of Methane, Ethane, and Ethylene Gases and Their Binary and Ternary Mixtures and Carbon Dioxide on Activated Carbon at 212-301 K and Pressures to 35 Atmosphers*, Ind. Eng.Chem. Process Des. Dev., <u>19</u> 336 (1980).

76. Reid, R.C., Prausnitz, J.M., Poling, B.E., "The Properties of Gases & Liquids, Fourth Ed.," McGraw-Hill Inc., New York, (1987).

77. Ritter, J.A., Yang, R.T., *Equilibrium Adsorption of Multicomponent Gas Mixtures at Elevated Pressures*, Ind. Eng. Chem. Res. <u>26</u> 1679-1686 (1987)

78. Rouquerol, F., Rouquerol, J., Sing, K., "Adsorption by Powders & Porous Solids: Principles, Methodology and Applications," Academic Press, London, (1999).

79. Salem, M.M.K., Braeuer, P., Szombathely M.v., Heuchel, M., Harting, P., Quitzsch, K., *Thermodynamics of High-Pressure Adsorption of Argon, Nitrogen, and Methane on Microporous Adsorbents,* Langmuir 14 3376-3389 (1998).

80. Sandler, S.I., "Chemical Engineering Thermodynamics, 3rd Ed.," Wiley, New York, (1998).

81. Span, R.,Wagner; W., *A New Equation of State for Carbon Dioxide Covering the Fluid Region from the Triple Point Temperature to 1100 K at Pressures up to 800 MPa,* J. Phys. Chem. Ref. Data, 25 1509-1590 (1996).

82. Steele, W.A., "The Interaction of Gases with Solid Surfaces," Pergamon Press, New York, (1974).

83. Sudibandriyo, M., Fitzgerald, J. E., Pan, Z., Robinson, Jr., R. L., Gasem, K. A. M., *Extension of Ono-Kondo Lattice Model to Mixture Adsorption,* Proceedings of the AIChE Spring National Meeting, New Orleans, Louisiana, March 31-April 3, (2003).

84. Sudibandriyo, M., Pan, Z., Fitzgerald, J. E., Robinson, Jr., R. L., Gasem, K. A. M., *Adsorption of Methane, Nitrogen, Carbon Dioxide and their Binary Mixtures on Dry Activated Carbon at 318.2 K and Pressures to 13.6 MPa,* Langmuir 19 (13), 5323-5331 (2003).

85. Stacy, T.D., Hough, E.W., Mc.Cain, W.D. Jr., *Adsorption of Methane on Carbon at Temperature to 121 °C and Pressures to 650 Atm.,* J.Chem. Eng. Data, 13 74-77 (1968).

86. Stevens, S.H., Spector, D., Riemer, P., *Enhanced Coalbed Methane Recovery Using CO_2 Injection: Worldwide Resource and CO_2 Sequestration Potential,* 1998 SPE International Conference in China, Beijing, China, Nov., (1998).

87. Stevens, S.H., Kuuskraa, V.A., Spector, D., *CO_2 Sequestration in Deep Coal Seams: Pilot Results and Worldwide Potential* in "Greenhouse Gas Control Technologies," Riemer, P., Eliasson, B., and Wokaun, A., Eds., Elsevier Science Ltd., (1999).

88. Suwanayuen, S., Danner, R. P., *A Gas Adsorption Isotherm Equation Based on Vacancy Solution Theory,* AIChE J 26 68-75 (1980).

89. Suwanayuen, S., Danner, R. P., *Vacancy Solution Theory of Adsorption From Gas Mixtures,* AIChE J 26 76-83 (1980).

90. Talu, O., Zwiebel, I., *Multicomponent Adsorption Equilibria of Nonideal Mixtures,* AIChE J 32 1263-1276 (1986).

91. Toda, Y., Hatami, M., Toyoda, S., Yoshida, Y., Honda, H., *Micropore Structure of Coal*, Fuel, 50 187 (1971).

92. Valenzuela, D.P., Myers, A.L., Talu, O., Zwiebel, I., *Adsorption of Gas Mixtures: Effect of Energetic Heterogeneity*, AIChE J. 34 397-402 (1988).

93. van der Vaart, R., Huiskes, C., Bosch, H., Reith, T., *Single and Mixed Gas Adsorption Equilibria of Carbon Dioxide/Methane on Activated Carbon*, Adsorption, 6 311-323 (2000).

94. Vermesse, J., Vidal, D., Malbrunot, P., *Gas Adsorption on Zeolites at High Pressure*, Langmuir, 12 4190-4196 (1996).

95. Wakasugi, Y., Ozawa, S., Ogino, Y., *Physical Adsorption of Gases at High Pressure, V. An Extension of a Generalized Adsorption Equation to System with Polar Adsorbents*, Journal of Colloid and Interface Science, 79 399-409 (1981).

96. Walker, P.L., "Chemistry and Physics of Carbon, Vol. 5," Marcel Dekker Inc., New York, (1969).

97. Webb, P.A., Powder Handling and Processing, 4 (4) 439 (1992).

98. Wong, S., Foy, C., Gunter, B., and Jack, T., *Injection of CO_2 for Enhanced Energy Recovery: Coalbed Methane Versus Oil Recovery* in "Greenhouse Gas Control Technologies," Riemer, P., Eliasson, B., and Wokaun, A., Eds., Elsevier Science Ltd., (1999).

99. Yang, R.T., "Adsorbents: Fundamentals and Applications," Wiley-Interscience, Hoboken, N.J., (2003).

100. Zhou, C., Hall, F., Gasem, K. A. M., Robinson, Jr., R. L., *Predicting Gas Adsorption Using Two-Dimensional Equation of State*, I&EC Research 33 1280-1289 (1994).

101. Zhou, C., "Modeling and Prediction of Pure and Multicomponent Gas Adsorption," Ph.D. Dissertation, Oklahoma State University, Stillwater, Oklahoma (1994).

102. Zhou, L., Zhou, Y., Li, M., Chen., P., and Wang., Y., *Experimental and Modeling Study of the Adsorption of Supercritical Methane on a High Surface Activated Carbon*. Langmuir, 16 5955-5959 (2000).

103. Zhou, L., Zhou, Y., Bai, S., Lu, C., Yang, B., *Determination of the Adsorbed Phase Volume and Its Application in Isotherm Modeling for the Adsorption of Supercritical Nitrogen on Activated Carbon*, Journal of Colloid and Interface Science, 239 33-38 (2001)

APPENDIX A

TEMPERATURE CALIBRATION

APPENDIX A

TEMPERATURE CALIBRATION

The temperature of the equilibrium cell section was measured using an RTD digital thermometer, model 2180A, manufactured by Fluke. The platinum probe was inserted inside a hole in an aluminum block, which was attached to the surface of the equilibrium cell. The pump section temperature was measured using a thermocouple mounted to the inside of the Ruska injection pump. In addition, the pump section temperature was also monitored by three other thermocouples attached on the surface and surrounding of the injection pump.

Calibrations were performed routinely during the course of the experiments. The temperature measuring devices were calibrated against a Minco platinum resistance reference thermometer model RT 88078. Table A1 presents an example of the calibration results conducted on July 2002. Figures A1 and A2 present linear fit of the reading cell and pump section temperatures to the Minco reference thermometer. Results showed root-mean-square errors (RMSE) of the fit to be 0.02°F and 0.07°F for the equilibrium cell and pump thermocouples, respectively.

Table A1. Temperature Calibration Results

| Points No.	Minco Reference Temperature (°F)	Cell Section Temperature (°F)	Pump Section Temperature (°F)
1	32.20	32.15	33.00
2	50.36	50.30	51.00
3	70.40	70.30	70.95
4	90.42	90.35	91.10
5	110.48	110.40	110.90
6	120.53	120.50	120.90
7	125.50	125.45	125.80
8	127.49	127.45	127.80
9	128.50	128.50	128.75
10	129.51	129.50	129.75
11	130.01	130.00	130.20
12	130.52	130.50	130.70
13	130.89	130.90	131.10
14	131.30	131.30	131.45
15	131.49	131.50	131.65
16	131.71	131.70	131.85
17	132.12	132.10	132.30
18	132.49	132.50	132.70
19	133.00	133.00	133.20
20	133.50	133.50	133.75
21	134.51	134.50	134.70
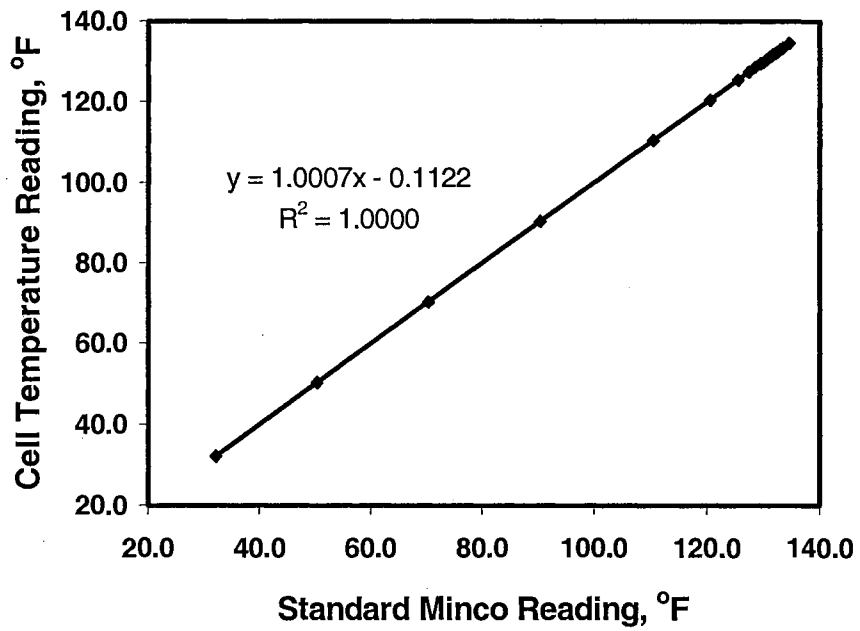
Figure A1. Temperature Calibration for Equilibrium Cell Temperature Measurement

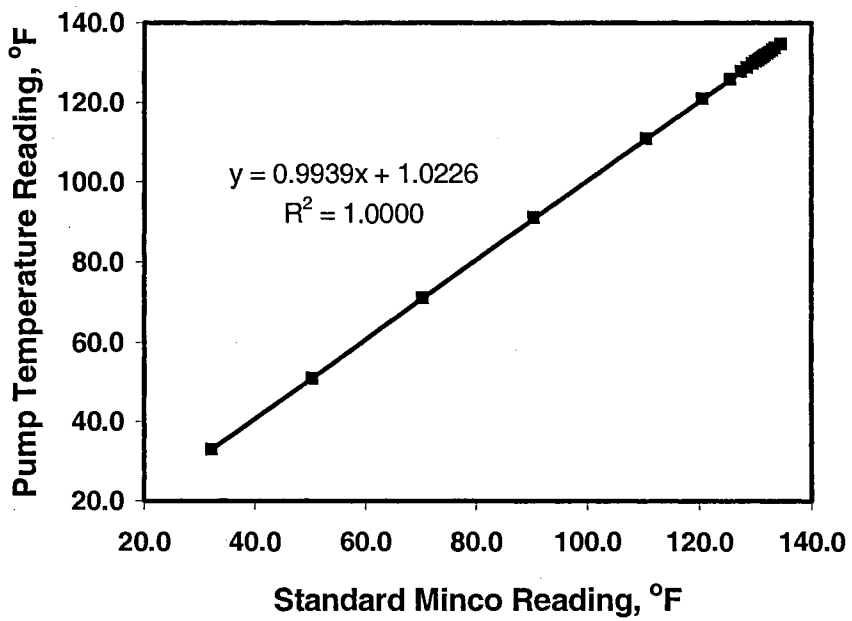

Figure A2. Temperature Calibration for Pump Temperature Measurement

179

APPENDIX B

PRESSURE CALIBRATION

APPENDIX B

PRESSURE CALIBRATION

The pressures measured by Super TJE transducers were calibrated against a Ruska deadweight tester with calibration traceable to the National Institute of Science and Technology. Calibrations were performed routinely during the course of the experiments. The pump and cell section pressure transducers were calibrated at pressures from zero to 1800 psia at intervals of about 100 psia. The results were used to construct pressure calibration plots similar to the one illustrated in Figure B1. Deviations between standard dead weight pressure and the transducer pressure were plotted as a function of transducer pressure. The pressure calibration data were fit to a second order polynomial in pressure using a least-squares method. Results showed root-mean-square errors (RMSE) of the fit to be 0.1 psia. The pressure calibration regression coefficients were entered into the data reduction software routines to make the appropriate pressure corrections.
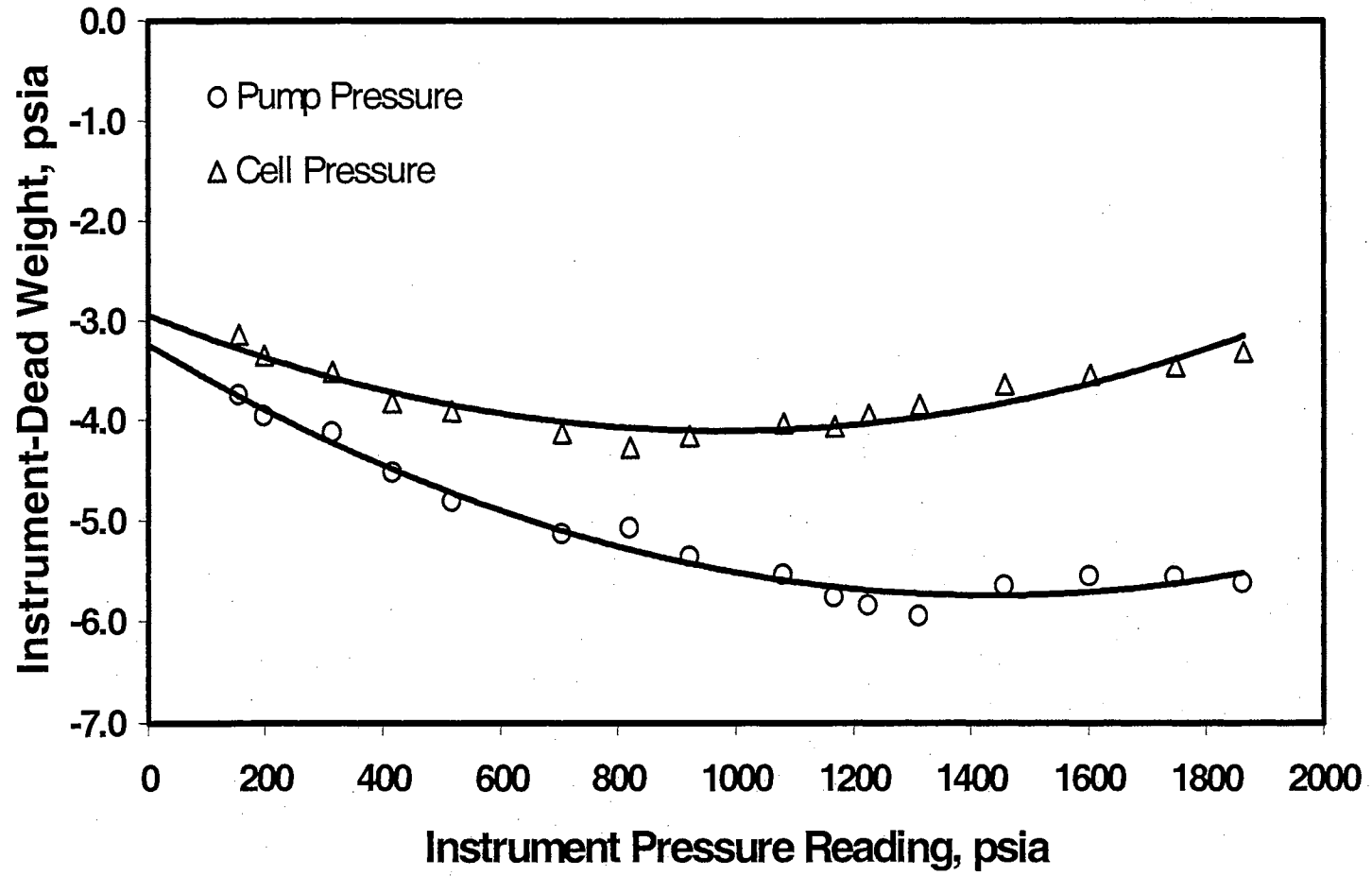
Figure B1. Pump and Equilibrium Cell Section Pressure Calibrations

APPENDIX C

GAS CHROMATOGRAPH CALIBRATION

APPENDIX C

GAS CHROMATOGRAPH CALIBRATION

For mixture adsorption, at equilibrium, a 20μL sample in the cell-section loop was transferred to the gas chromatograph for analysis. The GC used for composition analysis was a Varian Chrompack CP-3800 with the helium carrier gas maintained at a 0.25-mL/s flow rate. A 10-ft Haysep D packed-column was used for CH_4/CO_2, N_2/CO_2 and $CH_4/CO_2/N_2$ systems, and a molecular sieve 13X column was used for the CH_4/N_2 system; column temperature was 80°C. A thermal conductivity detector was used for all of the binary systems studied; its bath temperature was set at 100°C.

The gas chromatograph was calibrated against volumetrically-prepared mixtures at the nominal feed-gas concentrations. The chromatographic response factor, defined as $(A_2/A_1)(y_1/y_2)$ where A is the GC response percentage area, was found to depend slightly on pressure; as such, the GC was calibrated for each nominal composition at pressure intervals of 1.4 MPa (200 psi).

Table C1 presents the GC calibration fit for the binary systems used. P in the GC calibration equation is pressure in psia, and the relative response factors were defined as follows:

$$RF_1 = \frac{A_{CH_4} y_{N_2}}{A_{N_2} y_{CH_4}} \qquad \text{for methane/nitrogen system} \qquad \text{(C1)}$$

$$RF_2 = \frac{A_{CH_4} y_{CO_2}}{A_{CO_2} y_{CH_4}} \qquad \text{for methane/CO}_2 \text{ system} \qquad \text{(C2)}$$

$$RF_3 = \frac{A_{N_2} y_{CO_2}}{A_{CO_2} y_{N_2}} \qquad \text{for nitrogen/CO}_2 \text{ system.} \qquad (C3)$$

Table C1. GC Calibration Fit for Binary Mixtures

Binary System	GC Calibration Equation
Methane/Nitrogen	$RF_1 = -1.5243 \times 10^{-5} P + 0.31162\, y_{N_2} - 0.67741\, y_{N_2}^2$ $+ 48.643\, y_{N_2}^3 + 0.823605$
Methane/CO$_2$	$RF_2 = \left(-2.6972\, y_{CO_2}^2 + 4.2595\, y_{CO_2}\right) \times 10^{-8} P^2$ $+ \left(1.0987\, y_{CO_2}^2 - 0.89272\, y_{CO_2} - 0.38\right) \times 10^{-4} P + 0.791$
Nitrogen/CO$_2$	$RF_2 = (-5.0551\, y_{CO_2}^3 + 0.07028\, y_{CO_2}^2 - 0.025695\, y_{CO_2} +$ $0.00640681\,) \times 10^{-2} P - 0.00060852\, y_{CO_2} + 0.92786$

By knowing the GC response percentage area at a given pressure, the composition of the gas mixture can be determined, using the equations given in Table C1. Results showed the average deviations of the gas mole fraction determined by the calibration fit were less than 0.001 with the maximum deviation of 0.003.

Figure C1 shows the example of the GC calibration results for the methane/CO$_2$ binary system. The error bars in the figure represent the estimated uncertainties in determining RF from several samples taken.

For the ternary mixture, the GC response percentage areas of methane and CO$_2$ in the ternary mixture were normalized and the values were used to obtain the gas composition (y_{CH_4}'' and y_{CO_2}'') using methane/CO$_2$ calibration. Similarly, the GC response percentage areas of nitrogen and CO$_2$ in the ternary mixture were normalized and the values were used to obtain the gas composition (y_{N_2}' and y_{CO_2}') using nitrogen-CO$_2$

calibration. The ternary gas compositions were then calculated with the following equation:

$$y_{CO_2} = \frac{y''_{CO_2}}{\left(y''_{CO_2} + y''_{CH_4} + \dfrac{y''_{CO_2}}{y'_{CO_2}} y'_{N_2}\right)} \tag{C4}$$

$$y_{CH_4} = \frac{y''_{CH_4}}{\left(y''_{CO_2} + y''_{CH_4} + \dfrac{y''_{CO_2}}{y'_{CO_2}} y'_{N_2}\right)} \tag{C5}$$

and

$$y_{N_2} = 1 - y_{CO_2} - y_{CH_4} \tag{C6}$$

Using the above method, the ternary gas compositions can be determined within 0.004 deviations.
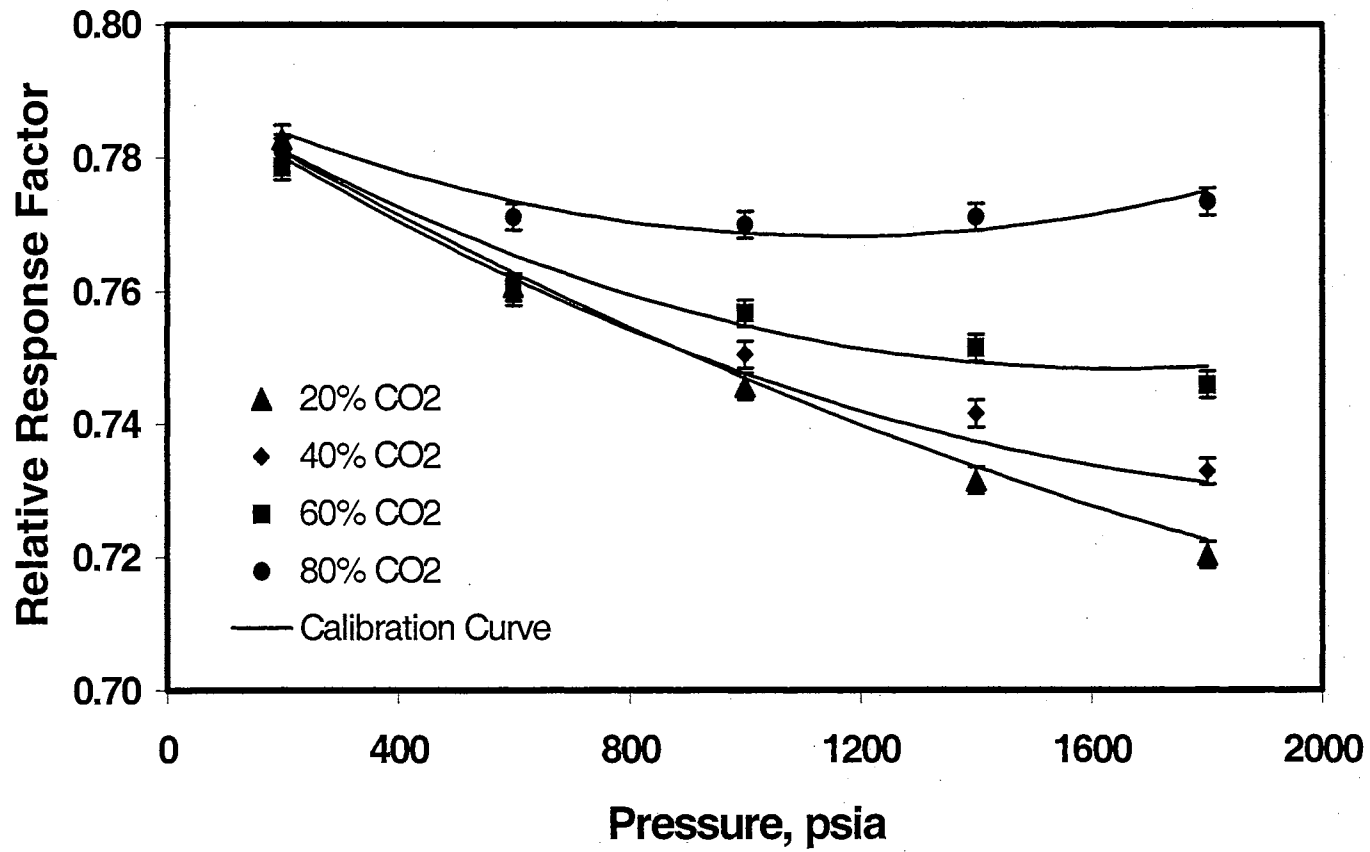
Figure C1. Gas Chromatograph Calibration for Methane/CO_2 Mixtures

APPENDIX D

ERROR ANALYSIS

APPENDIX D

ERROR ANALYSIS

Pure Component Adsorption

The Gibbs excess adsorption in units of mg mole/g adsorbent was calculated as follows:

$$n^{Gibbs} = \frac{1000\, n_{ads}}{L} \tag{D1}$$

where L is the amount of activated carbon loaded in the cell [g] and n_{ads} is the Gibbs excess adsorption obtained from the experiment according to Equation (4).

Therefore, the uncertainty in calculating the Gibbs excess adsorption is determined by:

$$\sigma^2_{n^{Gibbs}} = \left(\frac{\partial n^{Gibbs}}{\partial n_{ads}} \right)^2 \sigma^2_{n_{ads}} + \left(\frac{\partial n^{Gibbs}}{\partial L} \right)^2 \sigma^2_L \tag{D2}$$

or

$$\sigma^2_{n^{Gibbs}} = \left(\frac{1000}{L} \right)^2 \sigma^2_{n_{ads}} + \left(\frac{1000\, n_{ads}}{L^2} \right)^2 \sigma^2_L \tag{D3}$$

where σ_L was estimated to be 0.1 g, and n_{ads} was calculated as:

$$\sigma^2_{n_{ads}} = \sigma^2_{n_{inj}} + \sigma^2_{n_{unads}} + \sigma^2_{n_{sol}} \tag{D4}$$

$\sigma_{n_{inj}}$ is dependent on the uncertainty of determining the density of the gas in the pump, ρ_p and the uncertainty of the gas volume injected.

$$\sigma_{n_{inj}}^2 = (V_f^2 + V_i^2)\sigma_{\rho_p}^2 + 2\rho_p^2\sigma_V^2 \tag{D5}$$

where V_f and V_i are the final and initial volume in the pump.

The uncertainty of injected gas volumes, σ_v, is estimated to be equal to 0.02 cm^3, and σ_{ρ_p} is calculated as follow:

$$\rho_p = (P/ZRT)_p \tag{D6}$$

which leads to

$$\sigma_{\rho_p}^2 = \left(\frac{\partial\rho_p}{\partial T}\right)_P^2 \sigma_T^2 + \left(\frac{\partial\rho_p}{\partial P}\right)_T^2 \sigma_P^2 + \left(\frac{\partial\rho_p}{\partial Z}\right)_{T,P}^2 \sigma_Z^2 \tag{D7}$$

Therefore

$$\sigma_{\rho_p}^2 = \rho^2 \left(\left(\frac{1}{T} + \frac{(\partial Z/\partial T)_P}{Z}\right)^2 \sigma_T^2 + \left(\frac{1}{P} - \frac{(\partial Z/\partial P)_T}{Z}\right)^2 \sigma_P^2 + \left(\frac{1}{Z}\right)^2 \sigma_Z^2 \right) \tag{D8}$$

where σ_z is the accuracy of the compressibility factor model used. σ_T and σ_P are estimated to be 0.1 K and 6.9 kPa respectively.

Using similar technique $\sigma_{n_{unads}}$ in Equation (D4) can also be deriveded resulting the following expression:

$$\sigma_{unads}^2 = (\rho_{cell})^2 \sigma_{V_{void}}^2 + (V_{void})^2 \sigma_{\rho_{cell}}^2 \tag{D9}$$

The void volume is measured several times within the range of the operating pressure. Generally, each void volume measured is less than 0.3 cm^3 removed from the average void volume taken over at least five injections. So, $\sigma_{V_{void}}$ was estimated to be 0.3 cm^3.

Equation (D8) can also be used to calculate the uncertainty of the gas density in the cell, $\sigma_{\rho_{cell}}$.

For adsorption on a dry matrix, $\sigma_{n_{sol}}$ is equal to zero, and for adsorption on a wet matrix, the accuracy of the model for calculating the gas solubility in water is estimated to be 5 % of the amount of gas absorbed in water.

Error Estimates for Absolute Adsorption

Relation between Gibbs and absolute adsorption is expressed as:

$$n^{Abs} = \frac{n^{Gibbs}}{1 - \frac{\rho}{\rho_a}} \tag{D10}$$

Therefore, the uncertainty in calculating the absolute adsorption can be expressed as:

$$\sigma^2_{n^{Abs}} = \left(\frac{1}{1 - \frac{\rho}{\rho_a}} \right)^2 (\sigma_{n^{Gibbs}})^2 + \left(\frac{n^{Abs}}{(\rho_a - \rho)} \right)^2 \sigma^2_\rho \tag{D11}$$

Multicomponent Adsorption

The uncertainty of component Gibbs excess adsorption is calculated as follow:

$$n_1^{Gibbs} = x_1^{Gibbs} n_{tot}^{Gibbs} \tag{D12}$$

Therefore

$$(\sigma_{n_1^{Gibbs}})^2 = (n_{tot}^{Gibbs})^2 (\sigma_{x_1}^{Gibbs})^2 + x_1^{Gibbs} (\sigma_{n_{tot}^{Gibbs}})^2 \tag{D13}$$

The same method as used for pure-component adsorption is employed to determine $\sigma_{n_{tot}^{Gibbs}}$. The only difference is in the method used to calculate σ_ρ. For the multicomponent case, the compressibility factor, Z, also depends on the gas composition. Therefore Equation (D8) becomes:

$$\sigma_{\rho_P}^2 = \rho^2 \left(\left(\frac{1}{T} + \frac{(\partial Z/\partial T)_{P,y}}{Z} \right)^2 \sigma_T^2 + \left(\frac{1}{P} - \frac{(\partial Z/\partial P)_{T,y}}{Z} \right)^2 \sigma_P^2 + \left(\frac{(\partial Z/\partial y)_{T,P}}{Z} \right)^2 \sigma_y^2 + \left(\frac{1}{Z} \right)^2 \sigma_Z^2 \right)$$

(D14)

Equation (D14) can be applied for both the pump side and the cell side. The uncertainty of the Z value, σ_Z, calculated by the BWR equation of state (Pan, 2003) is estimated about 0.5% of the Z value.

The $\sigma_{x_1}^{Gibbs}$ is calculated as follow:

$$x_1^{Gibbs} n_{ads} = z_1 n_{inj} - y_1 n_{unads} - n_{sol,1}$$

(D15)

Therefore

$$\sigma_{x_1}^2 = \left(\frac{n_{inj}}{n_{ads}} \right)^2 \sigma_z^2 + \left(\frac{n_{unads}}{n_{ads}} \right)^2 \sigma_y^2 + \left((y_1 - z_1) \left(\frac{n_{inj}}{n_{ads}^2} \right) \right)^2 \sigma_{inj}^2$$

$$+ \left((z_1 - y_1) \left(\frac{n_{inj}}{n_{ads}^2} \right) \right)^2 \sigma_{unads}^2 + \left(\frac{1}{n_{ads}} \right)^2 \sigma_{n_{sol}}^2$$

(D16)

σ_y is the uncertainty in determinating the gas composition, which is equal to the accuracy of the gas chromatograph calibration used (=0.002 mole fraction). σ_z is the uncertainty of the feed composition, which depends on the accuracy of the injection method. Normally, the value is relatively small (=0.00015 mol fraction).

VITA

Mahmud Sudibandriyo

Candidate for the Degree of

Doctor of Philosophy

Thesis: A GENERALIZED ONO-KONDO LATTICE MODEL FOR HIGH-PRESSURE ADSORPTION ON CARBON ADSORBENTS

Major Field: Chemical Engineering

Biographical:

Personal Data: Born in Pati, Indonesia, on August 18, 1963, the son of Muhammad Oelwi and Siti Kamari

Education: Graduated from SMPP Negeri 10 High School, Yogyakarta, Indonesia, in July 1981; received Bachelor of Science in Chemical Engineering from Bandung Institute of Technology, Indonesia, in May 1985; received Masters of Science in Chemical Engineering from Oklahoma State University, Stillwater, Oklahoma, in May 1991. Completed the requirements for the Doctor of Philosophy degree with a major in Chemical Engineering at Oklahoma State University in December 2003.

Experience: Lecturer in the Gas & Petrochemical Engineering Department, University of Indonesia, 1987 to present; post-graduate fellow in Chemical Engineering, Tokyo Institute of Technology, 1992-1993; employed by Oklahoma State University, School of Chemical Engineering, as a teaching assistant and research assistant, 2000-present.

Professional Membership: American Institute of Chemical Engineers